Four – or Even Five? – Decades of CT Image Reconstruction

Marc Kachelrieß

German Cancer Research Center (DKFZ)

Heidelberg, Germany

www.dkfz.de/ct

DEUTSCHES KREBSFORSCHUNGSZENTRUM IN DER HELMHOLTZ-GEMEINSCHAFT

Major Progress Timeline

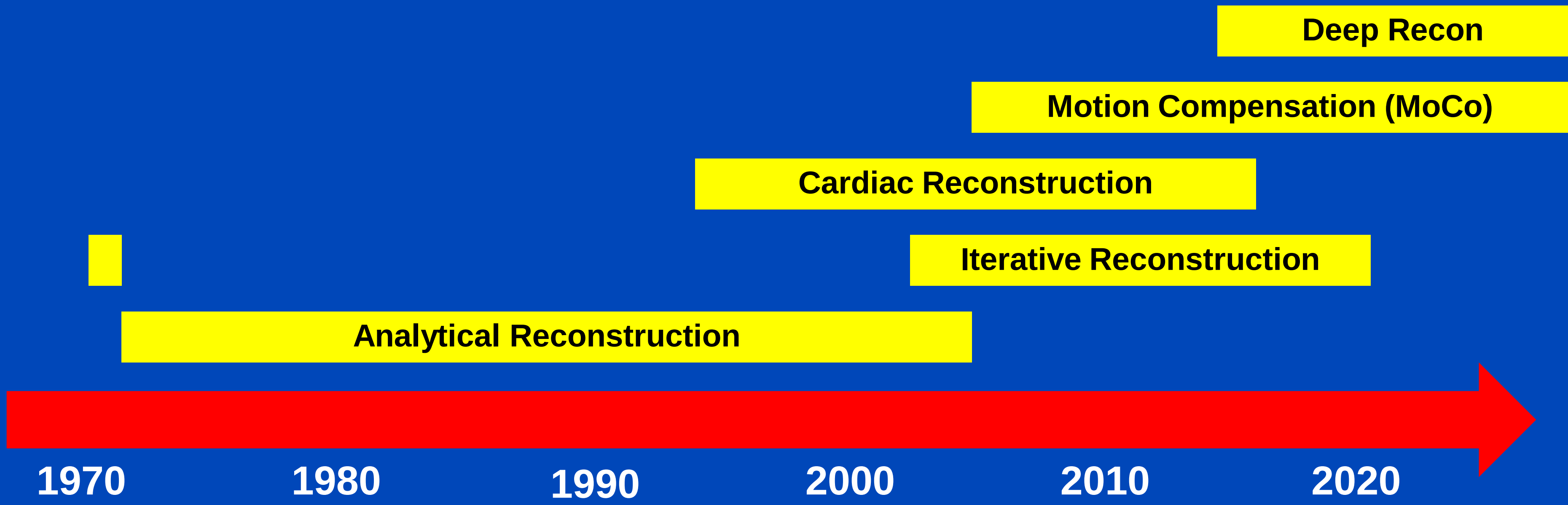

Analytical Image Reconstruction

- **Main progress:**
  - Mid seventies to around 2005

$$x^2 = y$$

Model

$$x = \sqrt{y}$$

Solution

Fan-beam geometry | Parallel-beam geometry

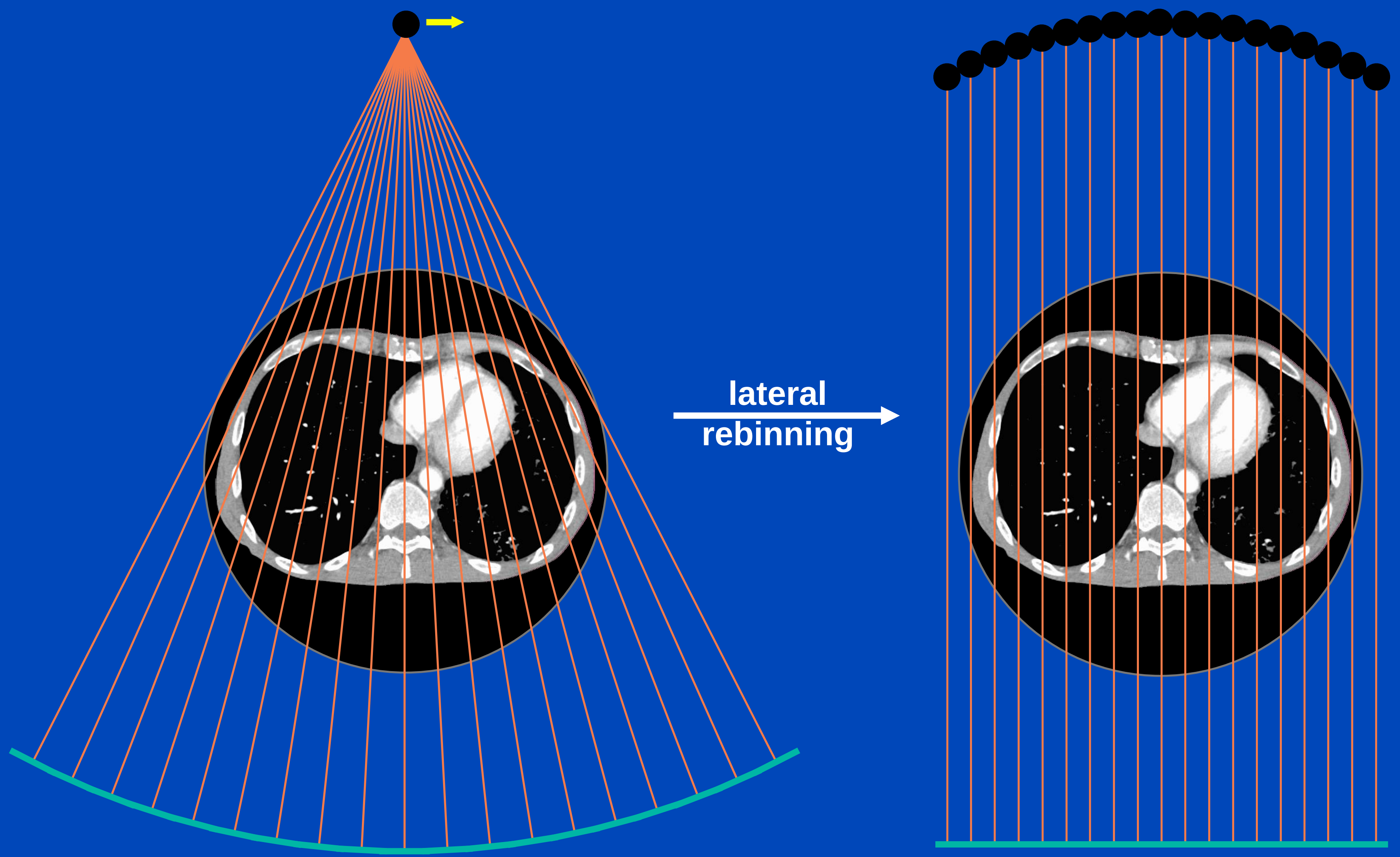

(β, α) (ξ, ϑ)

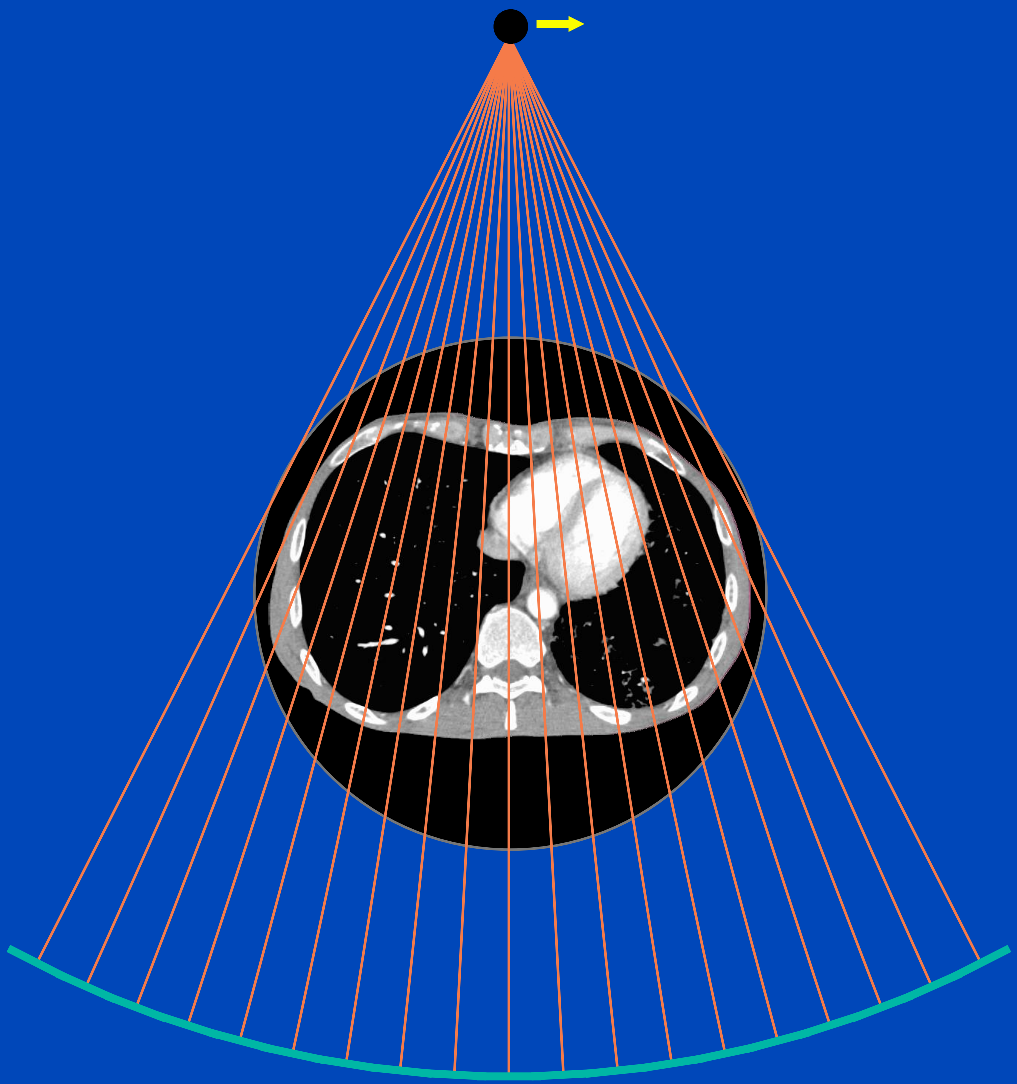

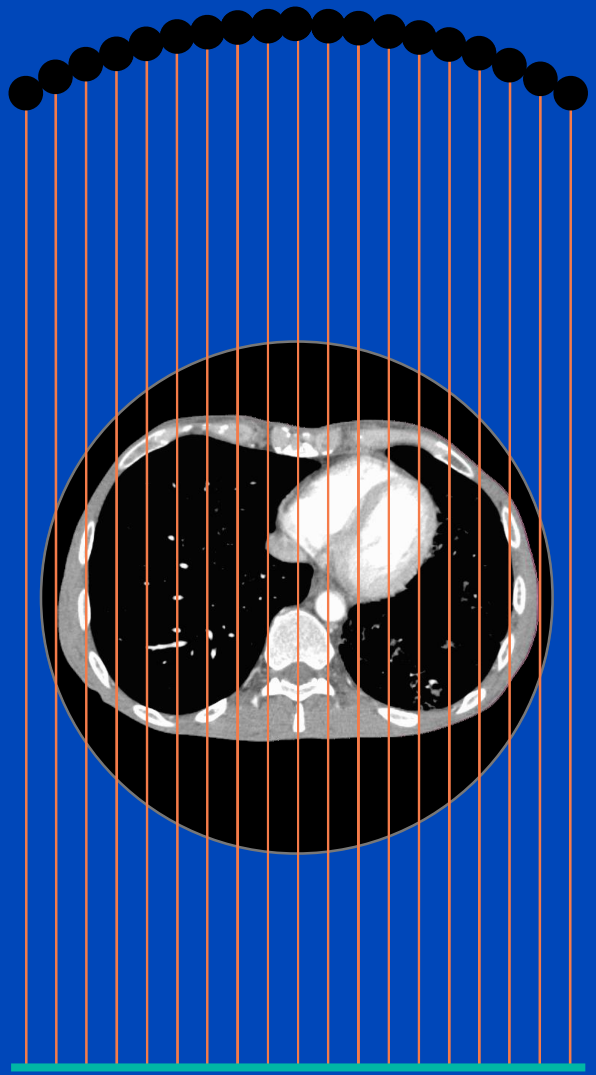

Fan-beam geometry

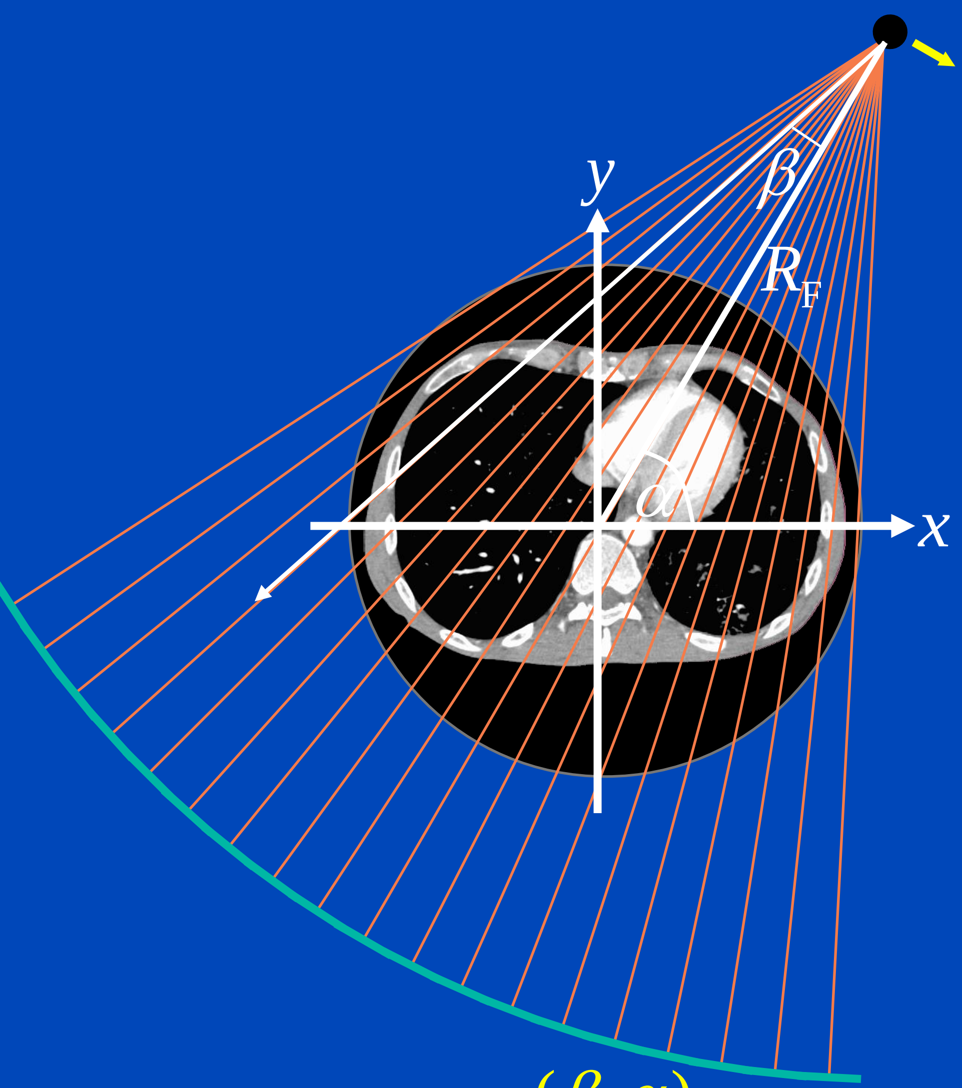

(β, α)

Parallel-beam geometry

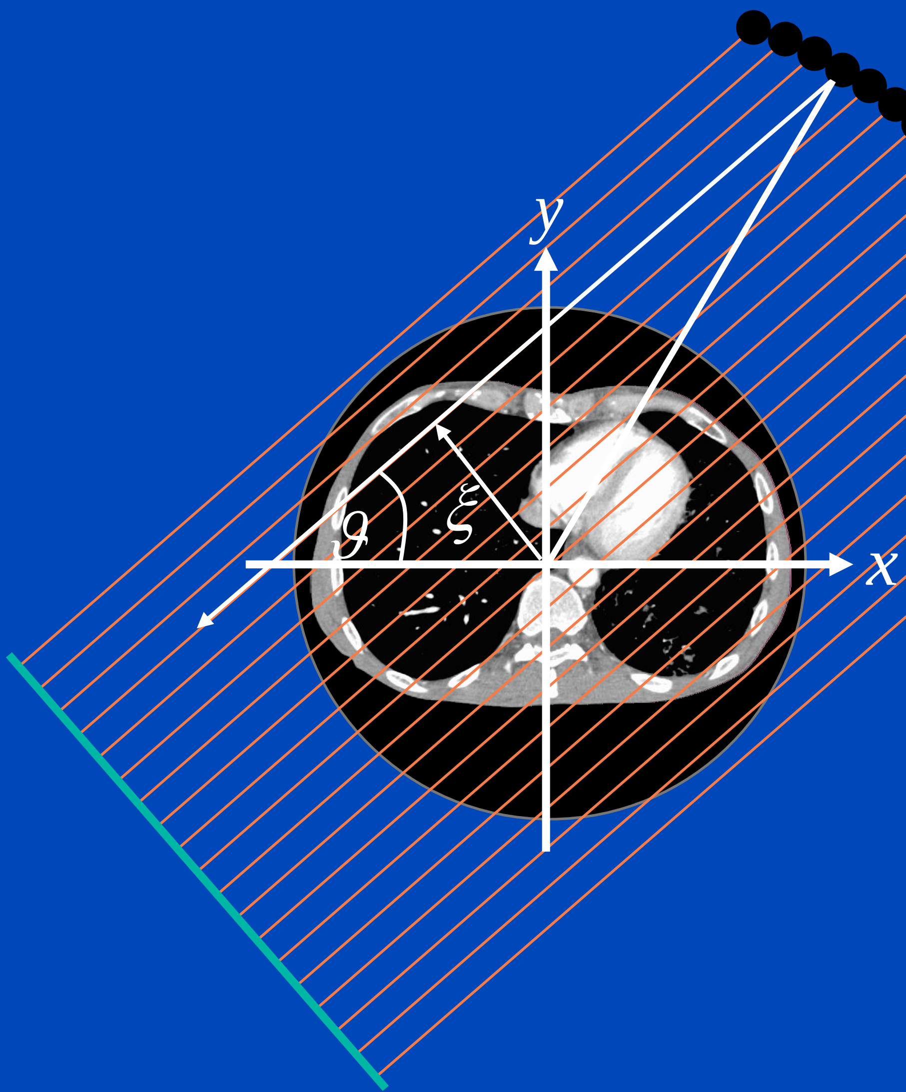

(ξ, ϑ)

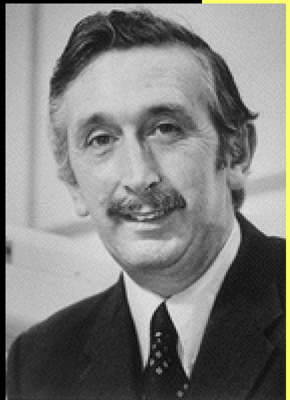

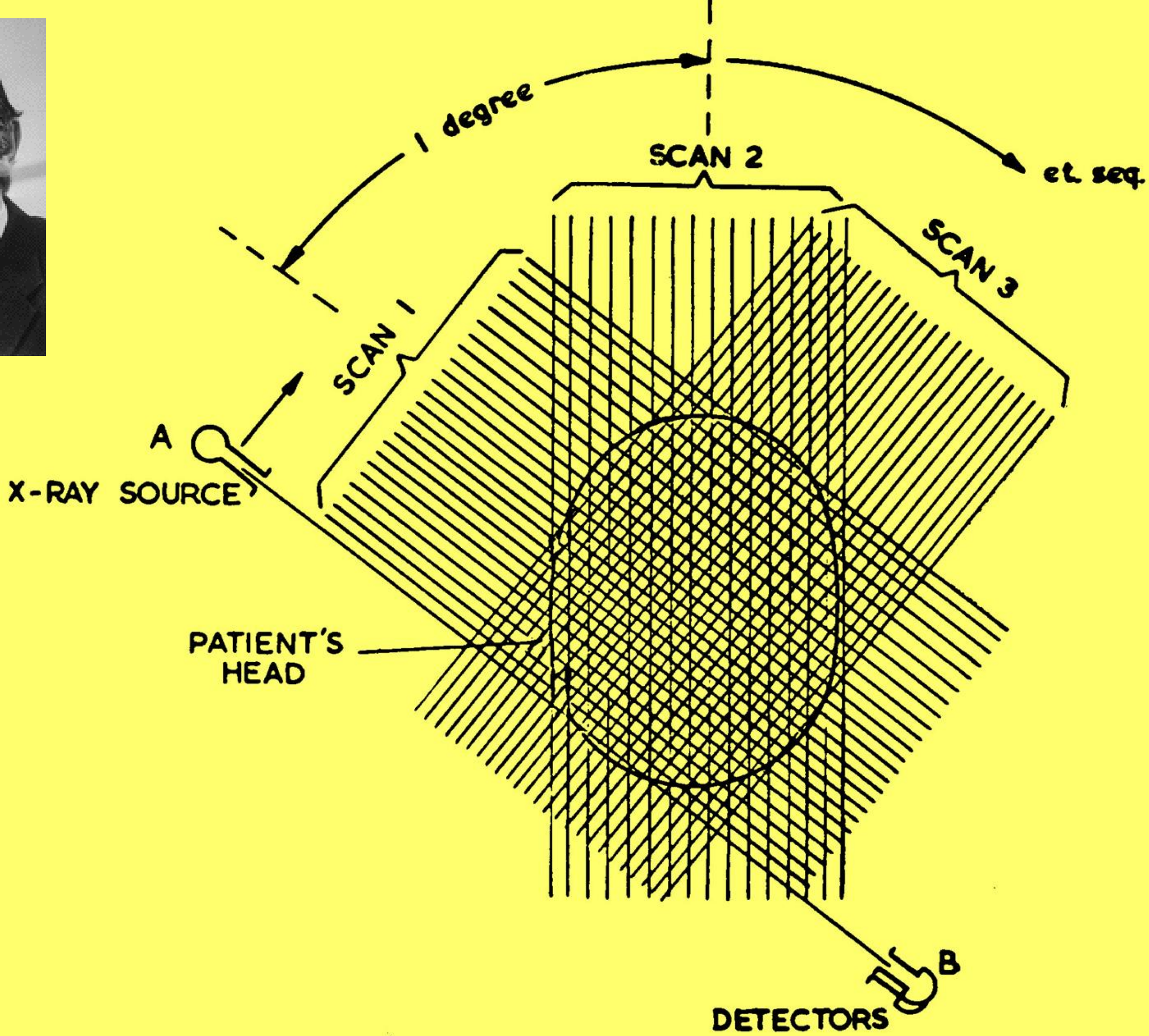

FIG. 3.
Simplified illustration of the scanning sequence.

EMI
and maybe others

Generation 1

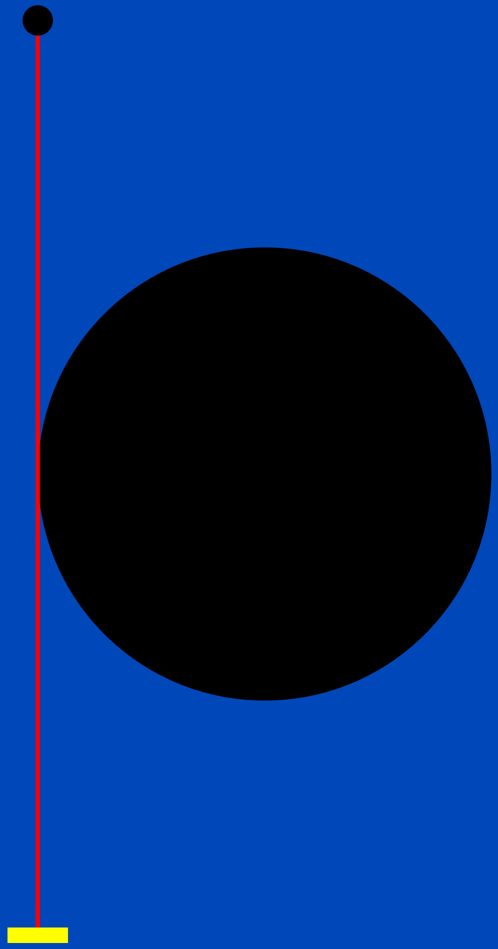

Generation 1

EMI
and maybe others

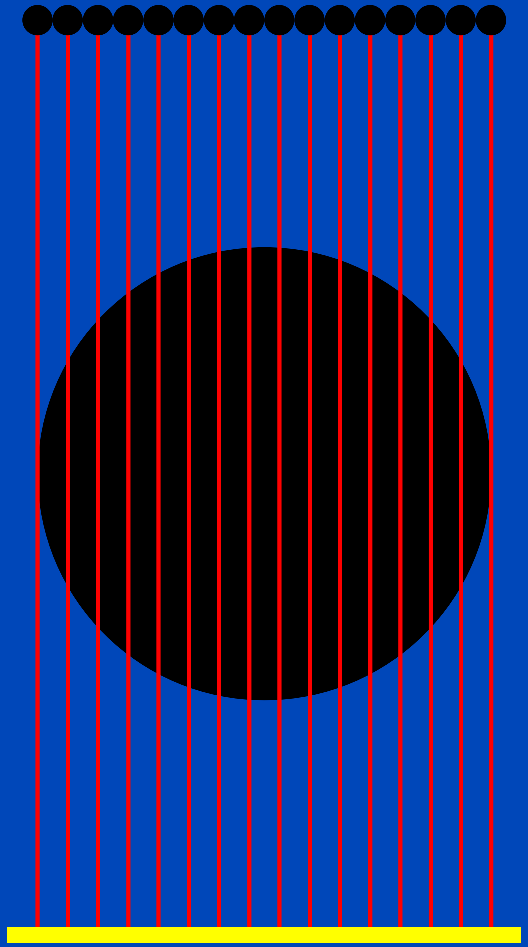

Generation 2

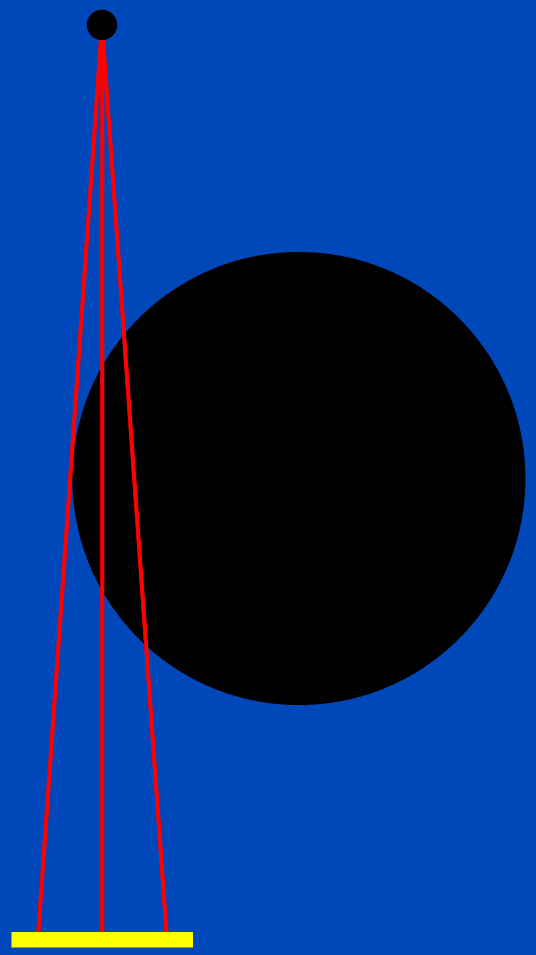

Generation 2

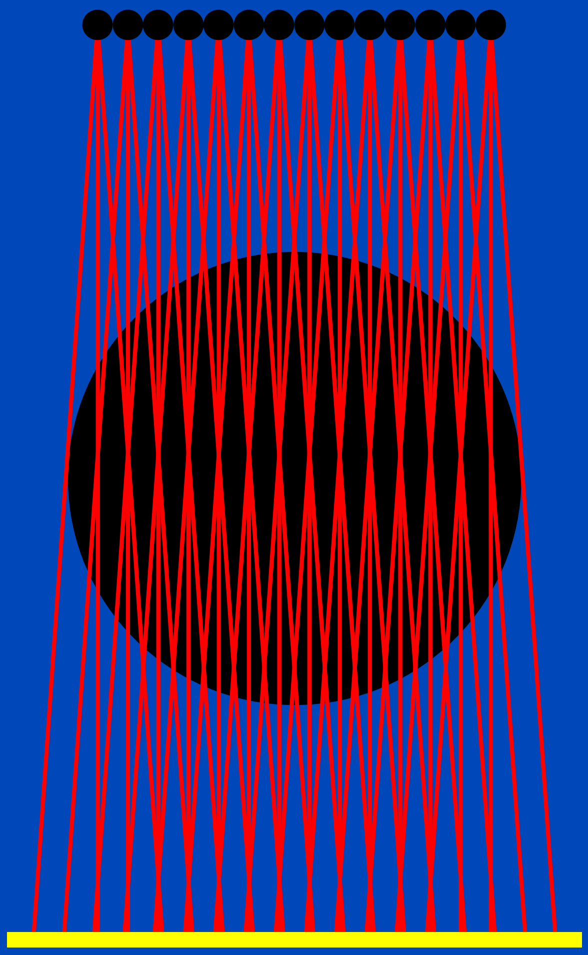

In-Plane Parallel Beam Geometry

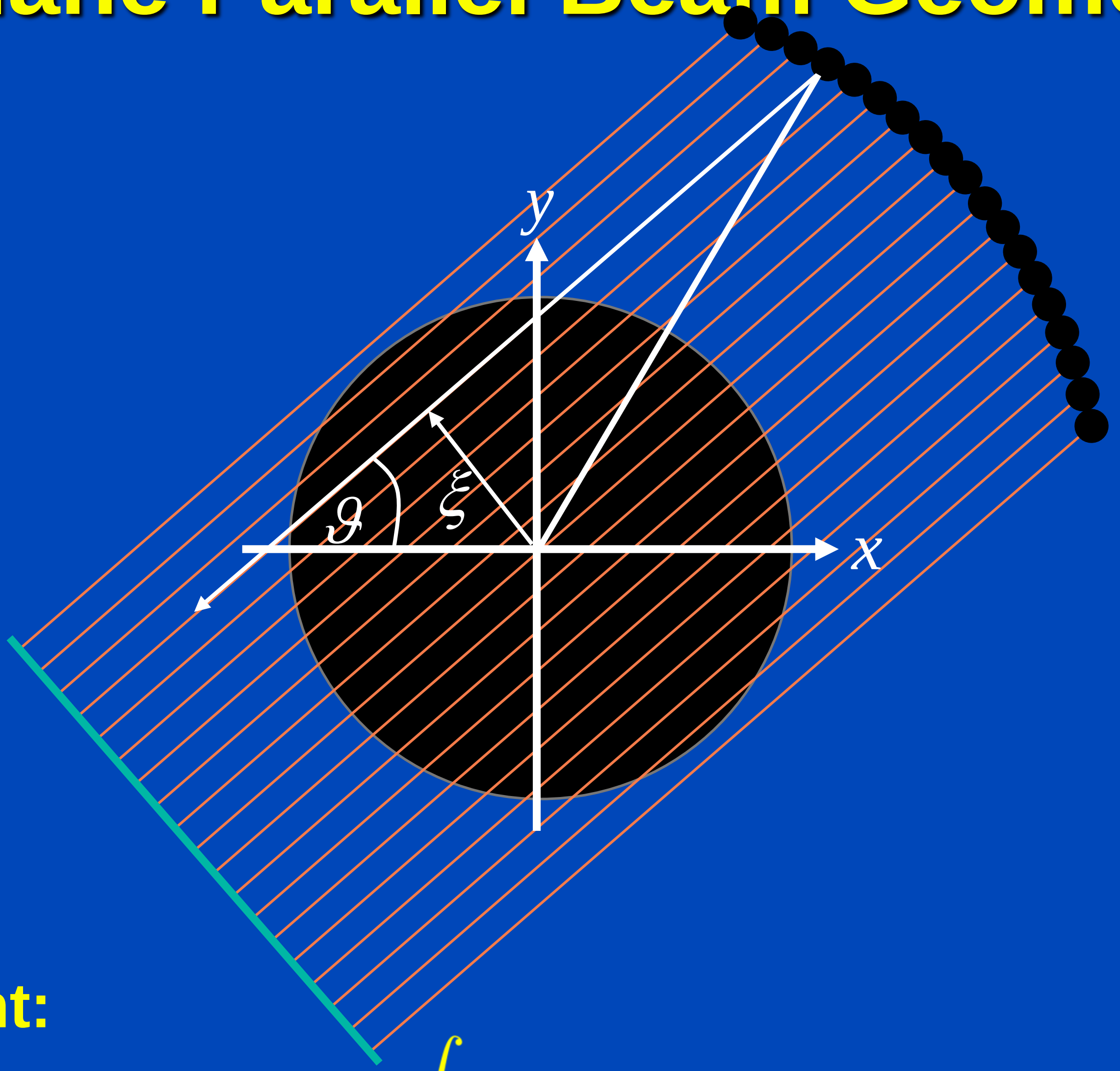

Measurement:

$$p(\vartheta,\xi) = \mathsf{R}f(\vartheta,\xi) = \int dxdy\, f(x,y)\delta(x\cos\vartheta + y\sin\vartheta - \xi)$$

Filtered Backprojection (FBP)

Measurement: $p(\vartheta,\xi) = \int dxdy\, f(x,y)\delta(x\cos\vartheta + y\sin\vartheta - \xi)$

Fourier transform:

$$\int d\xi\, p(\vartheta,\xi)e^{-2\pi i\xi u} = \int dxdy\, f(x,y)e^{-2\pi i u(x\cos\vartheta + y\sin\vartheta)}$$

This is the central slice theorem: $P(\vartheta,u) = F(u\cos\vartheta, u\sin\vartheta)$

Inversion: $f(x,y) = \int_0^\pi d\vartheta \int_{-\infty}^{\infty} du\, |u| P(\vartheta,u)e^{2\pi i u(x\cos\vartheta + y\sin\vartheta)}$

$$= \int_0^\pi d\vartheta\, p(\vartheta,\xi) * k(\xi)\Big|_{\xi = x\cos\vartheta + y\sin\vartheta}$$

Filtered Backprojection (FBP)

1. Filter projection data with the reconstruction kernel.
2. Backproject the filtered data into the image:

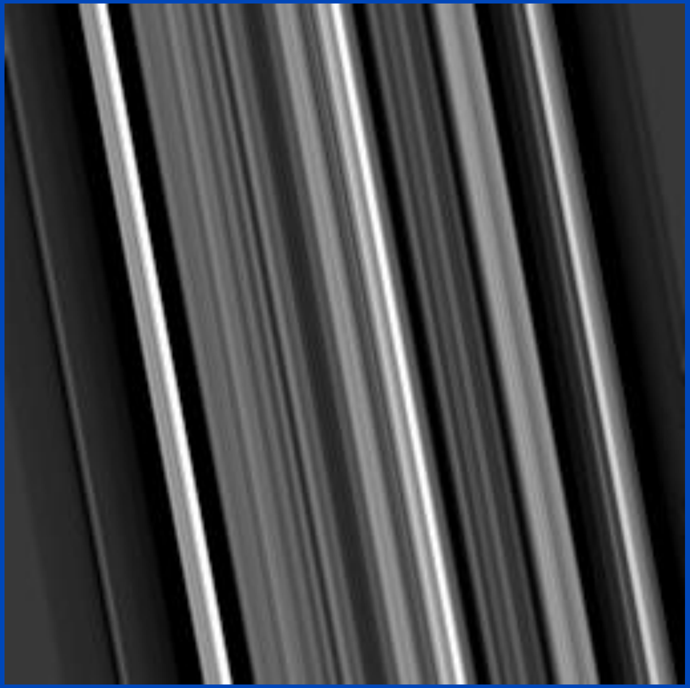

Smooth kernel (e.g. B30)

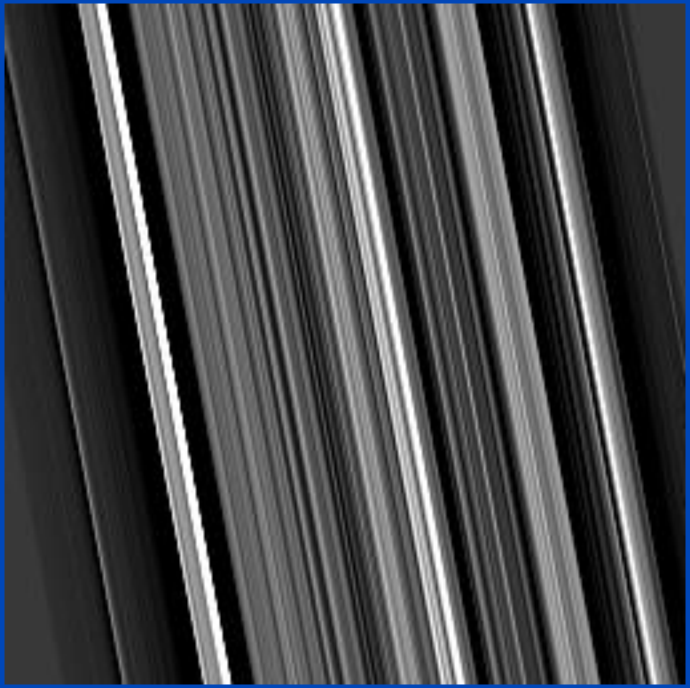

Sharp kernel (e.g. B70)

Reconstruction kernels balance between spatial resolution and image noise.

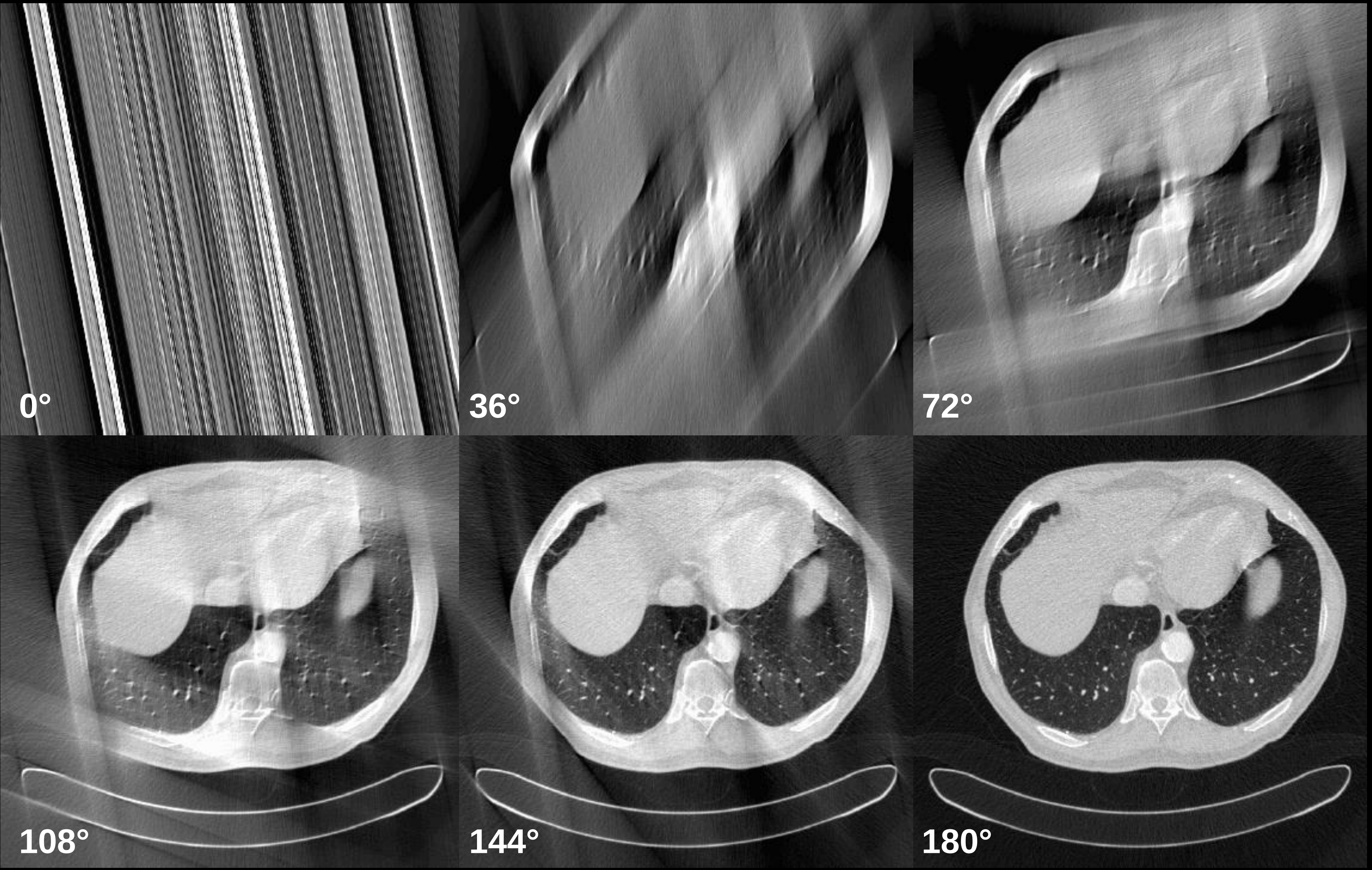
0°
36°
72°
108°
144°
180°

normalized

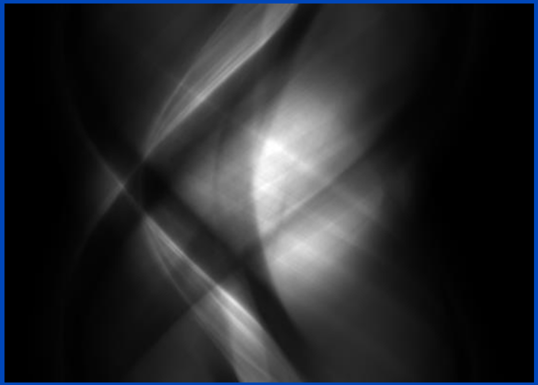

log normalized

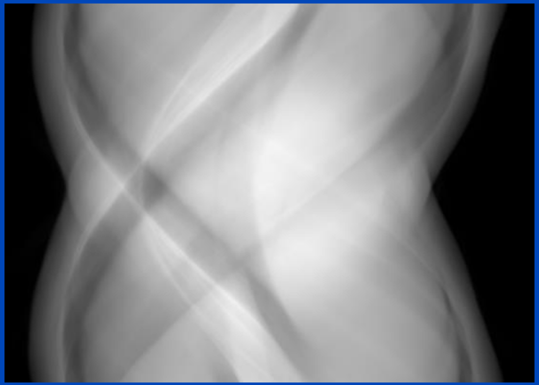

log normalized and convolved

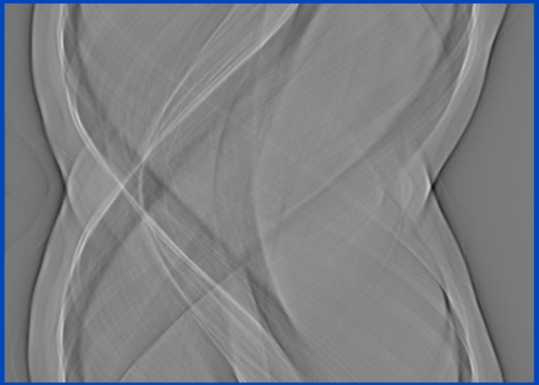

after 36°

after 72°

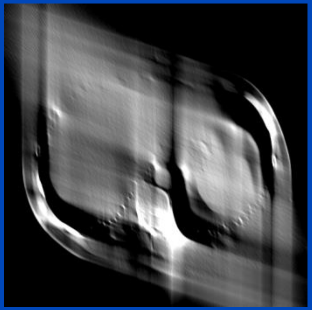

after 108°

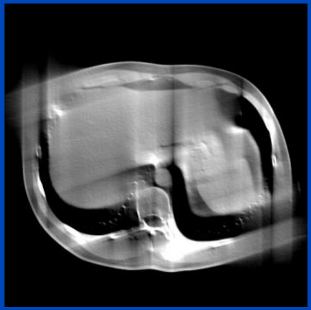

after 144°

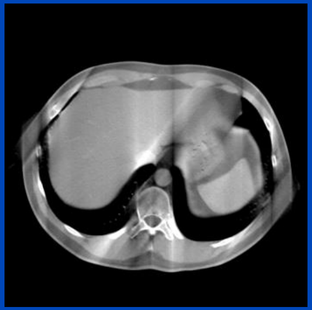

after 180°

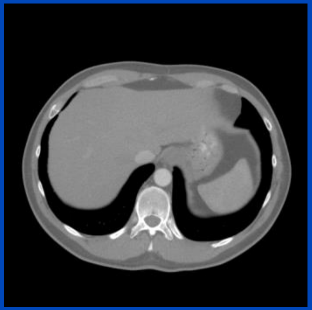

1 projection

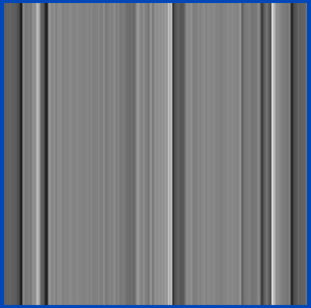

2 projections

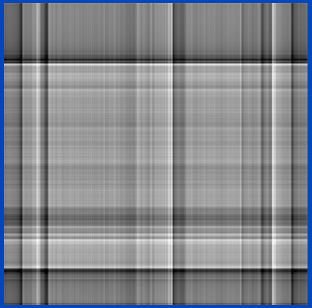

4 projections

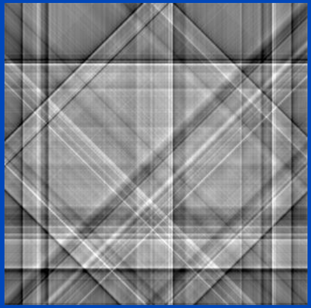

8 projections

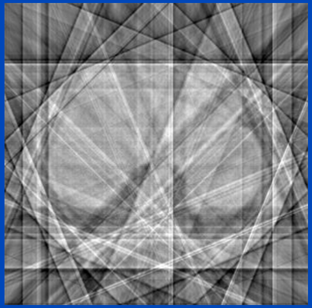

all projections

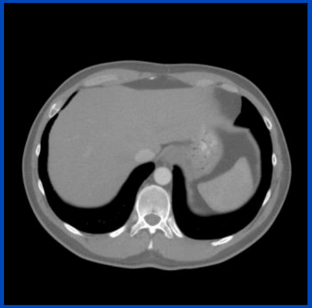

2D Fan-Beam FBP

- **Some fan-beam geometries lend themselved to filtered backprojection without rebinning[1,2].**
- **Among those geometries the geometry with equiangular sampling in β, i.e. in steps of $\Delta\beta$, is the most prominent one (although not necessarily optimal).**
- **The second most prominent geometry that allows for filtered backprojection in the native geometry is the one corresponding to a flat detector.**
- **The fourth generation CT geometry does not allow for shift-invariant filtering, unless the distance R_F of the focal spot to the isocenter equals the radius R_D of the detector ring.**

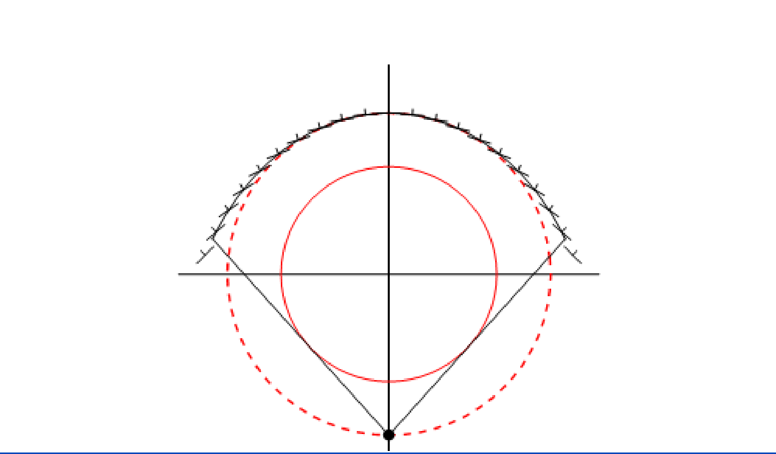

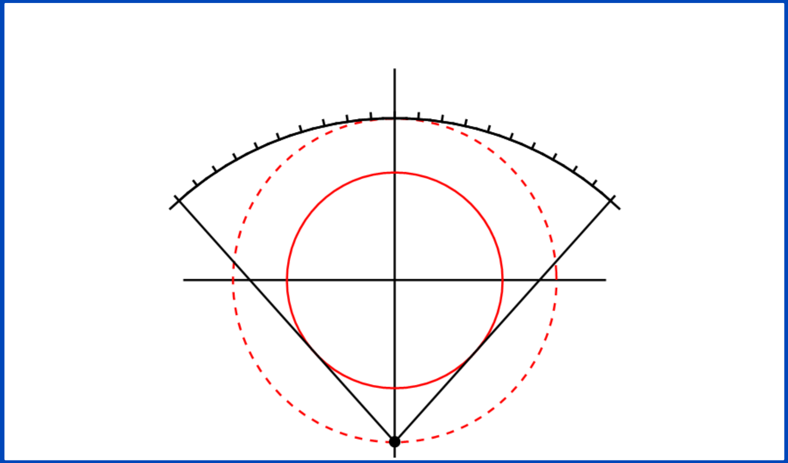

[1]Guy Besson. CT fan-beam parametrizations leading to shift-invariant filtering. Inv. Prob. 1996.
[2]Marc Kachelrieß. Interesting detector shapes for third generation CT scanners. Med. Phys. 2013.

2D Fan-Beam FBP

- **Classical way (coordinate transform):**

$$f(\boldsymbol{r}) = \tfrac{1}{2}\int_0^{2\pi} d\alpha \frac{1}{|\boldsymbol{r}-\boldsymbol{s}(\alpha)|^2} \; R_{\mathrm{F}} \cos\beta \, q(\alpha,\beta) \; * \; k(\sin\beta)\Big|_{\beta=\hat{\beta}(\alpha,\boldsymbol{r})}$$

- **Modern way[1] (inspired by Katsevich's work):**

$$f(\boldsymbol{r}) = \tfrac{1}{2}\int_0^{2\pi} d\alpha \frac{1}{|\boldsymbol{r}-\boldsymbol{s}(\alpha)|} \Big(\big(\partial_\beta - \partial_\alpha\big)\, q(\alpha,\beta)\Big) * K(\sin\beta)\Big|_{\beta=\hat{\beta}(\alpha,\boldsymbol{r})}$$

- **Parallel beam FBP for comparison:**

$$f(\boldsymbol{r}) = \tfrac{1}{2}\int_0^{2\pi} d\vartheta \, p(\vartheta,\xi) * k(\xi)\Big|_{\xi=\hat{\xi}(\vartheta,\boldsymbol{r})}$$

$$\hat{\beta}(\alpha,\boldsymbol{r}) = -\sin^{-1}\frac{x\cos\alpha + y\sin\alpha}{|\boldsymbol{r}-\boldsymbol{s}(\alpha)|}$$

$$\hat{\xi}(\vartheta,\boldsymbol{r}) = x\cos\vartheta + y\sin\vartheta$$

[1]F. Noo et al. Image reconstruction from fan-beam projections on less than a short scan. PMB 2002.

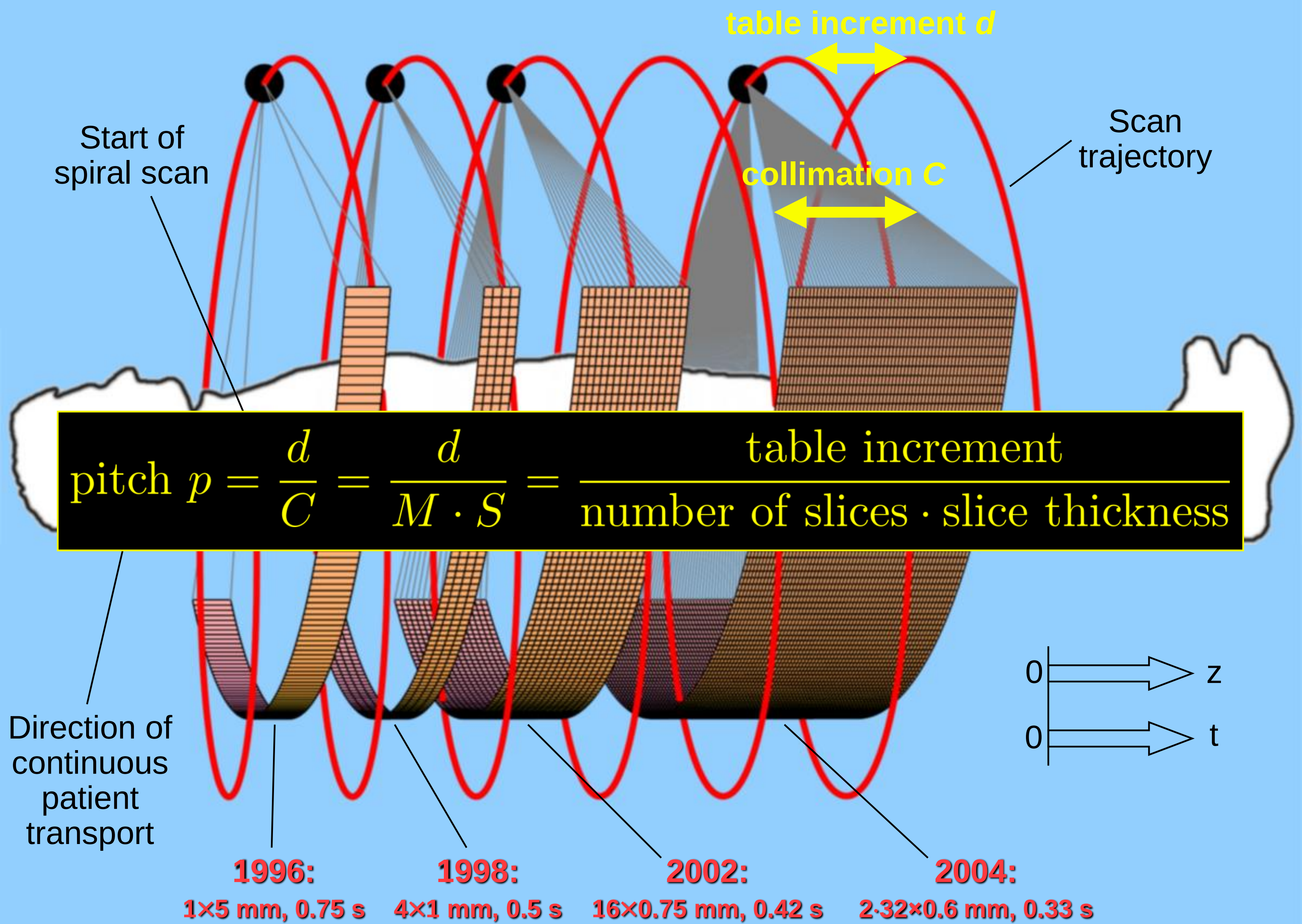

$$\text{pitch } p = \frac{d}{C} = \frac{d}{M \cdot S} = \frac{\text{table increment}}{\text{number of slices} \cdot \text{slice thickness}}$$

Kalender et al., Radiology 173(P):414 (1989) and 176:181-183 (1990)

360° LI Spiral z-Interpolation for Single-Slice CT (M=1)

$$p = \frac{d}{MS} \leq 2$$

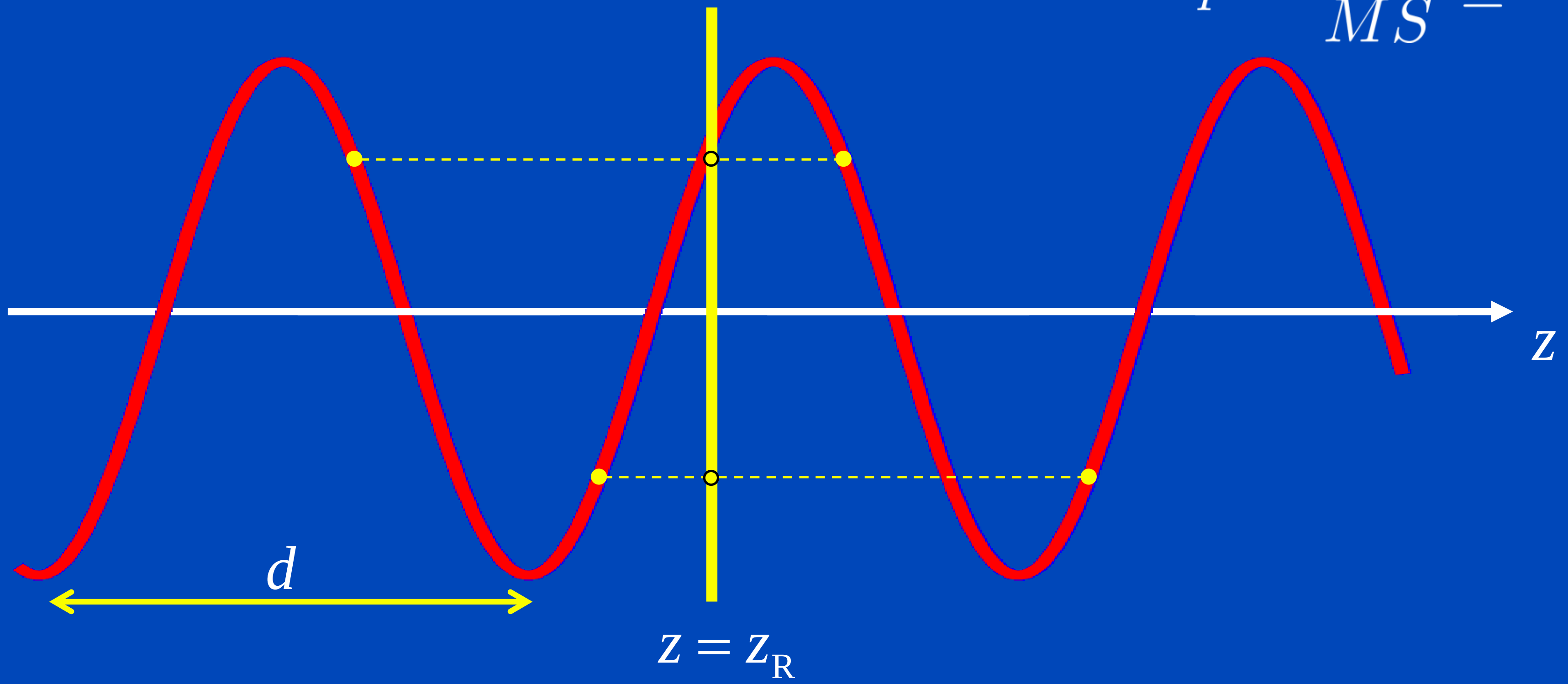

Spiral z-interpolation is typically a linear interpolation between points adjacent to the reconstruction position to obtain circular scan data.

without *z*-interpolation

with *z*-interpolation

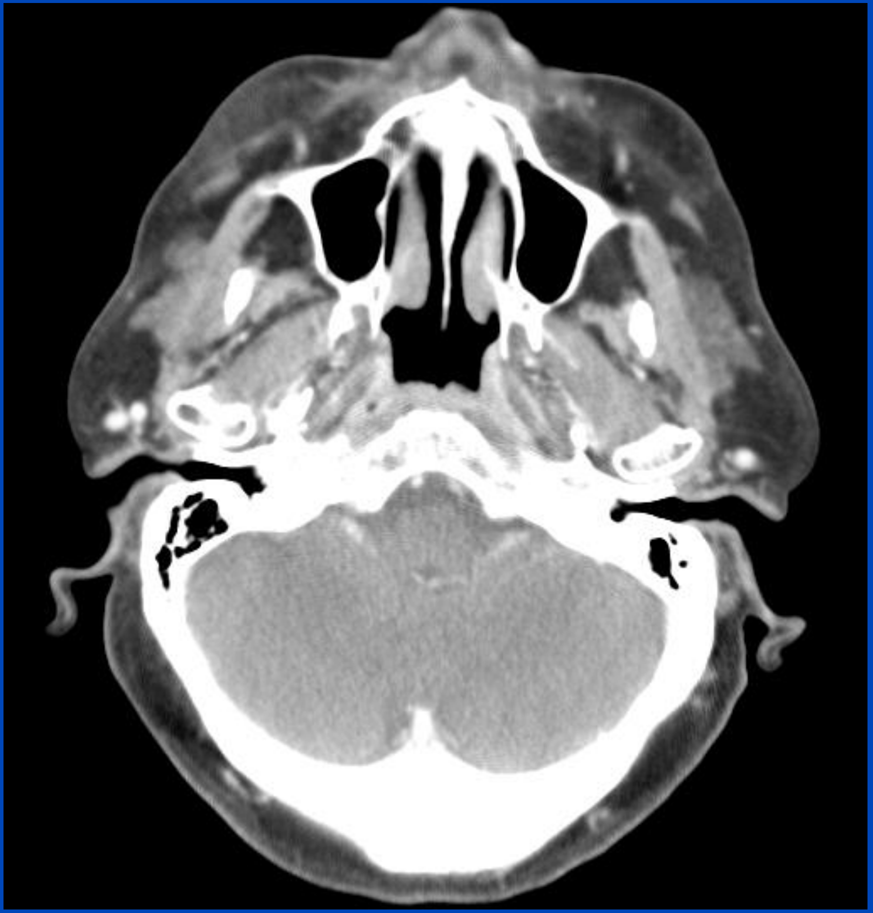

180° LI Spiral z-Interpolation for Single-Slice CT (*M*=1)

$$p = \frac{d}{MS} \le 2$$

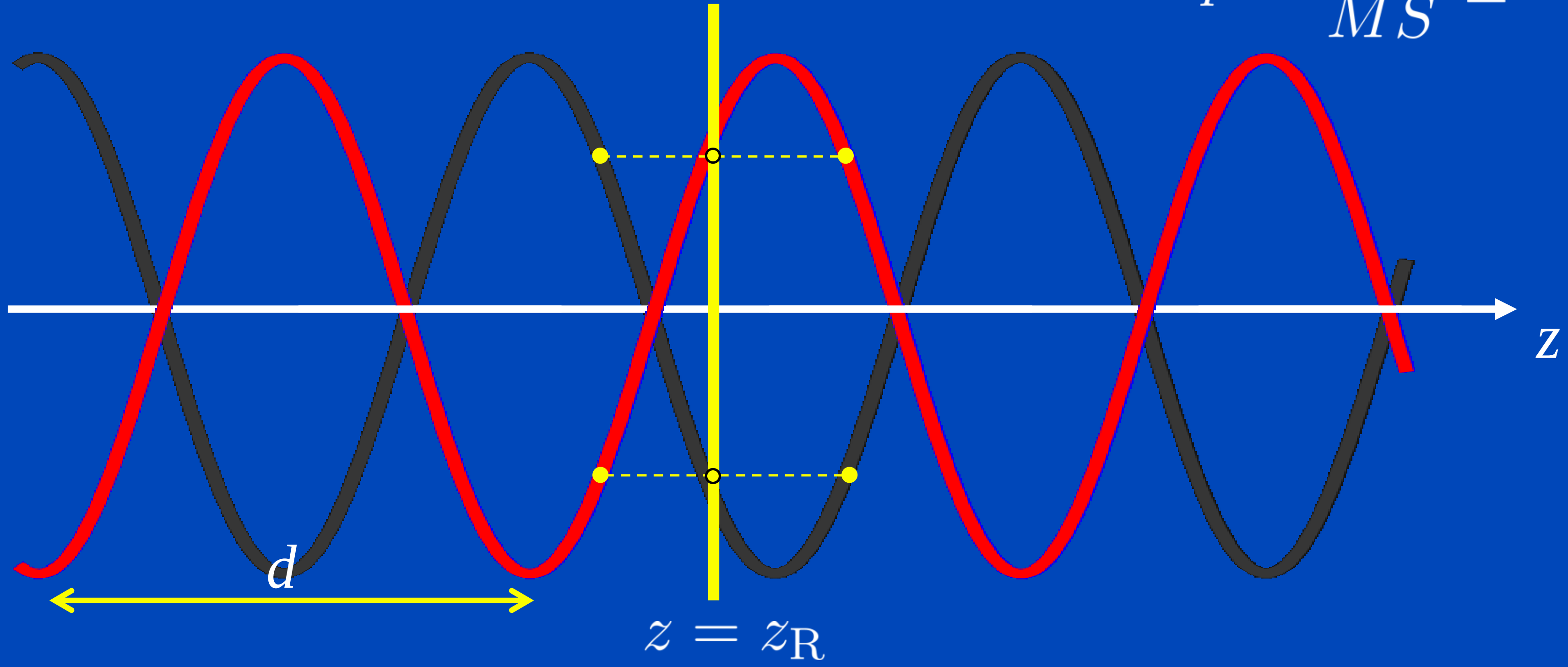

180° spiral z-interpolation interpolates between direct and complementary rays.

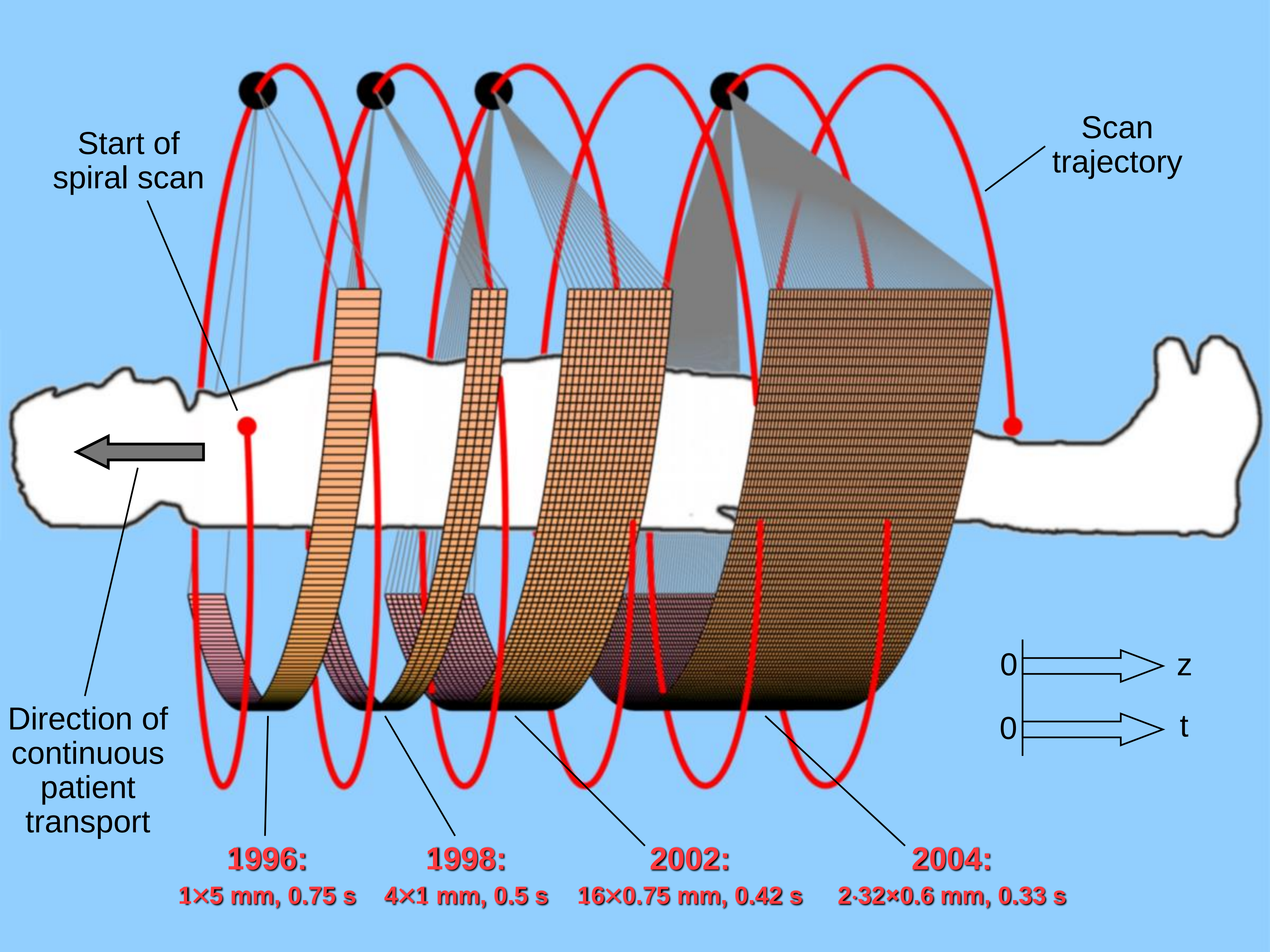

Start of spiral scan
Scan trajectory
Direction of continuous patient transport
0
z
0
t
1996:
1×5 mm, 0.75 s
1998:
4×1 mm, 0.5 s
2002:
16×0.75 mm, 0.42 s
2004:
2·32×0.6 mm, 0.33 s

Spiral z-Filtering for Multi-Slice CT
M=2, …, 6

$$p = \frac{d}{MS} \leq 1.5$$

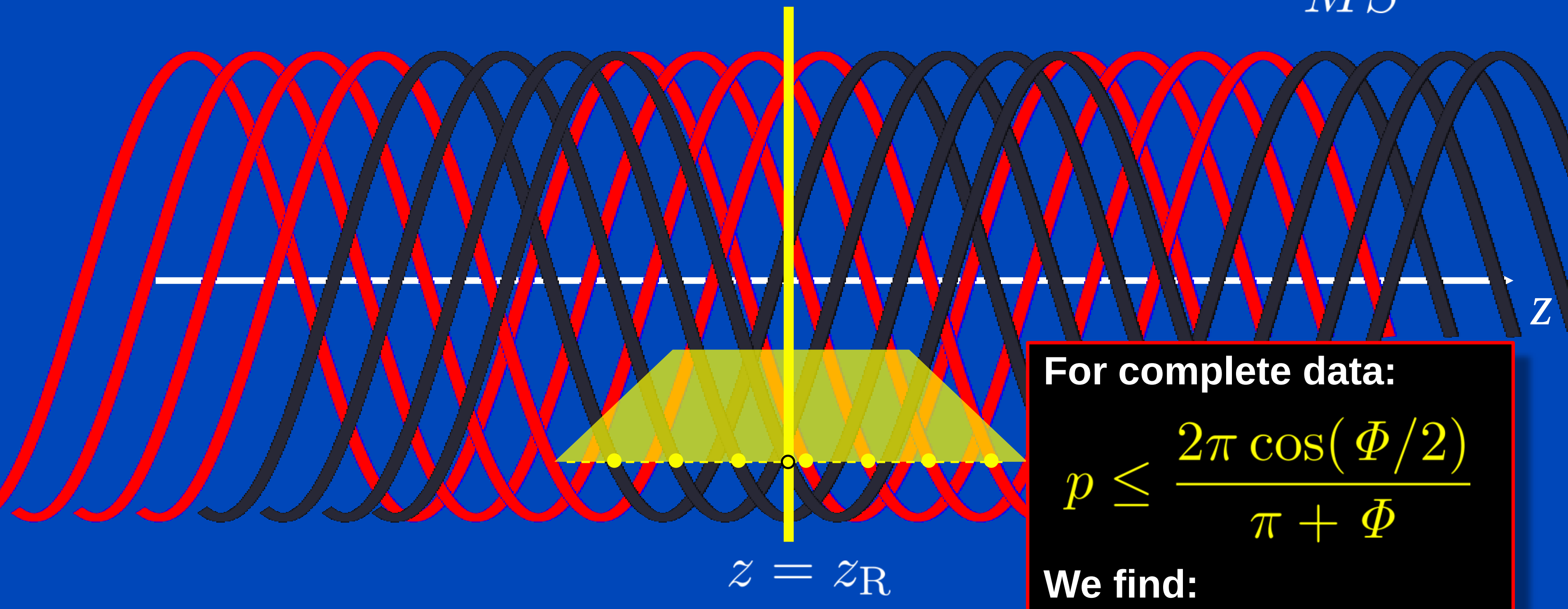

For complete data:

$$p \leq \frac{2\pi \cos(\Phi/2)}{\pi + \Phi}$$

We find:
$p \leq 1.4$ for 52° fan angle
$p \leq 1.5$ for 43° fan angle

Spiral z-filtering is collecting data points weig
trapezoidal distance weight to obtain circular scan data.

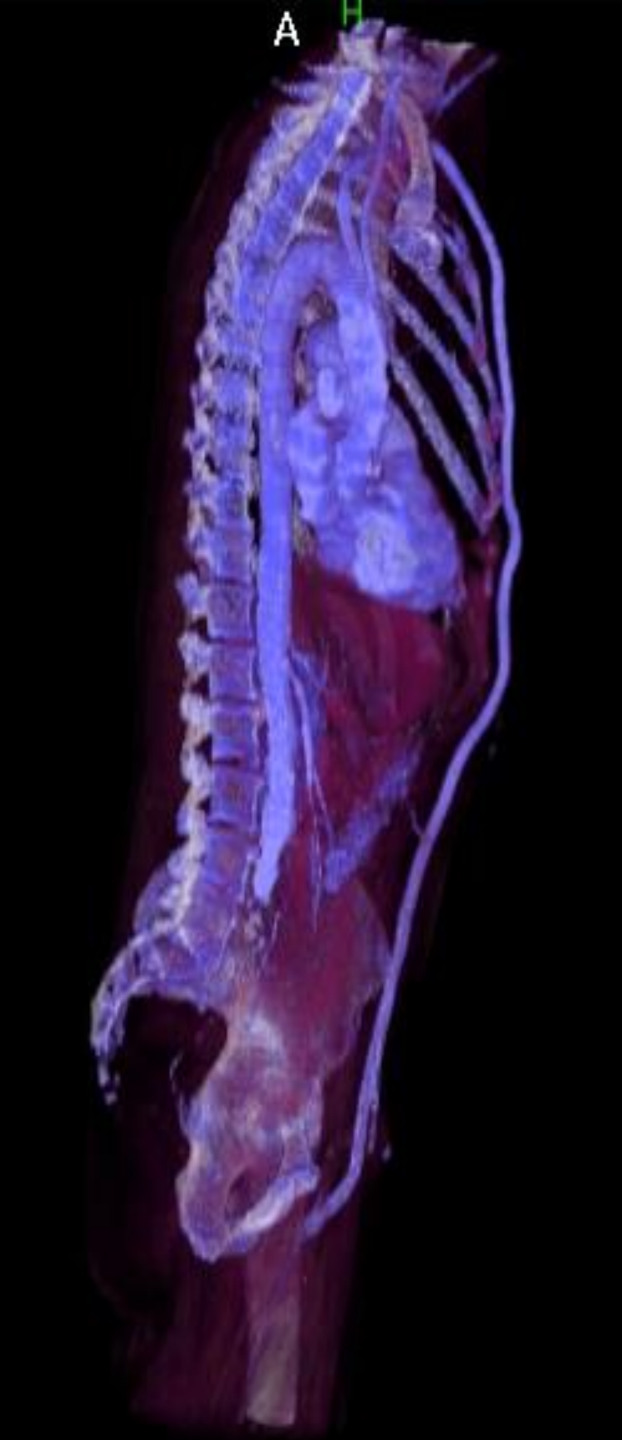

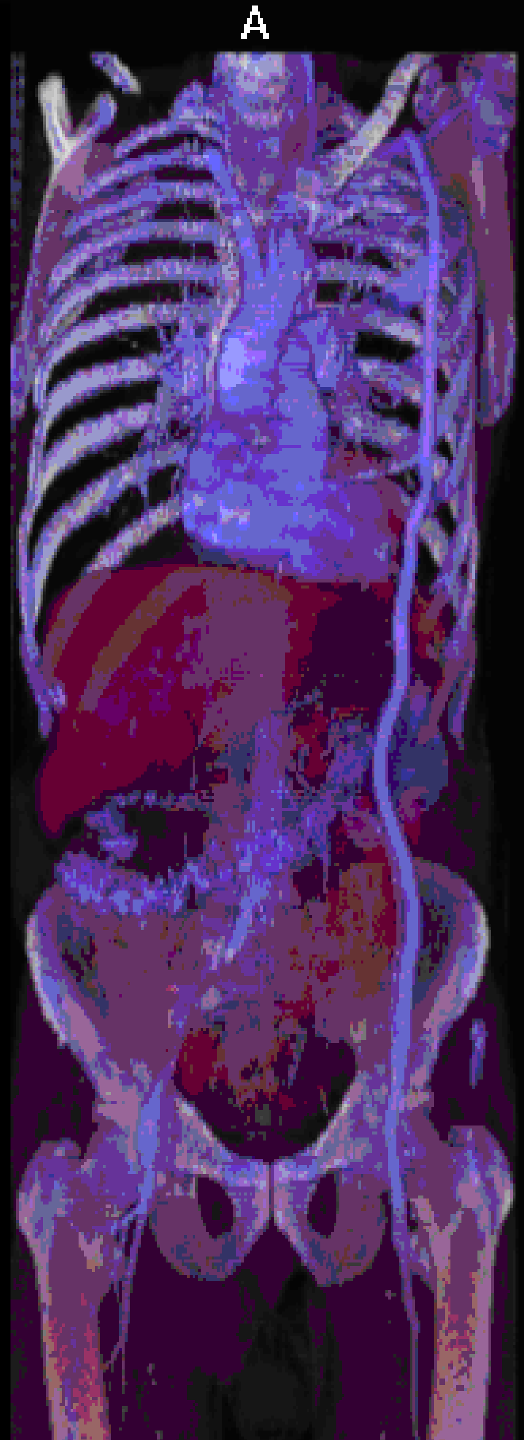

CT Angiography: Axillo-femoral bypass

***M* = 4**

120 cm in 40 s

0.5 s per rotation
4×2.5 mm collimation
pitch 1.5

RSNA 1989
SSCT (*M* = 1)

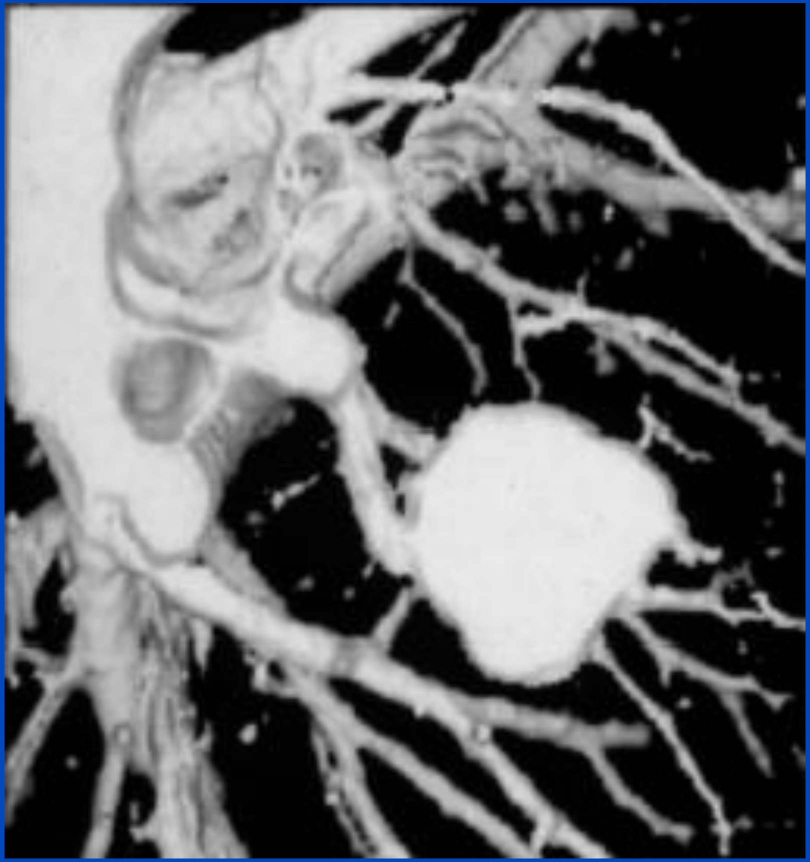

RSNA 2001
MSCT (*M* = 16)

The Cone-Beam Problem

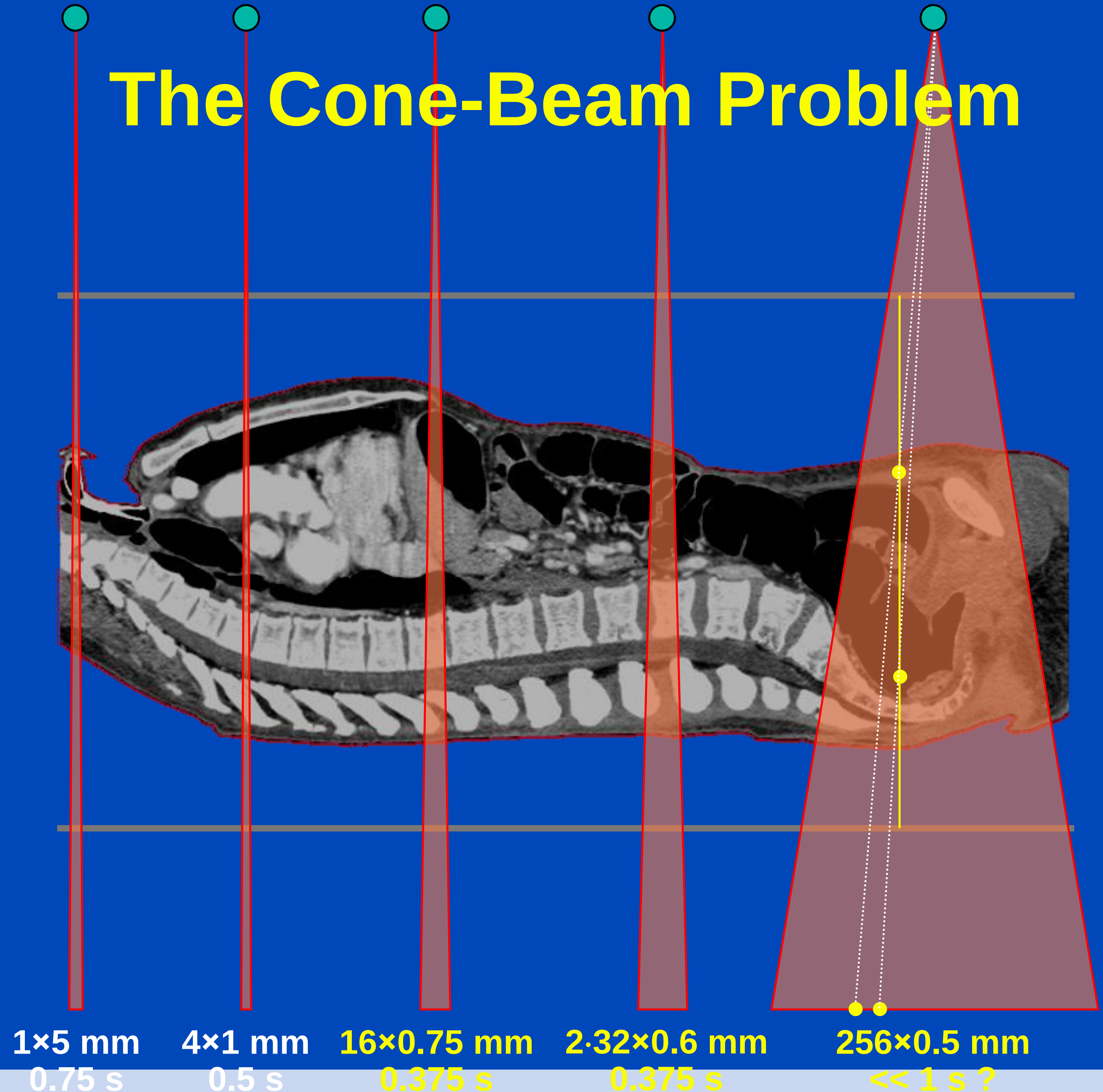

Advanced single-slice rebinning in cone-beam spiral CT

Marc Kachelrieß[a)]
Institute of Medical Physics, University of Erlangen–Nürnberg, Germany

Stefan Schaller
Siemens AG, Medical Engineering Group, Forchheim, Germany

Willi A. Kalender
Institute of Medical Physics, University of Erlangen–Nürnberg, Germany

(Received 11 August 1999; accepted for publication 12 January 2000)

To achieve higher volume coverage at improved z-resolution in computed tomography (CT), systems with a large number of detector rows are demanded. However, handling an increased number of detector rows, as compared to today's four-slice scanners, requires to accounting for the cone geometry of the beams. Many so-called cone-beam reconstruction algorithms have been proposed during the last decade. None met all the requirements of the medical spiral cone-beam CT in regard to the need for high image quality, low patient dose and low reconstruction times. We therefore propose an approximate cone-beam algorithm which uses virtual reconstruction planes tilted to optimally fit 180° spiral segments, i.e., the advanced single-slice rebinning (ASSR) algorithm. Our algorithm is a modification of the single-slice rebinning algorithm proposed by Noo *et al.* [Phys. Med. Biol. **44**, 561–570 (1999)] since we use tilted reconstruction slices instead of transaxial slices to approximate the spiral path. Theoretical considerations as well as the reconstruction of simulated phantom data in comparison to the gold standard 180°LI (single-slice spiral CT) were carried out. Image artifacts, z-resolution as well as noise levels were evaluated for all simulated scanners. Even for a high number of detector rows the artifact level in the reconstructed images remains comparable to that of 180°LI. Multiplanar reformations of the Defrise phantom show none of the typical cone-beam artifacts usually appearing when going to larger cone angles. Image noise as well as the shape of the respective slice sensitivity profiles are equivalent to the single-slice spiral reconstruction, z-resolution is slightly decreased. The ASSR has the potential to become a practical tool for medical spiral cone-beam CT. Its computational complexity lies in the order of standard single-slice CT and it allows to use available 2D backprojection hardware. [S0094-2405(00)00804-X]

Key words: computed tomography (CT), spiral CT, multi-slice CT, cone-beam detector systems, 3D reconstruction

The ASSR Algorithm

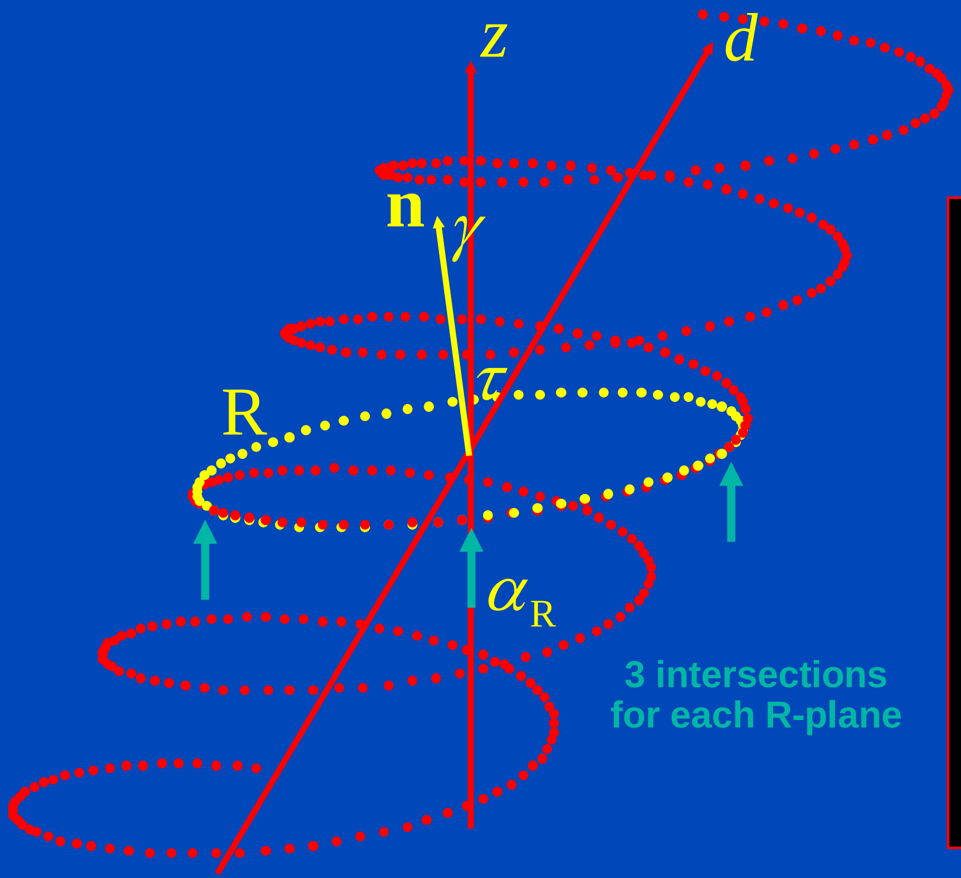

$$p = \frac{d}{MS} \leq 1.5$$

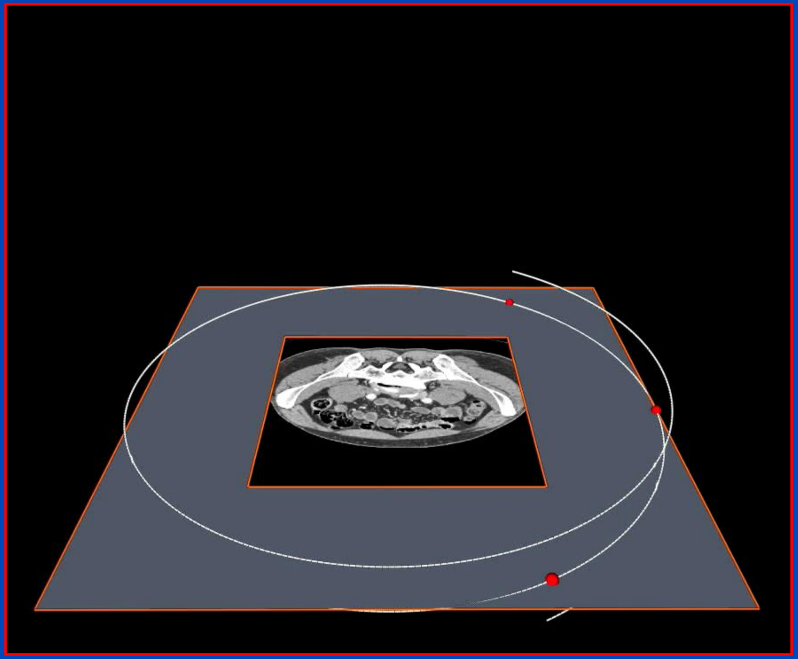

Mean deviation at distance R_M:	$\Delta \approx 0.007 \cdot d$
at distance R_F:	$\Delta \approx 0.014 \cdot d$

Comparison to Other Approximate Algorithms

180°LI d=1.5mm | Π d=64mm | MFR d=64mm | ASSR d=64mm

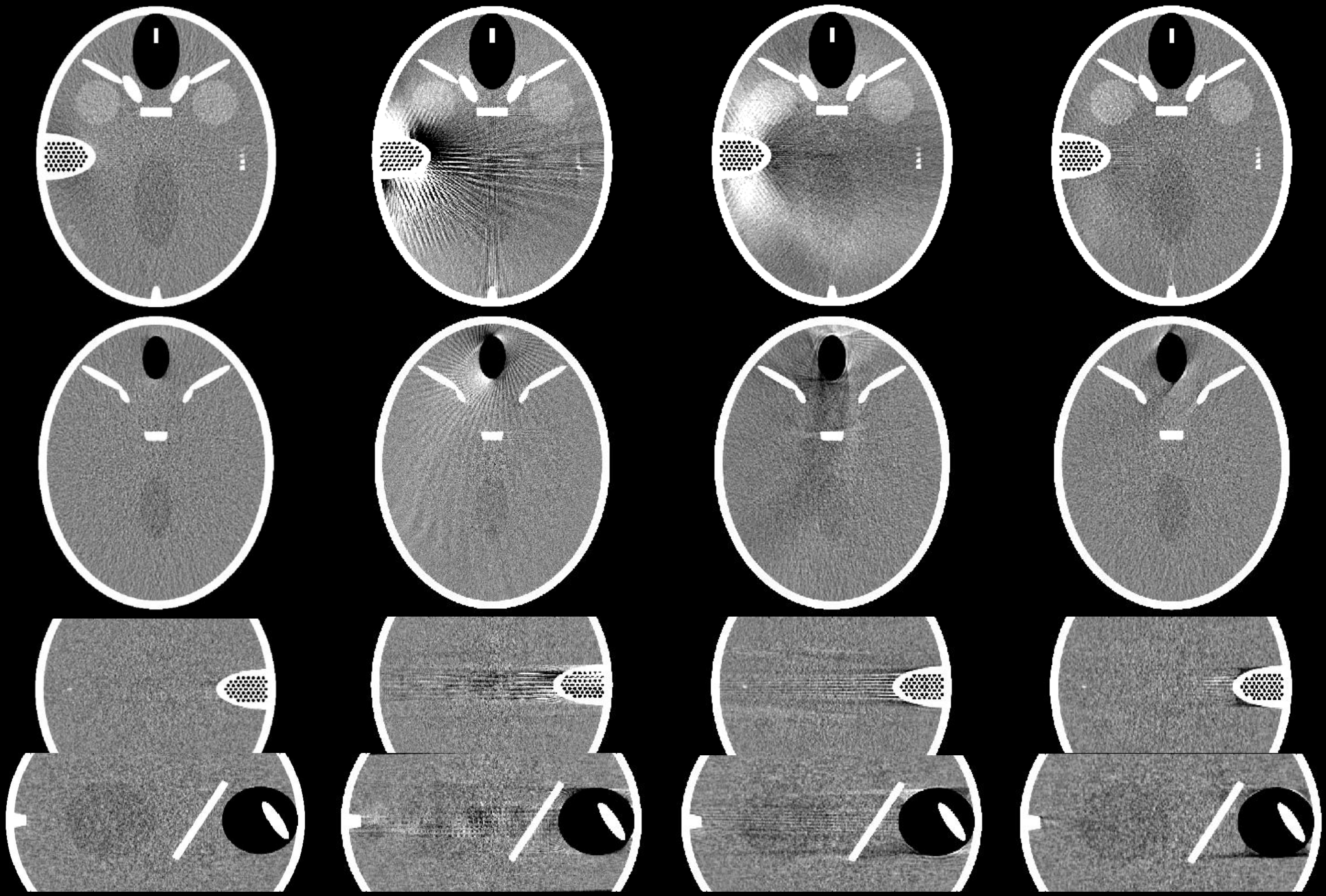

H. Bruder, M. Kachelrieß, S. Schaller. SPIE Med. Imag. Conf. Proc., 3979, 2000

Patient Images with ASSR

- High image quality
- High performance
- Use of available 2D reconstruction hardware
- 100% detector usage
- Arbitrary pitch

- Sensation 16
- 0.5 s rotation
- 16×0.75 mm collimation
- pitch 1.0
- 70 cm in 29 s
- 1.4 GB rawdata
- 1400 images

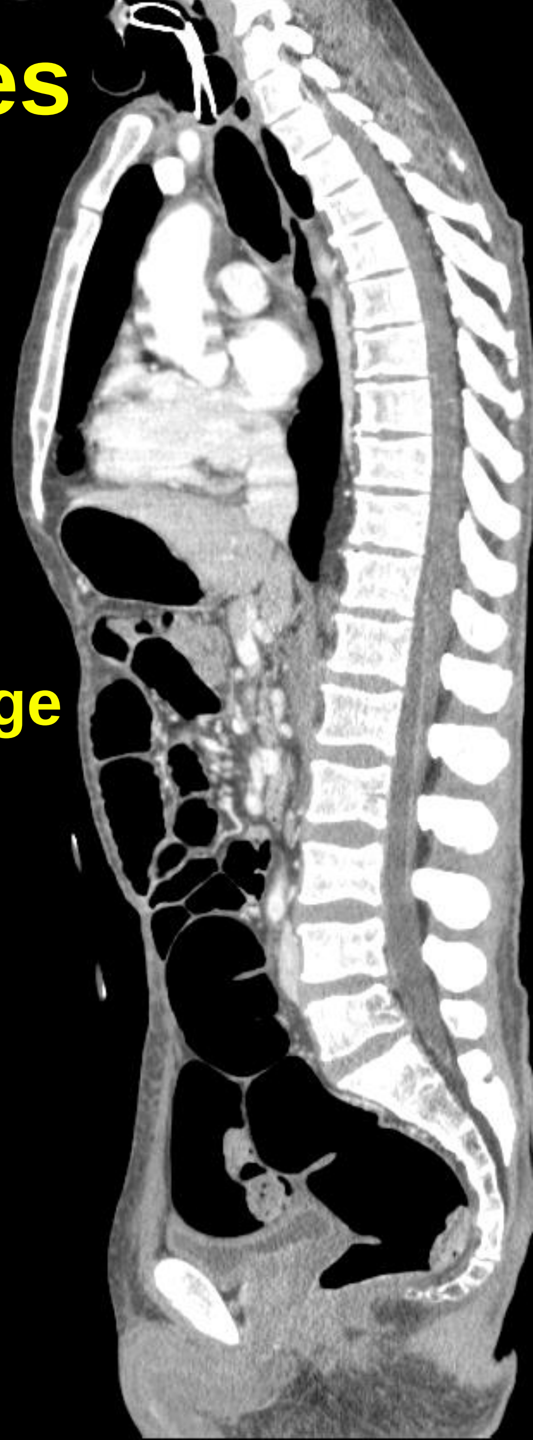

CTA, Sensation 16

Data courtesy of Dr. Michael Lell, Erlangen, Germany

Feldkamp-Type Reconstruction

- **Approximate**
- **Similar to 2D reconstruction:**
  - row-wise filtering of the rawdata
  - followed by backprojection
- **True 3D volumetric backprojection along the original ray direction**
- **Compared to ASSR:**
  - larger cone-angles possible
  - lower reconstruction speed
  - requires 3D backprojection hardware

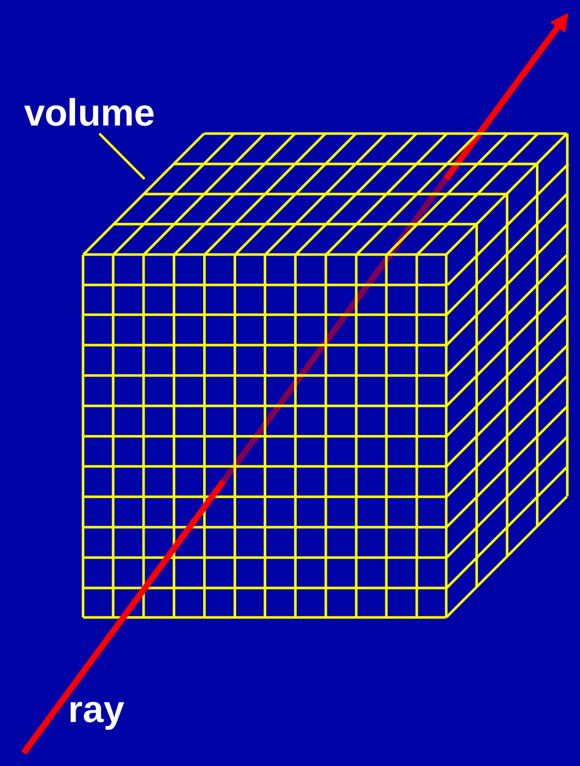

3D backprojection

Perspective Geometry

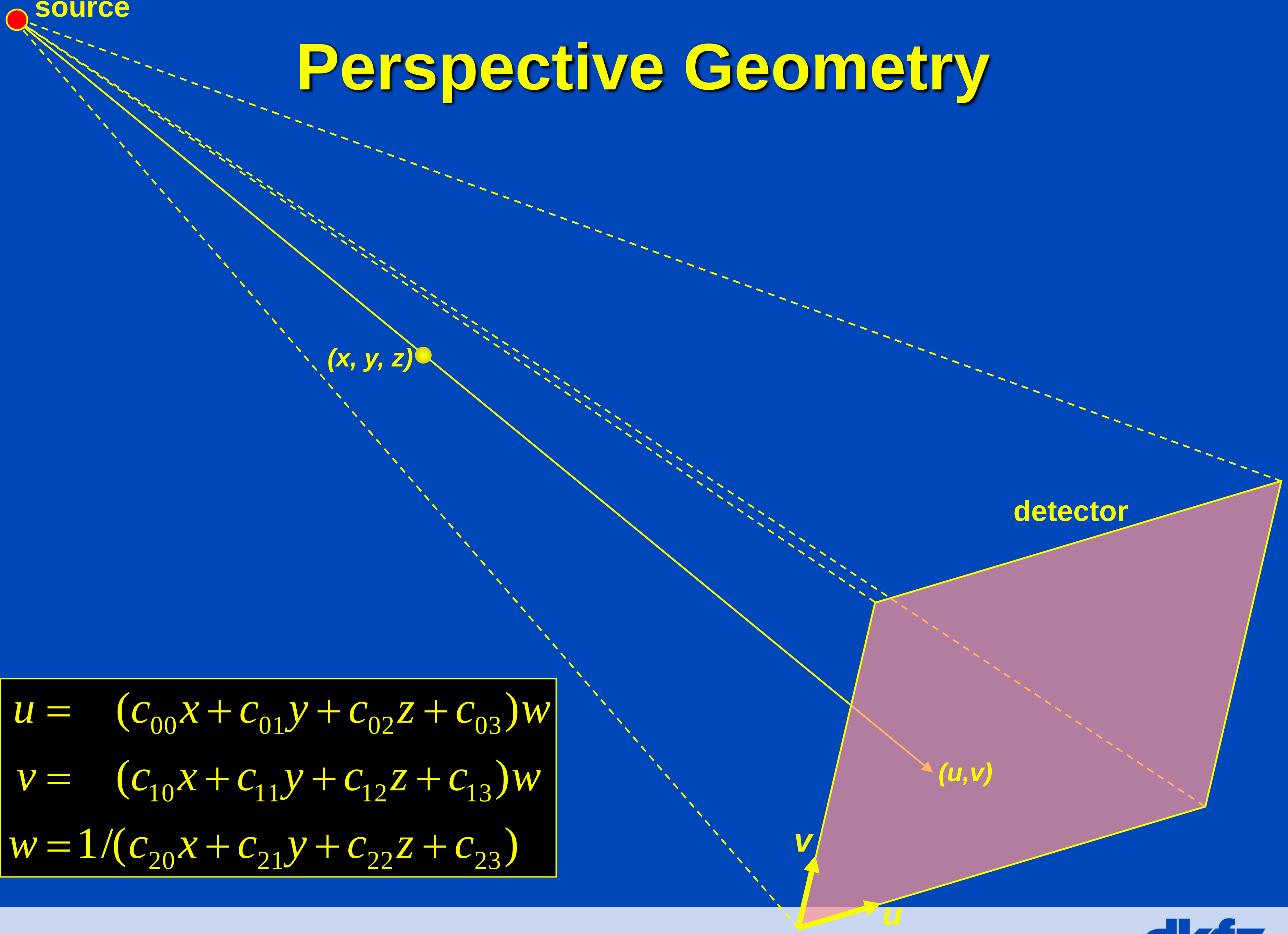

$$u = (c_{00}x + c_{01}y + c_{02}z + c_{03})w$$
$$v = (c_{10}x + c_{11}y + c_{12}z + c_{13})w$$
$$w = 1/(c_{20}x + c_{21}y + c_{22}z + c_{23})$$

Perspective Backprojection: Geometry

voxel position

projection data

$$f(\mathbf{r}) = \int d\alpha \, w^2(\alpha, \mathbf{r}) \, p(\alpha, u(\alpha, \mathbf{r}), v(\alpha, \mathbf{r}))$$

reconstructed volume

distance weight

$$u(\alpha, \mathbf{r}) = \quad (c_{00}x + c_{01}y + c_{02}z + c_{03}) w(\alpha, \mathbf{r})$$

$$v(\alpha, \mathbf{r}) = \quad (c_{10}x + c_{11}y + c_{12}z + c_{13}) w(\alpha, \mathbf{r})$$

$$w(\alpha, \mathbf{r}) = 1/(c_{20}x + c_{21}y + c_{22}z + c_{23})$$

$$c_{ij} = c_{ij}(\alpha)$$

trajectory parameter

transform coefficients

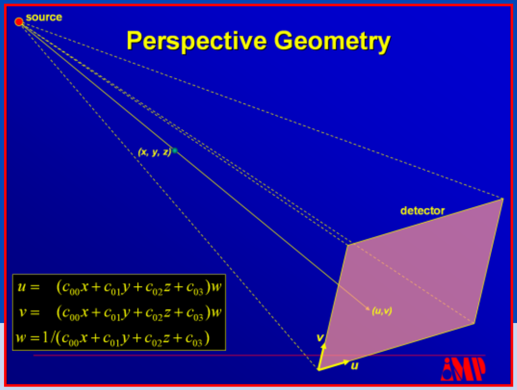

Extended Parallel Backprojection (EPBP)

3D and 4D Feldkamp-Type Image Reconstruction for Large Cone Angles

- Trajectories: circle, sequence, spiral
- Scan modes: standard, phase-correlated
- Rebinning: azimuthal + longitudinal + radial
- Feldkamp-type: convolution + true 3D backprojection
- 100% detector usage
- Fast and efficient

Kachelrieß et al., Med. Phys. 31(6), June 2004

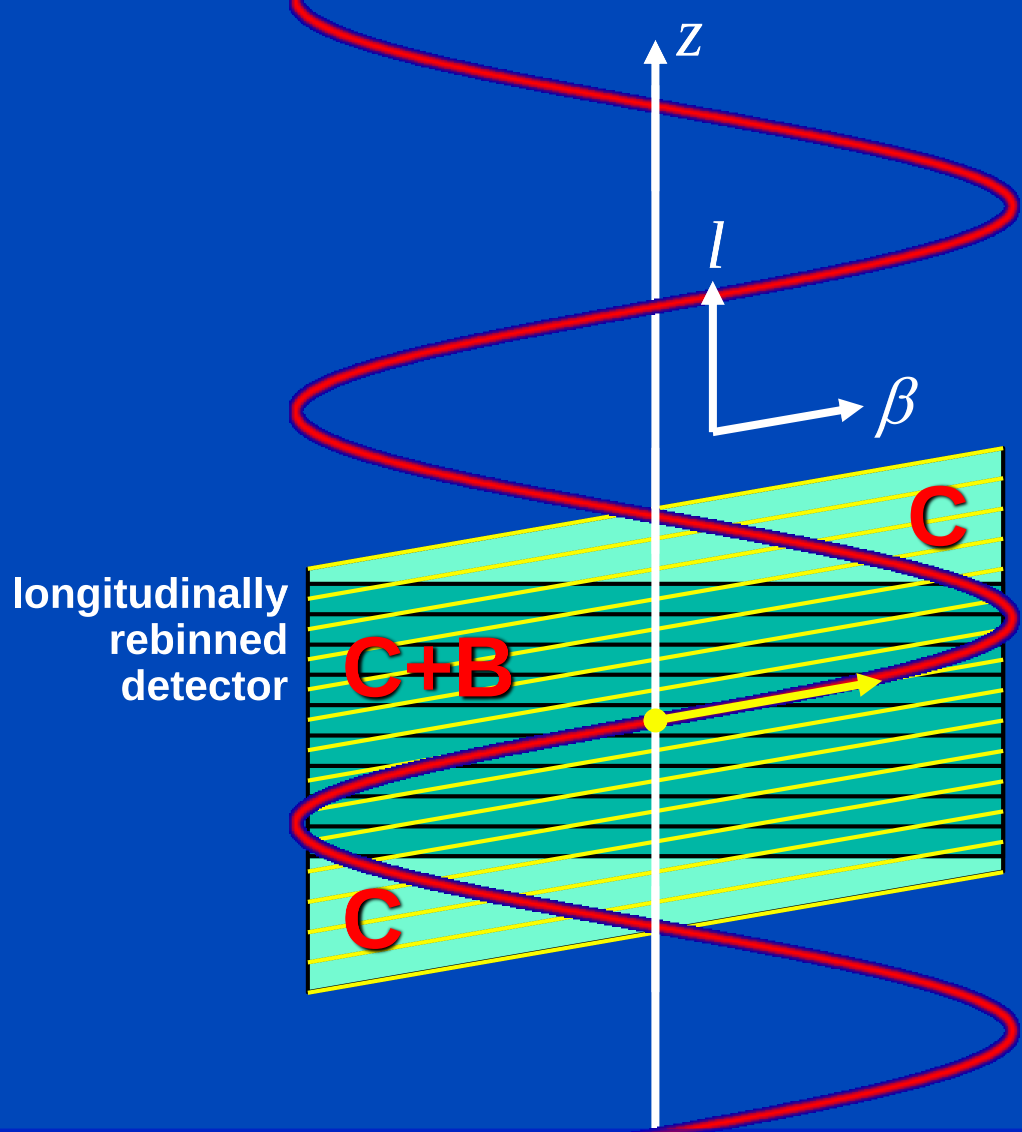

$$p = \frac{d}{MS} \leq 1.5$$

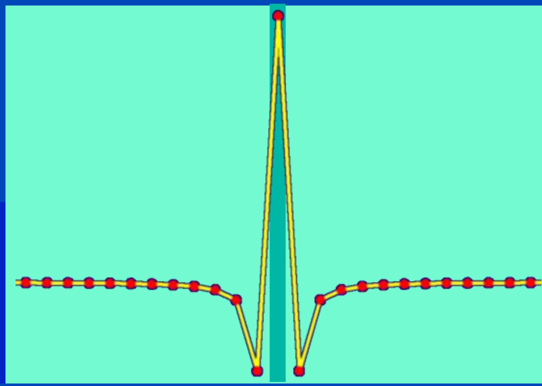

C: Area used for convolution
B: Area used for backprojection

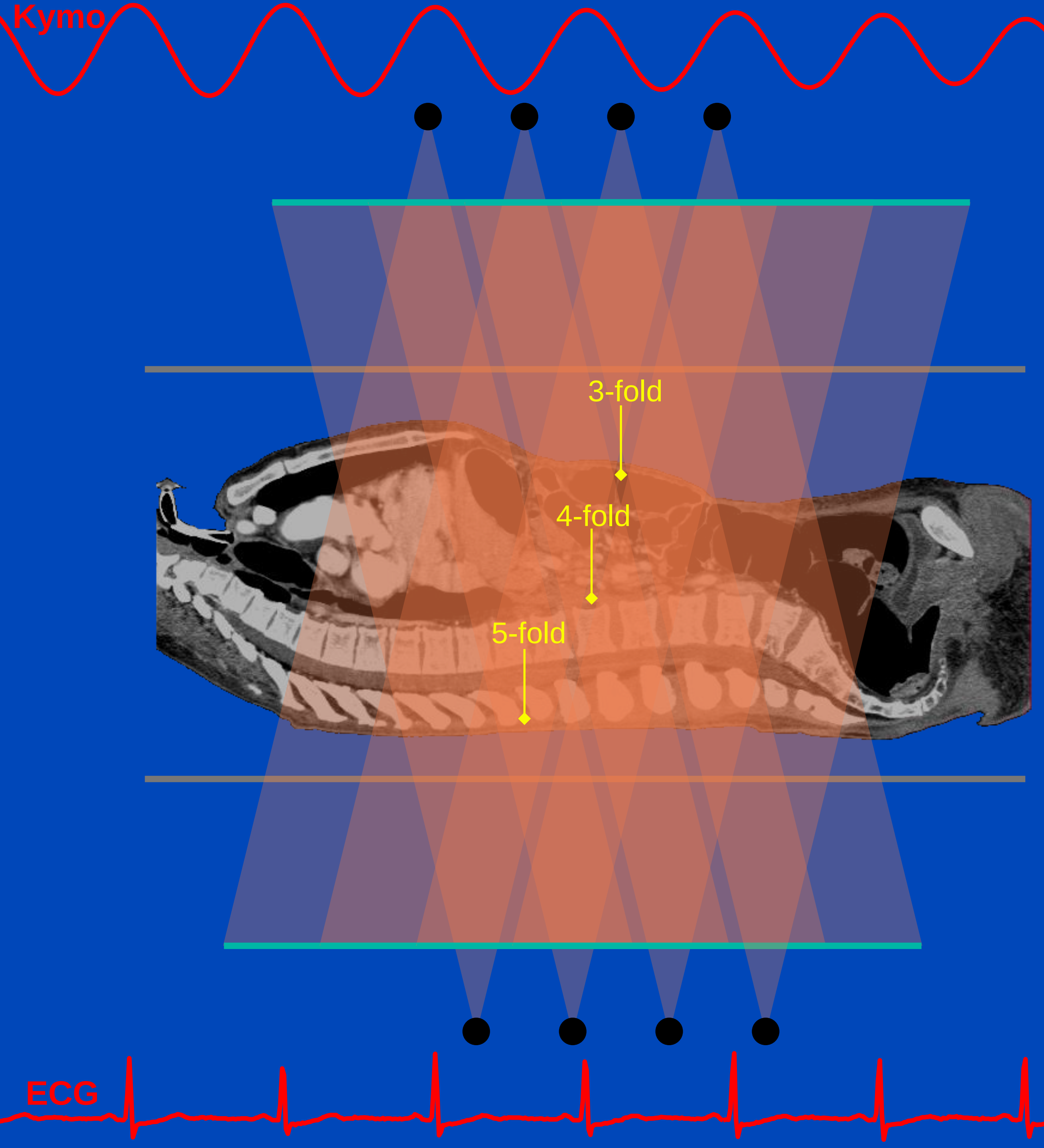

The complicated pattern of overlapping data …

… will become even more complicated with phase-correlation.

⇒ Individual voxel-by-voxel weighting and normalization.

The 180° Condition

$$\int d\vartheta\, w(\vartheta) = \pi$$

and

$$\sum_k w(\vartheta + k\pi) = 1$$

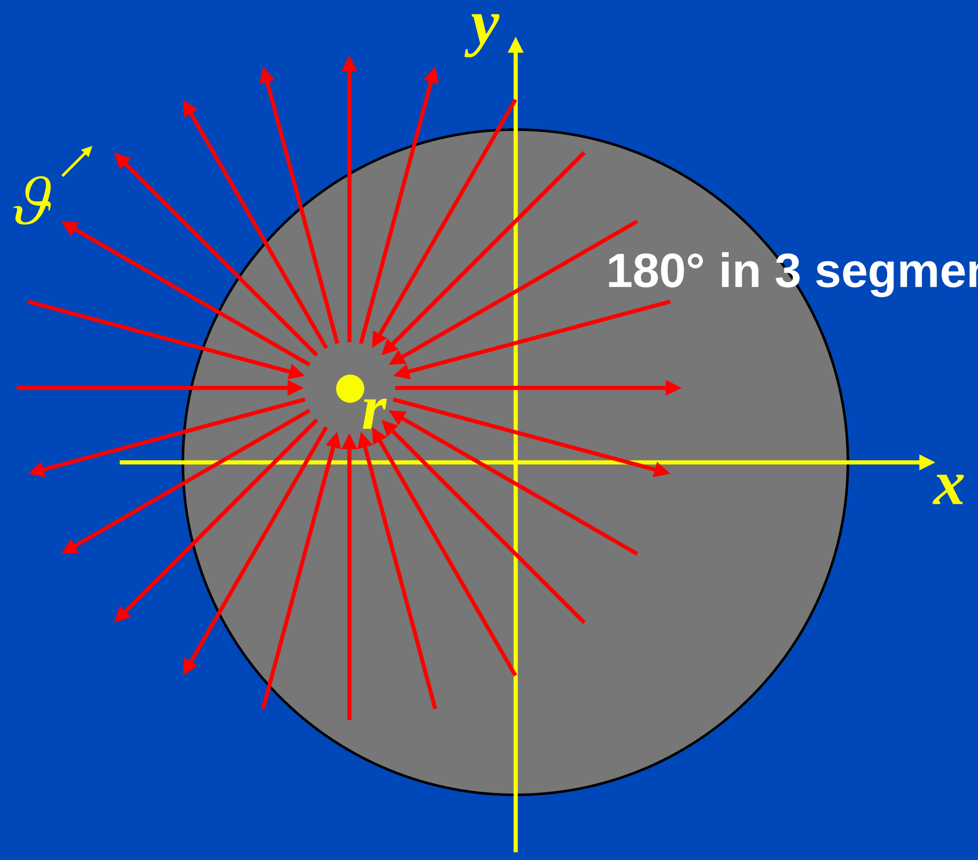

The (weighted) contributions to each object point must make up an interval of 180° and weight 1.

- Spiral
- EPBP Std
- *p* = 0.375

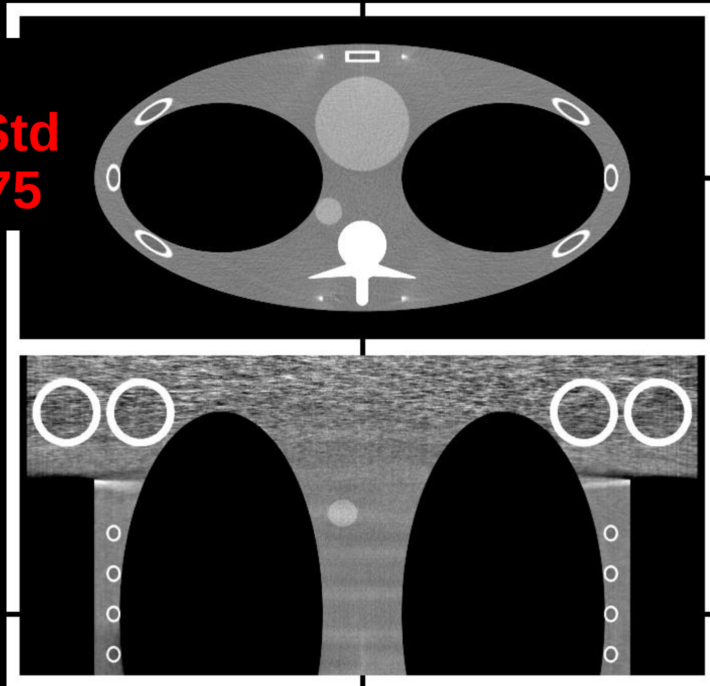

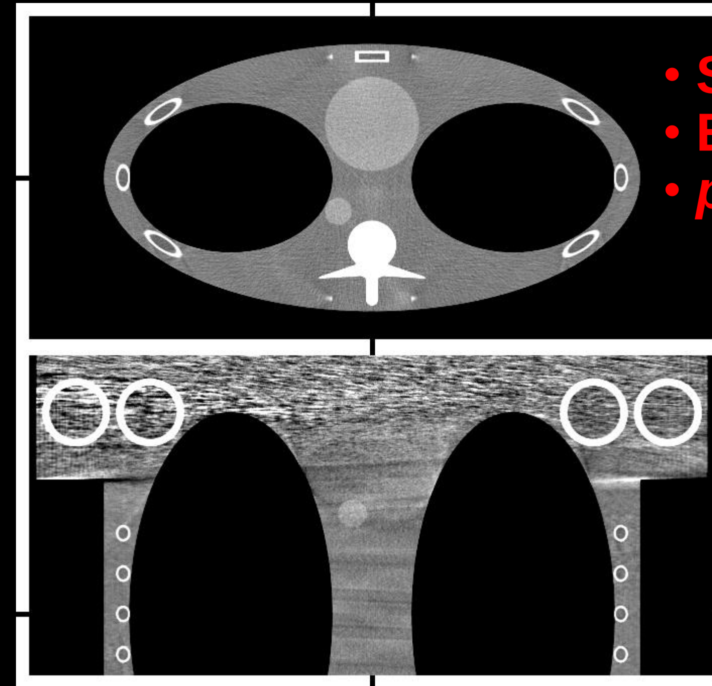

- Spiral
- EPBP Std
- *p* = 1.0

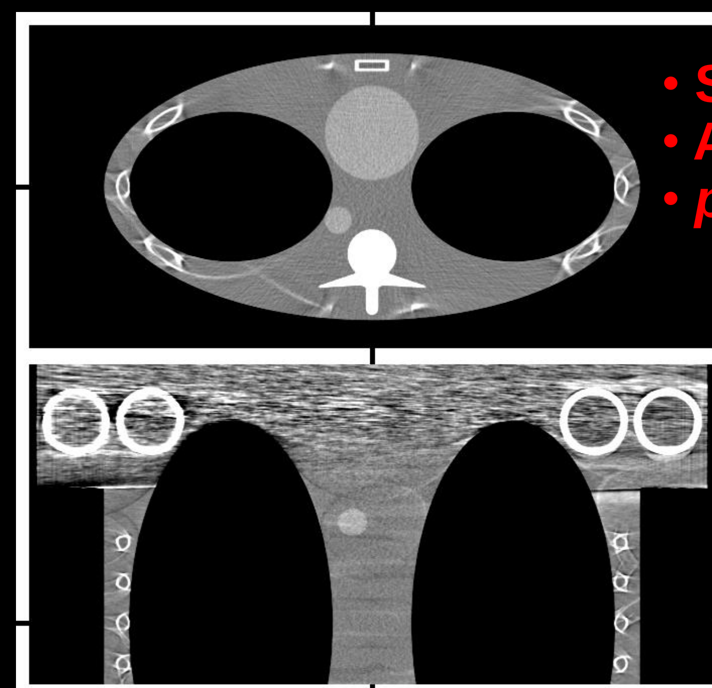

- Spiral
- ASSR Std
- *p* = 1.0

- 256 slices
- (0/300)

Kachelrieß et al., RSNA 2002, Fully3D 2003 and
Med. Phys. 31(6): 1623-1641, 2004

EPBP Std | **EPBP CI, 0% K-K** | **EPBP CI, 50% K-K**

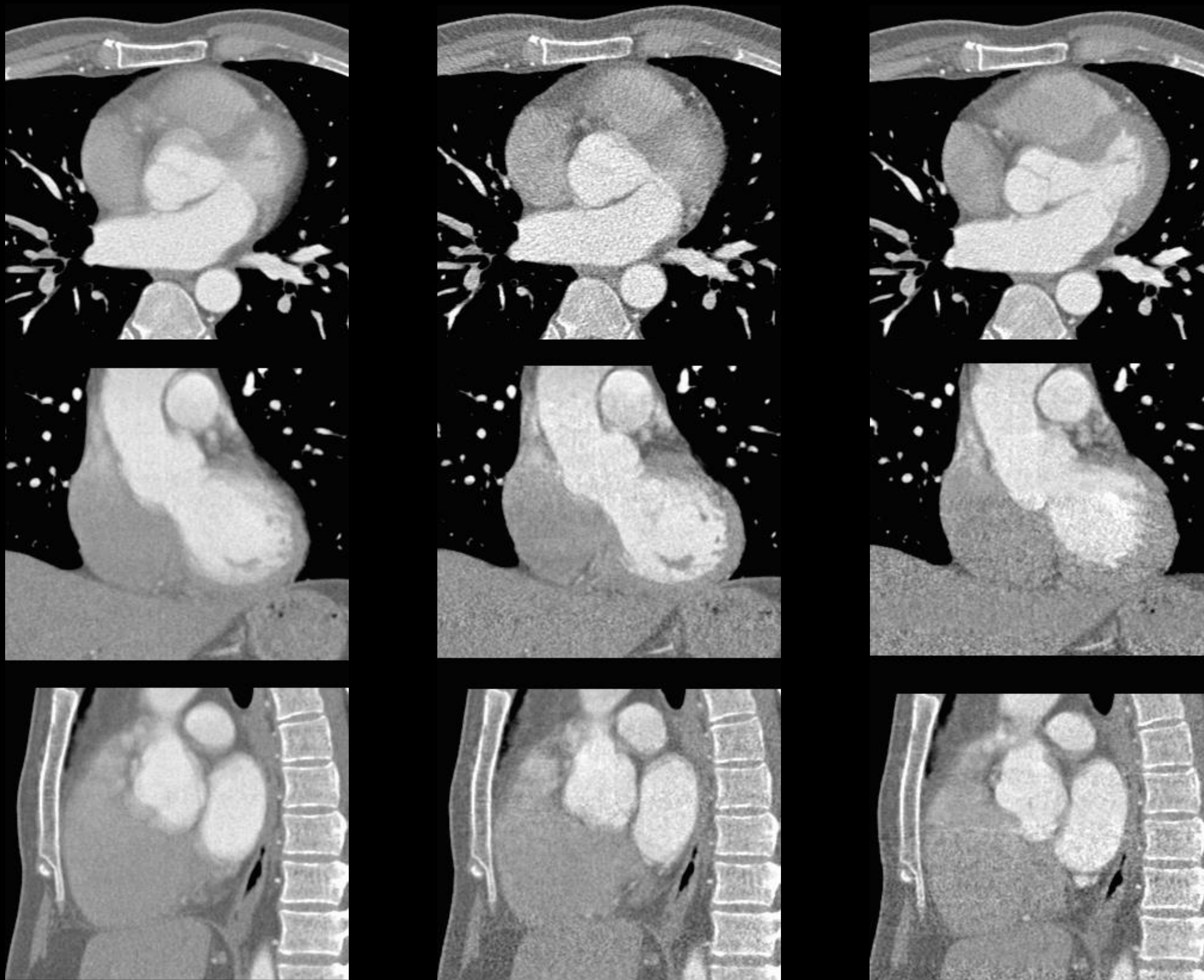

Kachelrieß et al., RSNA 2002, Fully3D 2003 and Med. Phys. 31(6): 1623-1641, 2004

Patient example, 32x0.6 mm, z-FFS, p=0.23, t_{rot}=0.375 s.

Iterative Image Reconstruction

- **Main progress:**
  - early 70ies
  - between about 2000 and 2020

$$x^2 = y$$

Model

$$\cancel{x = \sqrt{y}}$$

$$(x_n + \Delta x_n)^2 = y$$

$$x_n^2 + 2x_n\Delta x_n + \cancel{\Delta x_n^2} = y$$

$$x_n^2 + 2x_n\Delta x_n \approx y$$

$$\Delta x_n = \tfrac{1}{2}(y - x_n^2)/x_n$$

$$x_{n+1} = x_n + \Delta x_n$$

Update equation

Influence of Update Equation and Model

$0.5\,(3 - x_n^2)/x_n$	$0.4\,(3 - x_n^2)/x_n$	$0.5\,(3 - x_n^{2.1})/x_n$
$x_0 = 1.$	$x_0 = 1.$	$x_0 = 1.$
$x_1 = 2.$	$x_1 = 1.8$	$x_1 = 2.$
$x_2 = 1.75$	$x_2 = 1.74667$	$x_2 = 1.67823$
$x_3 = 1.73214$	$x_3 = 1.73502$	$x_3 = 1.68833$
$x_4 = 1.73205$	$x_4 = 1.73265$	$x_4 = 1.68723$
$x_5 = 1.73205$	$x_5 = 1.73217$	$x_5 = 1.68734$
$x_6 = 1.73205$	$x_6 = 1.73207$	$x_6 = 1.68733$
$x_7 = 1.73205$	$x_7 = 1.73206$	$x_7 = 1.68733$
$x_8 = 1.73205$	$x_8 = 1.73205$	$x_8 = 1.68733$

$$x^2 = 3, \quad x_0 = 1, \quad x_{n+1} = x_n + \Delta x_n$$

CT System Matrix

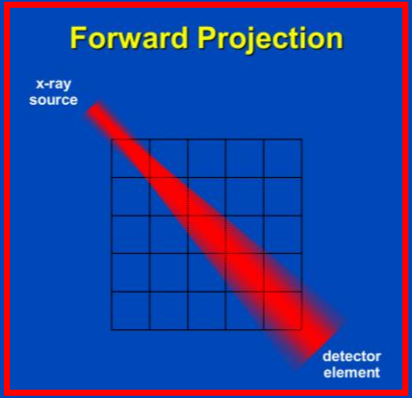

$$\underbrace{\boldsymbol{R}}_{\text{Radon or x-ray transform}} \cdot \underbrace{\boldsymbol{f}}_{\text{image to be reconstructed}} = \underbrace{\boldsymbol{p}}_{\text{measured rawdata}}$$

$$\boldsymbol{R} = \begin{pmatrix} r_{11} & r_{12} & \cdots & r_{1M} \\ r_{21} & r_{22} & \cdots & r_{2M} \\ \vdots & \vdots & \ddots & \vdots \\ r_{N1} & r_{N2} & \cdots & r_{NM} \end{pmatrix}, \quad \boldsymbol{f} = \begin{pmatrix} f_1 \\ f_2 \\ \vdots \\ f_M \end{pmatrix}, \quad \boldsymbol{p} = \begin{pmatrix} p_1 \\ p_2 \\ \vdots \\ p_N \end{pmatrix}$$

Kaczmarz's Method

$$\underbrace{\boldsymbol{R}}_{N \times M} \cdot \underbrace{\boldsymbol{f}}_{M \times 1} = \underbrace{\boldsymbol{p}}_{N \times 1}$$

$$\boldsymbol{R} = \begin{pmatrix} \boldsymbol{r}_1 \\ \boldsymbol{r}_2 \\ \vdots \\ \boldsymbol{r}_N \end{pmatrix}, \quad |\boldsymbol{r}_n| = 1$$

$$\boldsymbol{r}_n \cdot \boldsymbol{f} = p_n$$

Kaczmarz's Method (2)

- **Successively solve** $\boldsymbol{r}_n \cdot \boldsymbol{f} = p_n$
- **To do so, project onto the hyperplanes**

$$\boldsymbol{r}_n \cdot \big(\boldsymbol{f} + \lambda \boldsymbol{r}_n\big) = p_n$$

$$\lambda = p_n - \boldsymbol{r}_n \cdot \boldsymbol{f}$$

$$\boldsymbol{f}_{\text{new}} = \boldsymbol{f} + \lambda \boldsymbol{r}_n$$

$$\boldsymbol{f}_{\text{new}} = \boldsymbol{f} + \boldsymbol{r}_n \big(p_n - \boldsymbol{r}_n \cdot \boldsymbol{f}\big)$$

- **Repeat until some convergence criterion is reached**

$$\boldsymbol{f}_{\nu+1} = \boldsymbol{f}_\nu + \boldsymbol{r}_n \big(p_n - \boldsymbol{r}_n \cdot \boldsymbol{f}_\nu\big)$$

Kaczmarz‘s Method (3)

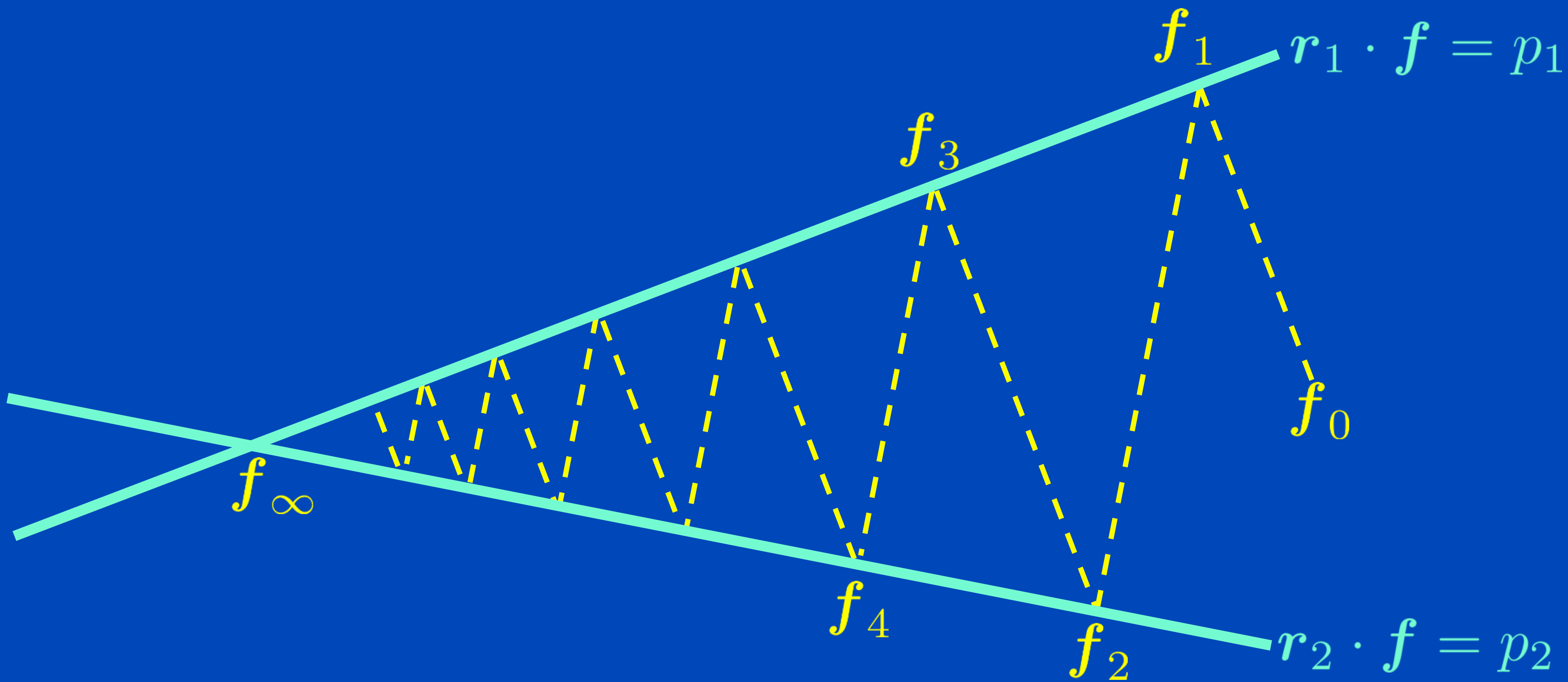

$$\boldsymbol{f}_{\nu+1} = \boldsymbol{f}_\nu + \boldsymbol{r}_n \big(p_n - \boldsymbol{r}_n \cdot \boldsymbol{f}_\nu \big)$$

Kaczmarz‘s Method = ART

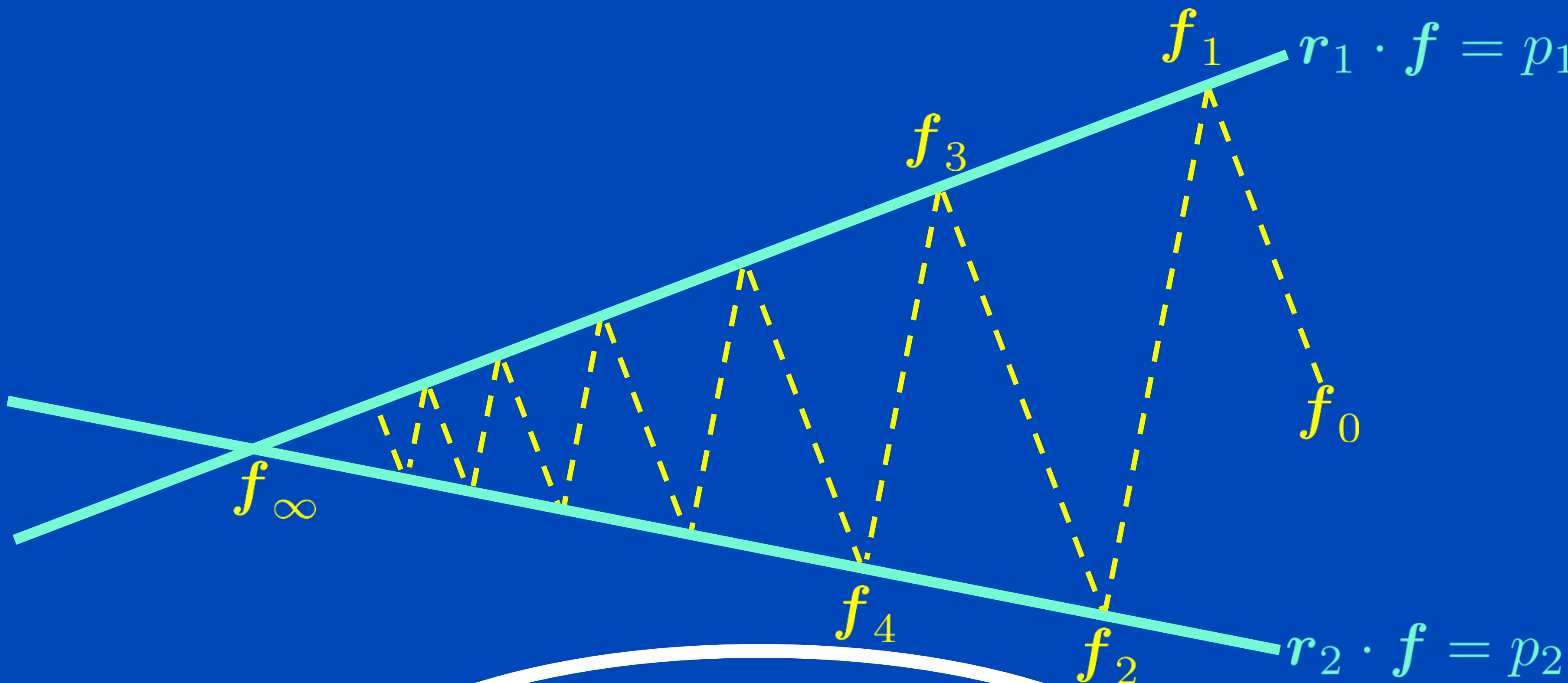

Model

$$f_{\nu+1} = f_\nu + R^{\mathrm{T}} \cdot \frac{p - R \cdot f_\nu}{R^2 \cdot 1}$$

Update equation

Kaczmarz‘s Method = ART

$$\boldsymbol{f}_{\nu+1} = \boldsymbol{f}_{\nu} + \boldsymbol{R}^{\mathrm{T}} \cdot \frac{\boldsymbol{p} - \boldsymbol{R} \cdot \boldsymbol{f}_{\nu}}{\boldsymbol{R}^{2} \cdot \boldsymbol{1}}$$

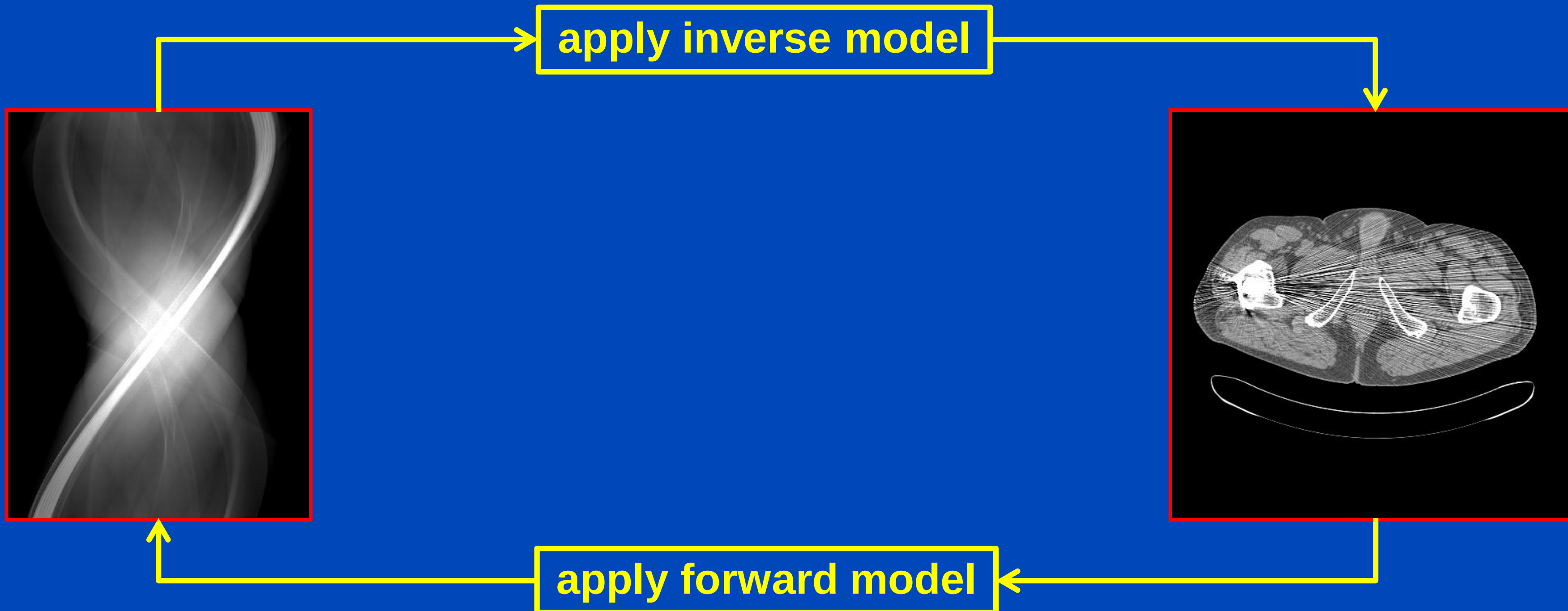

$$\boldsymbol{f}_{\nu+1} = \boldsymbol{f}_{\nu} + \boldsymbol{R}^{\mathrm{T}} \cdot \frac{\boldsymbol{p} - \boldsymbol{R} \cdot \boldsymbol{f}_{\nu}}{\boldsymbol{R}^{2} \cdot \mathbf{1}}$$

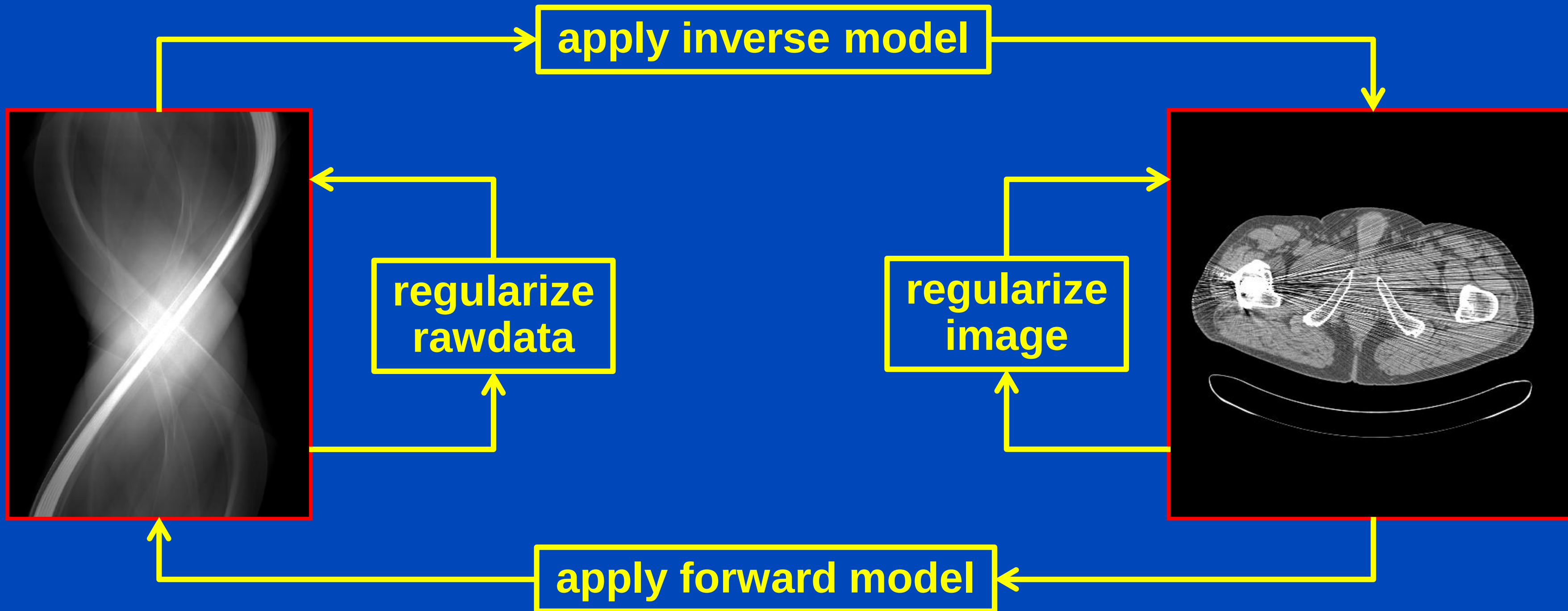

- Rawdata regularization: adaptive filtering[1], precorrections, filtering of update sinograms...
- Inverse model: backprojection (R^{T}) or filtered backprojection (R^{-1}). In clinical CT, where the data are of high fidelity and nearly complete, one would prefer filtered backprojection to increase convergence speed.
- Image regularization: edge-preserving filtering. It may model physical noise effects (amplitude, direction, correlations, …). It may reduce noise while preserving edges. It may include empirical corrections.
- Forward model (R_{phys}): Models physical effects. It can reduce beam hardening artifacts, scatter artifacts, cone-beam artifacts, noise, …

[1] M. Kachelrieß et al., Generalized Multi-Dimensional Adaptive Filtering, MedPhys 28(4), 2001

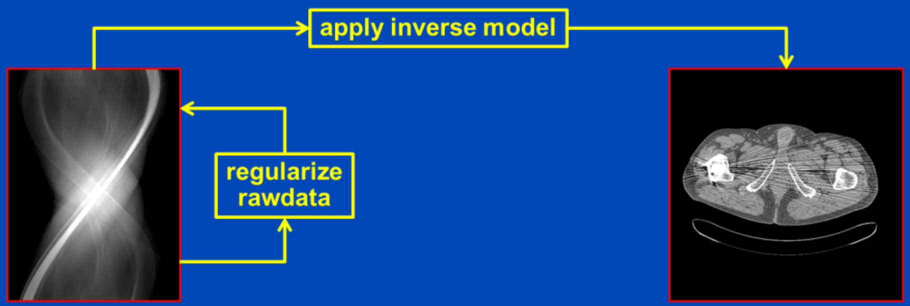

Conventional FBP with rawdata denoising (all vendors)

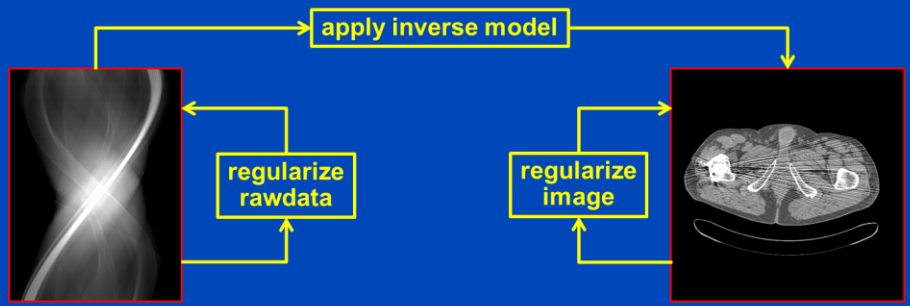

AIDR3D (Canon), ASIR, ASIR-V (Ge), IRIS (Siemens), iDose (Philips), SnapShot Freeze (GE), iTRIM (Siemens)

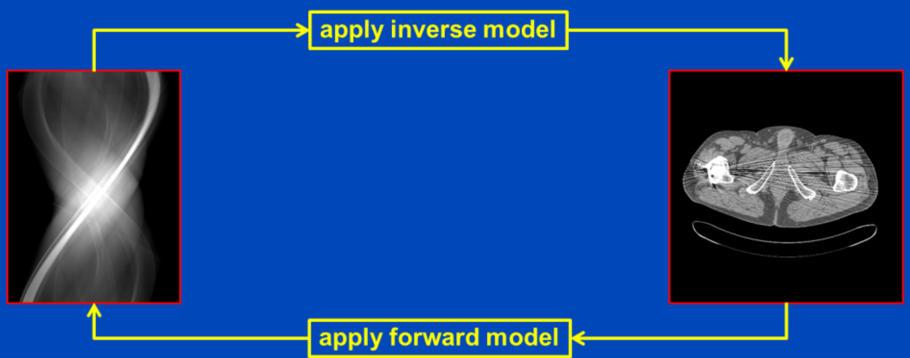

Veo123/MBIR (Ge)

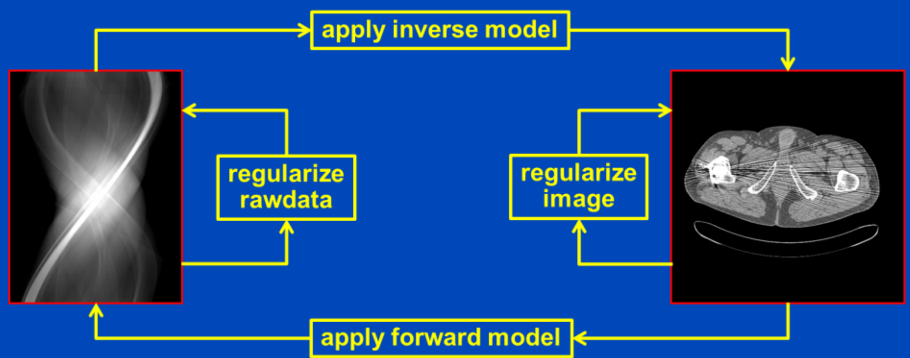

FIRST (Canon), IMR (Philips), SAFIRE, ADMIRE, QIR (Siemens)

Premium Recon Algorithms 2021/2022

Vendor	Algorithm	Additional parameters	Sinogram restoration	Image restoration	Full iterations	Deep learning
all	FBP	-	✓	-	-	-
Canon	AIDR-3D enhanced FIRST AiCE	Body, Bone, Brain, Cardiac, Lung each with Mild, Standard, or Strong	✓ ✓ ?	✓ ✓ ✓	- ✓ -	- - ✓
GE	ASIR, ASIR-V True Fidelity	0 – 100% (e.g. ASIR 30%) ???	✓ ?	✓ ✓	- -	- ✓
Philips	iDose IMR	Levels 1 – 7 Soft, Routine, or SharpPlus	✓ ?	✓ ?	- ?	- -
Siemens	IRIS SAFIRE ADMIRE QIR (PC-specific)	Strength 1 – 5 Strength 1 – 5 Strength 1 – 5 Strength 1 – 4	✓ ✓ ✓ ✓	✓ ✓ ✓ ✓	- ✓ ✓ ✓	- - - -

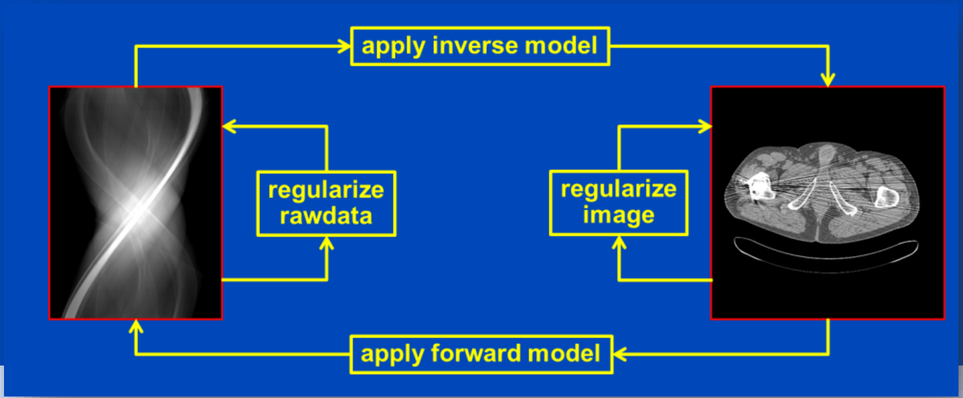

M. Lell and M. Kachelrieß. Recent and upcoming technological developments in CT. Invest. Radiol. Feb. 2020

Plain FBP

σ = 26.8 HU

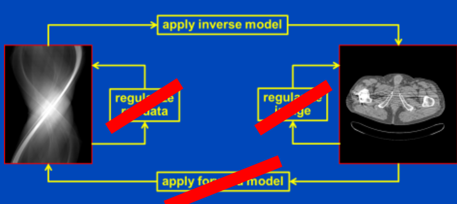

Siemens Standard

σ = 17.6 HU

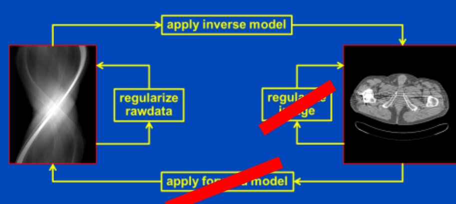

IRIS VA34

σ = 12.3 HU

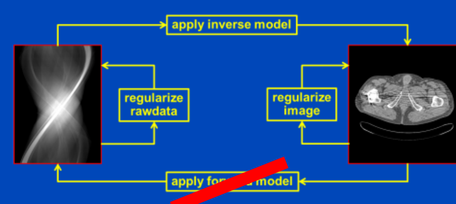

SAFIRE VA40

σ = 7.8 HU

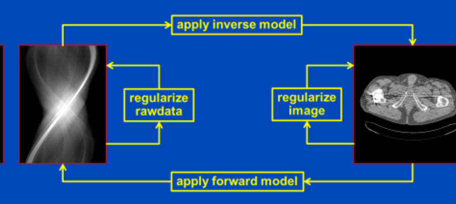

CT images provided by Siemens Healthcare, Forchheim, Germany

FBP


apply inverse model

ASIR

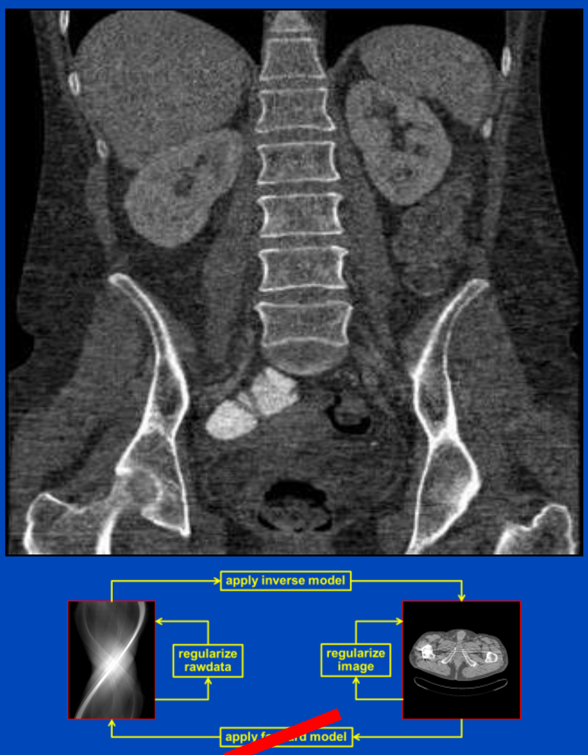
apply inverse model
regularize rawdata
regularize image

Veo

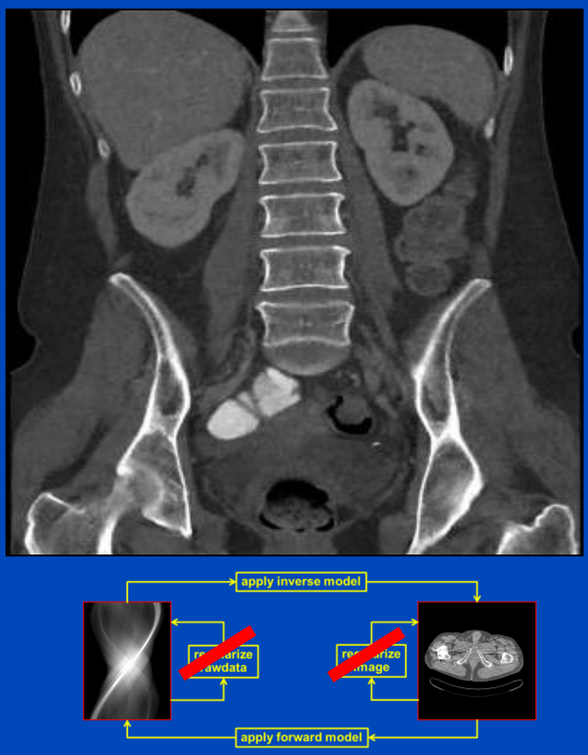
apply inverse model
apply forward model

Original CBCT Reconstruction

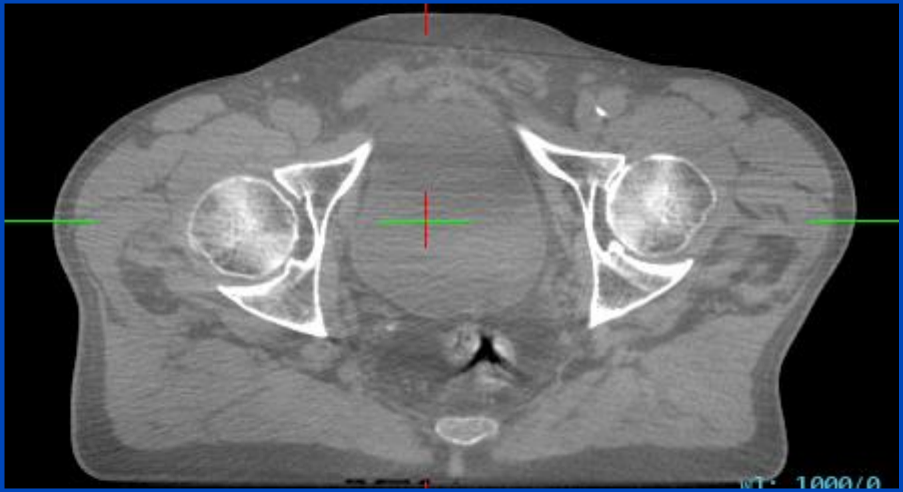

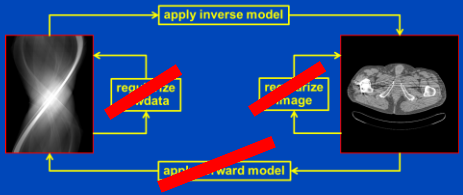

iCBCT Reconstruction

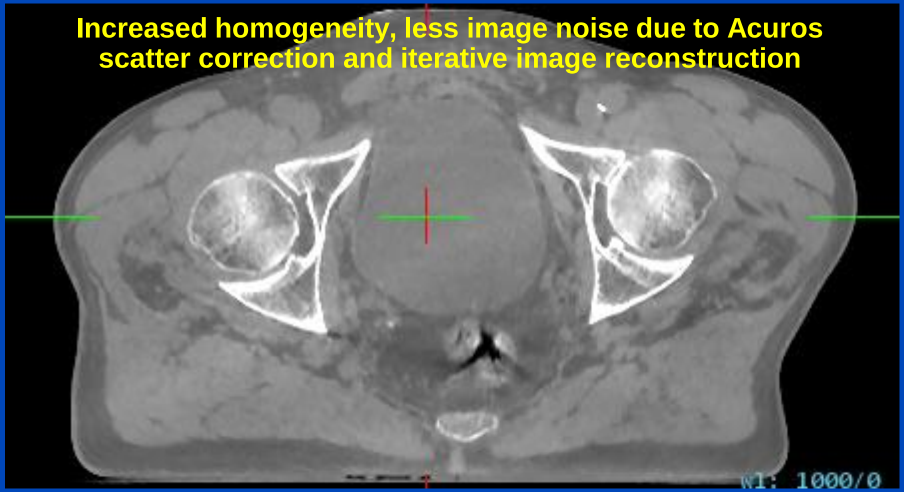

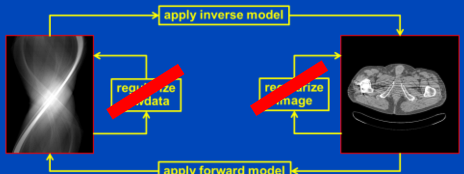

Planning CT for reference

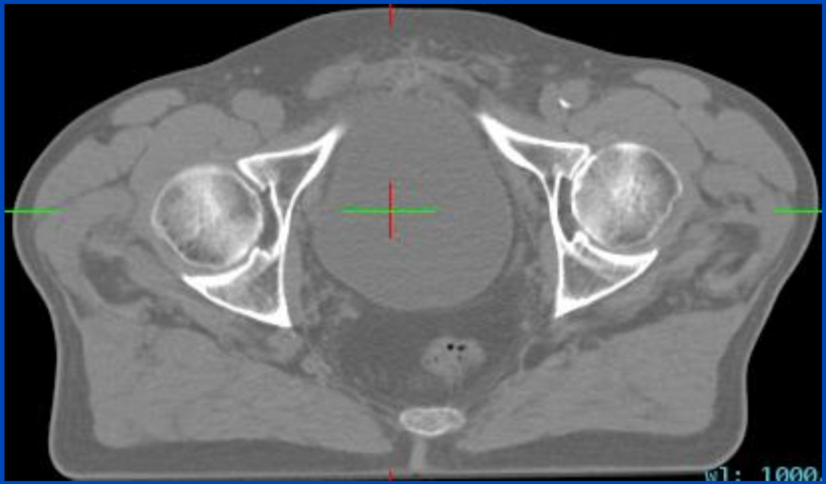

C = 0 HU, *W* = 1000 HU

Courtesy of Dr. Pascal Paysan, Varian iLab, Baden, Switzerland.

dkfz.

Deep Learning-Based Reconstruction

- Main progress:
  - Since about 2015
  - Still ongoing

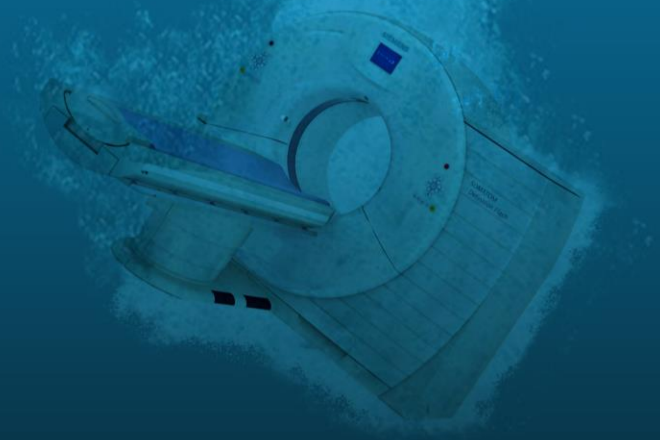

$$\cancel{x^2 = y}$$

$$\cancel{x = \sqrt{y}}$$

$$\cancel{\begin{aligned} \Delta x_n &= \tfrac{1}{2}(y - x_n^2)/x_n \\ x_{n+1} &= x_n + \Delta x_n \end{aligned}}$$

$$\{(y^{(d)}, x^{(d)}) \mid d = 1, \ldots, D \quad \text{with } D \text{ being large}\}$$

Data

$$f_{c_1, c_2, \ldots c_P}(y) \quad \text{with } P \text{ being large}$$

Model

$$\boldsymbol{c} = \arg\min_{\boldsymbol{c}} \sum_d \left(f_{\boldsymbol{c}}(y^{(d)}) - x^{(d)}\right)^2$$

Loss

$$x = f_{c_1, c_2, \ldots c_P}(y)$$

Inference

This is a data-driven solution.

dkfz.

Fully Connected Neural Network

- Each layer fully connects to previous layer
- Difficult to train (many parameters in *W* and *b*)
- Spatial relations not necessarily preserved

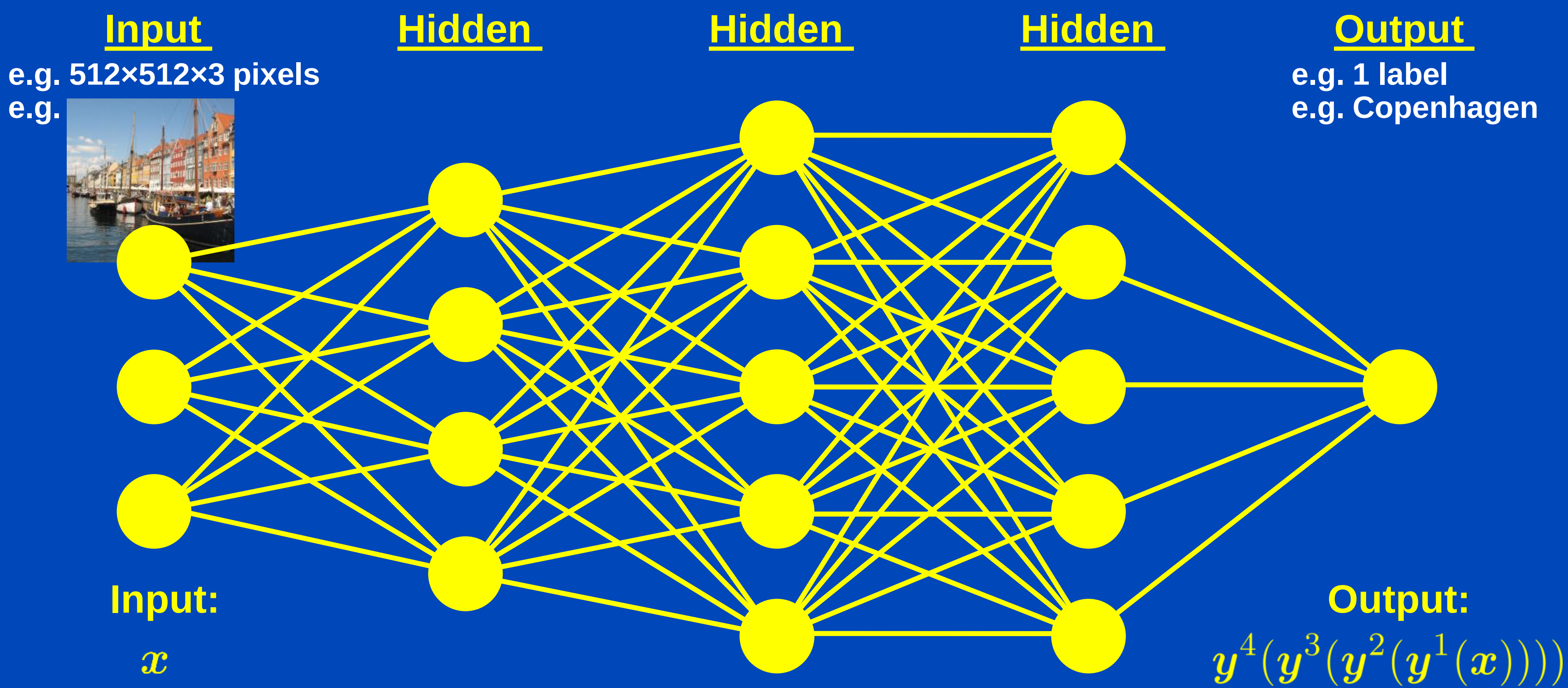

$\boldsymbol{y}(\boldsymbol{x}) = \boldsymbol{f}(\boldsymbol{W}\cdot\boldsymbol{x}+\boldsymbol{b})$ with $\boldsymbol{f}(\boldsymbol{x}) = \big(f(x_1), f(x_2), \ldots\big)$ point-wise scalar, e.g. $f(x) = x \vee 0 = \mathrm{ReLU}$

Canon‘s AiCE

- Advanced intelligent Clear-IQ Engine (AiCE)
- Trained to restore low-dose CT data to match the properties of FIRST, the model-based IR of Canon.
- FIRST is applied to high-dose CT images to obtain a high fidelity training target

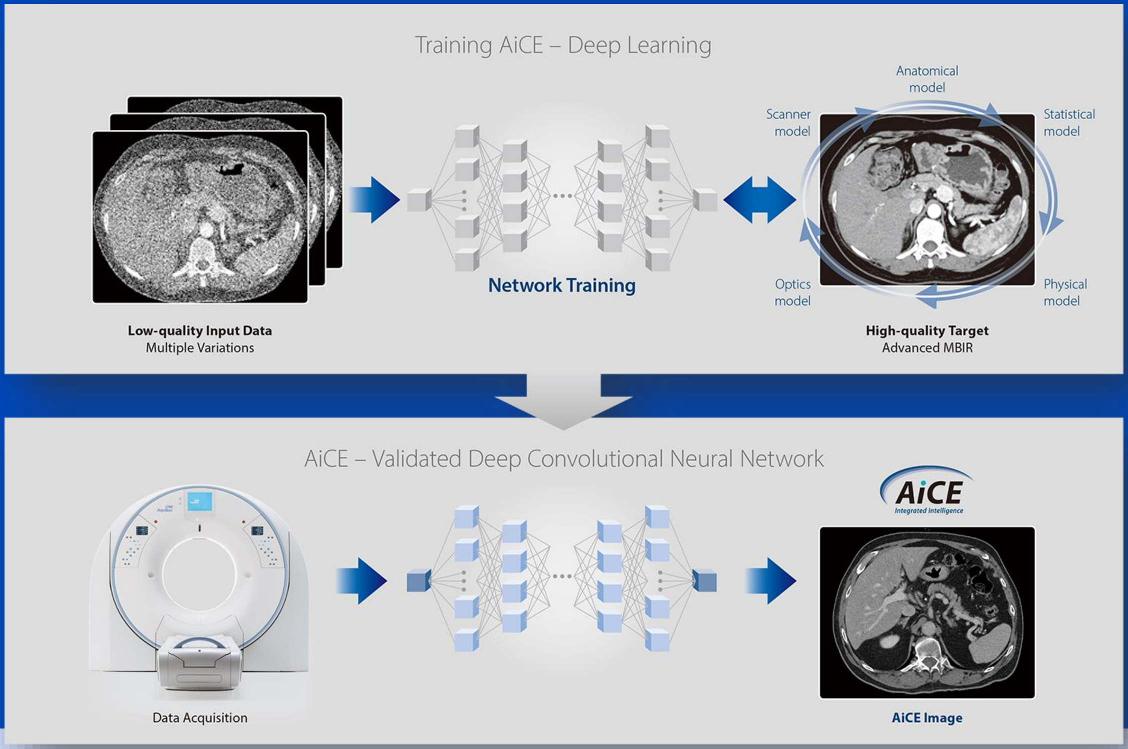

U = 100 kV
CTDI = 0.6 mGy
DLP = 24.7 mGy·cm
D_{eff} = 0.35 mSv

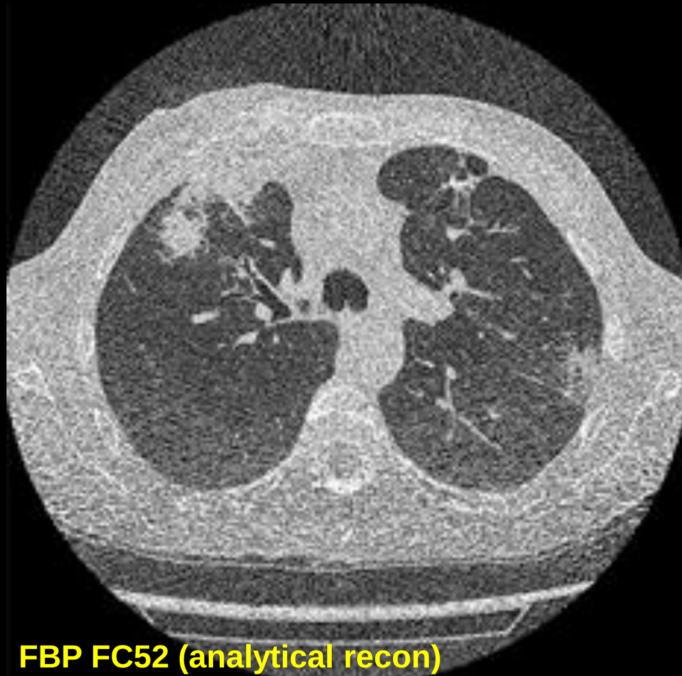

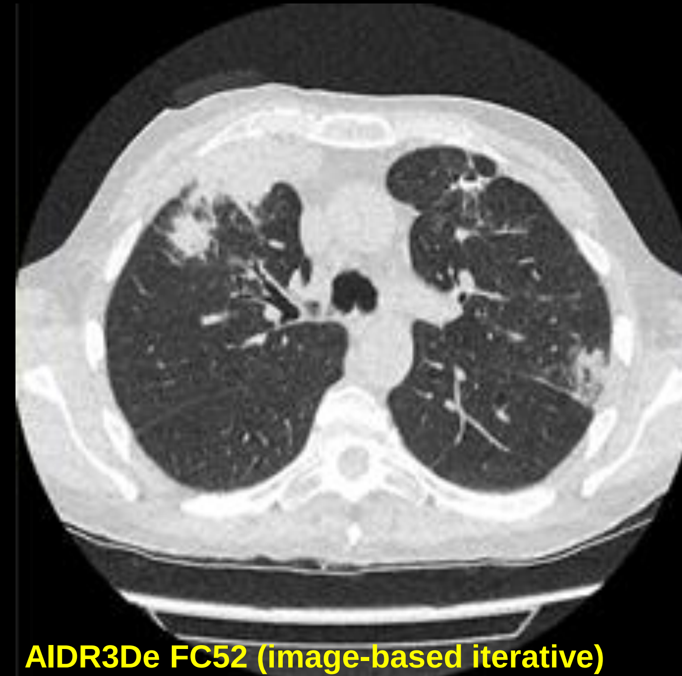

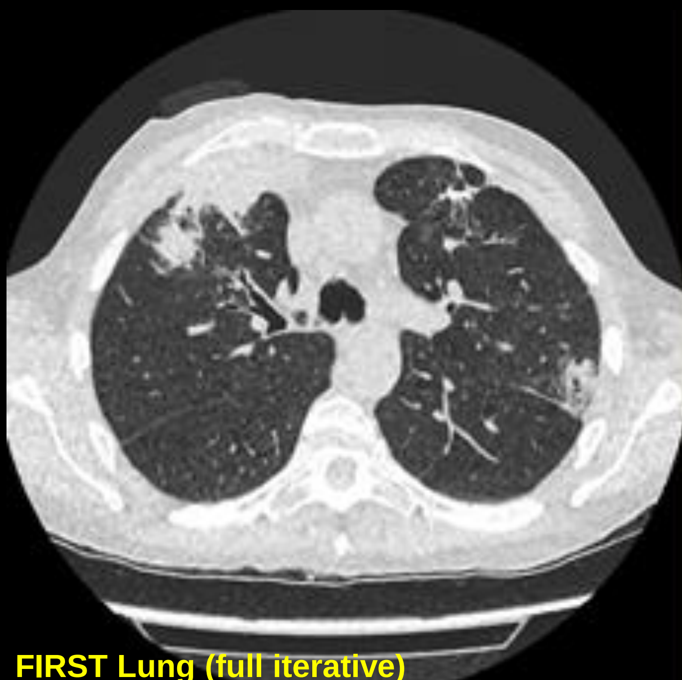

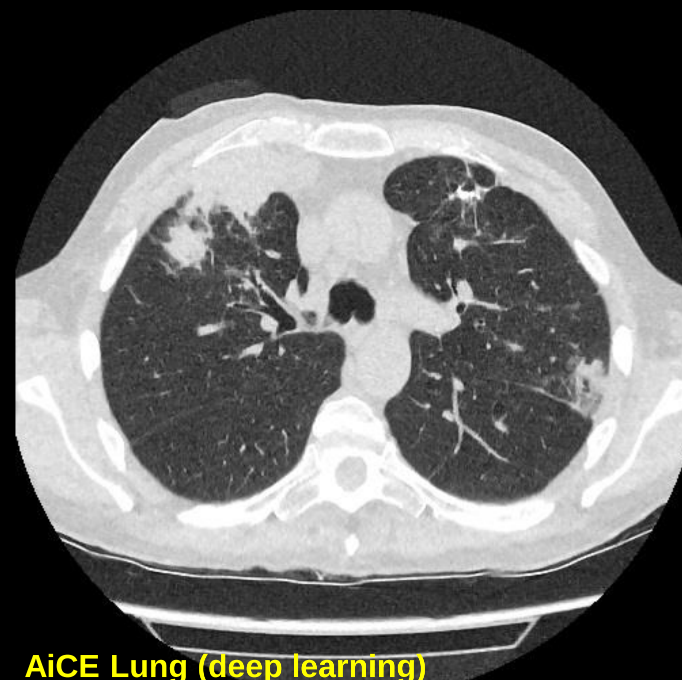

Courtesy of
Radboudumc,
the Netherlands

Noise Removal Example 7
GE's True Fidelity

- Based on a deep CNN
- Trained to restore low-dose CT data to match the properties of Veo, the model-based IR of GE.
- No information can be obtained in how the training is conducted for the product implementation.

2.5D DEEP LEARNING FOR CT IMAGE RECONSTRUCTION USING A MULTI-GPU IMPLEMENTATION

Amirkoushyar Ziabari[⋆], *Dong Hye Ye*[⋆ †], *Somesh Srivastava*[‡], *Ken D. Sauer*[⊕]
Jean-Baptiste Thibault[‡], *Charles A. Bouman*[⋆]

[⋆] Electrical and Computer Engineering at Purdue University
[†] Electrical and Computer Engineering at Marquett University
[‡] GE Healthcare
[⊕] Electrical Engineering at University of Notre Dame

ABSTRACT

While Model Based Iterative Reconstruction (MBIR) of CT scans has been shown to have better image quality than Filtered Back Projection (FBP), its use has been limited by its high computational cost. More recently, deep convolutional neural networks (CNN) have shown great promise in both denoising and reconstruction applications. In this research, we propose a fast reconstruction algorithm, which we call Deep

streaking artifacts caused by sparse projection views in CT images [8]. More recently, Ye, et al. [9] developed method for incorporating CNN denoisers into MBIR reconstruction as advanced prior models using the Plug-and-Play framework [10, 11].

In this paper, we propose a fast reconstruction algorithm, which we call Deep Learning MBIR (DL-MBIR), for approximately achieving the improved quality of MBIR using a deep residual neural network. The DL-MBIR method is trained to

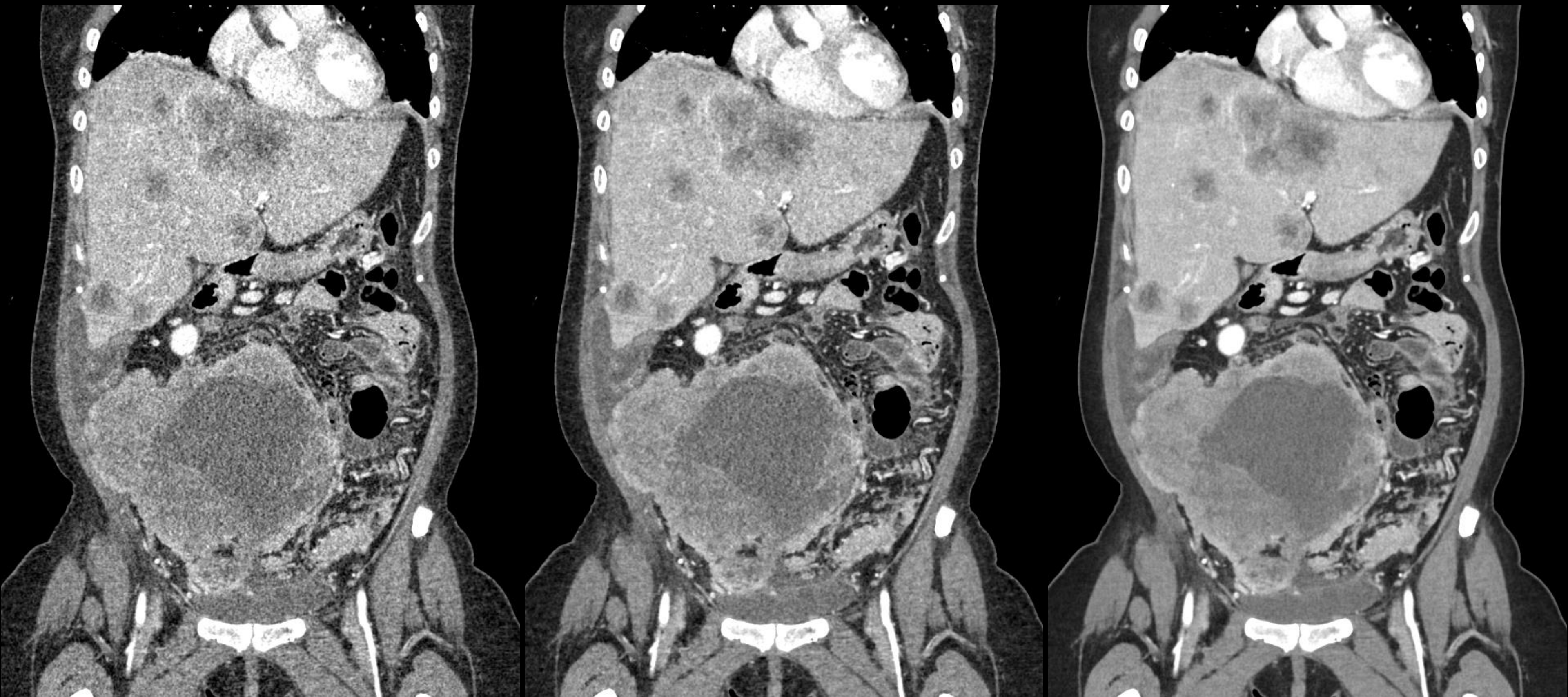

FBP　　ASIR V 50%　　True Fidelity

Courtesy of GE Healthcare

Cardiac CT Image Reconstruction

- **Main progress:**
  - **From about 1995 to 2015**

Electrocardiogram-correlated image reconstruction from subsecond spiral computed tomography scans of the heart

Marc Kachelriess and Willi A. Kalender[a)]
Institute of Medical Physics, University of Erlangen-Nürnberg, Erlangen, Germany

(Received 31 December 1997; accepted for publication 17 September 1998)

Subsecond computed tomography (CT) scanning offers potential for improved heart imaging. We therefore developed and validated dedicated reconstruction algorithms for imaging the heart with subsecond spiral CT utilizing electrocardiogram (ECG) information. We modified spiral CT z-interpolation algorithms on a subsecond spiral CT scanner. Two new classes of algorithms were investigated: (a) 180°CI (cardio interpolation), a piecewise linear interpolation between adjacent spiral data segments belonging to the same heart phase where segments are selected by correlation with the simultaneously recorded ECG signal and (b) 180°CD (cardio delta), a partial scan reconstruction of $180° + \delta$ with $\delta <$ fan angle, resulting in reduced effective scan times of less than 0.5 s. Computer simulations as well as processing of clinical data collected with 0.75 s scan time were carried out to evaluate these new approaches. Both 180°CI and 180°CD provided significant improvements in image quality. Motion artifacts in the reconstructed images were largely reduced as compared to standard spiral reconstructions; in particular, coronary calcifications were delineated more sharply and multiplanar reformations showed improved contiguity. However, new artifacts in the image plane are introduced, mostly due to the combination of different data segments. ECG-oriented image reconstructions improve the quality of heart imaging with spiral CT significantly. Image quality and the display of coronary calcification appear adequate to assess coronary calcium measurements with conventional subsecond spiral CT. [S0094-2405(98)00712-3]

Key words: computed tomography (CT), spiral CT, heart, coronary vessels, calcium

I. INTRODUCTION

Coronary artery disease is one of the most important causes of death in western civilizations. Therefore, noninvasive

heart cycle. Even for 180° algorithms[3] a data range acquired over $2 \times (180° + \Phi)/360° \times t_{rot}$ is accessed where Φ is the fan angle and t_{rot} is the time for a 360° rotation. Thus for a

Imaging the Heart with CT

(Cardiac-CT = phase-correlated CT)

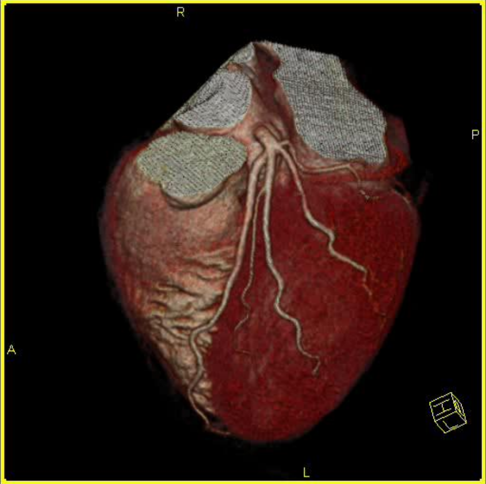

- **Periodic motion**
- **Synchronisation (ECG, Kymogram, …)**
- **Phase-correlated scanning = Prospective Gating**
  - Used in the 80s and 90s with little success.
  - Came into use again in the 10s due to large cone-angles.
- **Phase-correlated reconstruction = Retrospective Gating**
  - Single-phase (partial scan) approaches, e.g. 180°MCD
  - Bi-phase approaches, e.g. ACV (Flohr et al.)
  - Multi-phase Cardio Interpolation methods, e.g. 180°MCI (gold-standard)
  - Generations
    - » Single-slice spiral CT: 180°CD, 180°CI (introduced 1996[1])
    - » Multi-slice spiral CT: 180°MCD, 180°MCI (introduced 1998[2])
    - » Cone-beam spiral CT: ASSR CD, ASSR CI (introduced 2000[3])
    - » Wide cone-beam CT: EPBP (introduced 2002[4])
    - » Multi-source CBCT: EPBP (introduced 2005[5])

[1]Med. Phys. 25(12):2417-2431 (1998), [2]Med. Phys. 27(8):1881-1902 (2000), [3]Proc. Fully 3D-2001:179-182 (2001),
[4]Med. Phys. 31(6): 1623-1641 (2004), [5]Med. Phys. 33(7): 2435-2447 (2006)

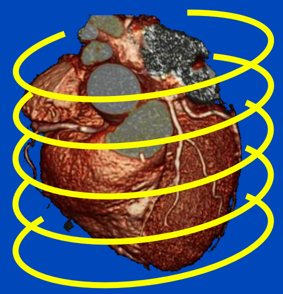

Retrospective Gating

=

Standard scan + ECG-correlated recon

Standard spiral scan with low pitch value ($p \leq f_H \cdot t_{rot}$)

Phase-correlated reconstruction

$p \cdot T_{rot} / 2 \leq$ Temp. resolution $\leq T_{rot} / 2$

Works also at high heart rates

Dose management: ECG-based TCM

Full phase selectivity

Highly robust (also with arrhythmia)

Good dose usage

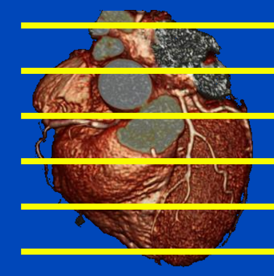

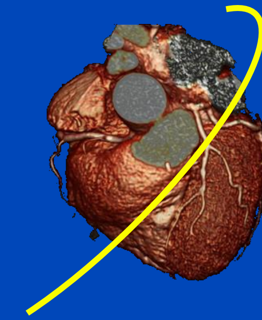

Prospective Gating

=

ECG-triggered scan + standard recon

ECG-triggered sequence- or spiral scan with high pitch value

Standard image reconstruction

Temporal resolution = $T_{rot} / 2$

Good at low heart rates

Dose management: inherent

No phase selectivity

Sufficiently robust (not with arrythmia)

Very good dose usage

Synchronization with the Heart Phase

t_{eff} = width / heart rate

e.g. 15% / 60 bpm = 150 ms

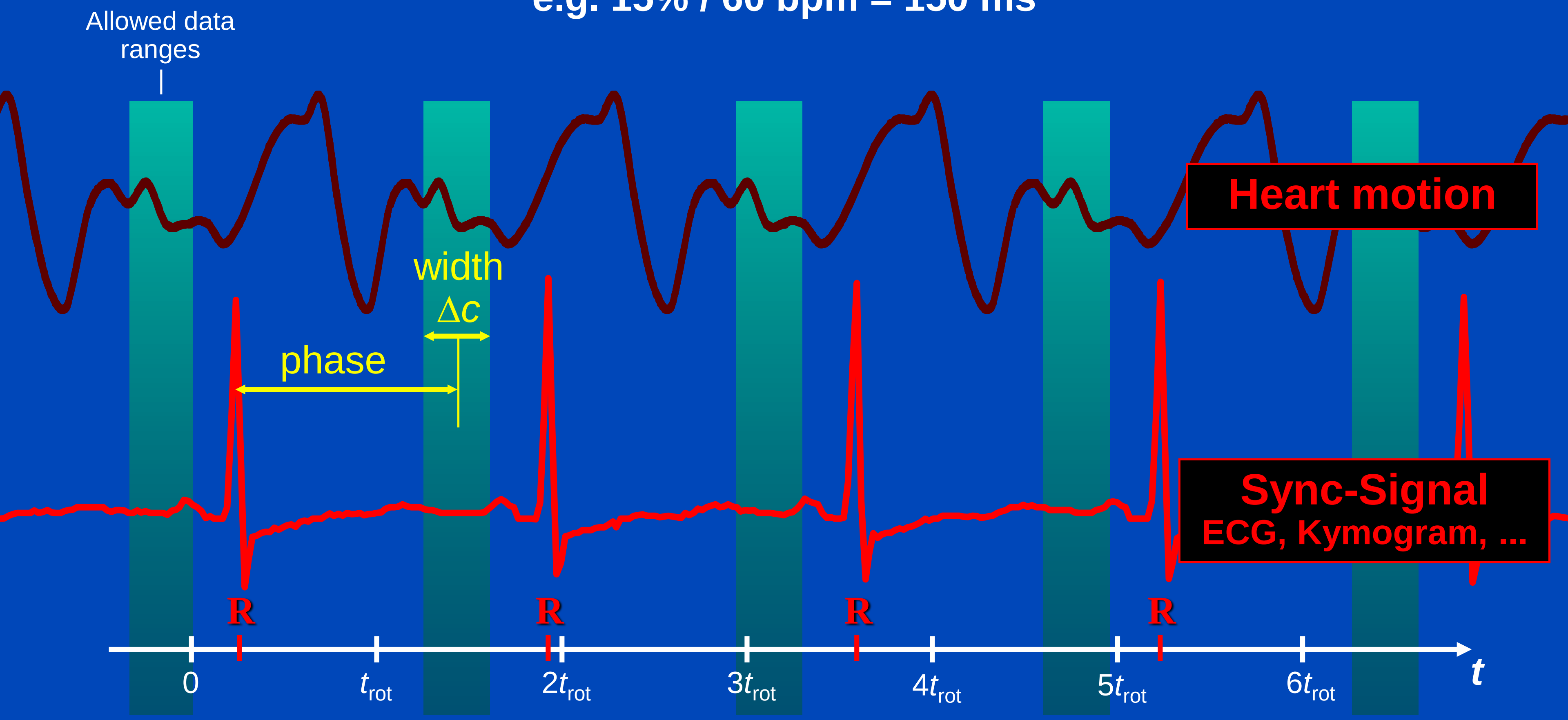

Width, and thus t_{eff}, corresponds to the FWTM of the phase contribution profile.

Partial Scan Reconstruction

Use one segment
of $180°+\delta$ data
of phase-coherent data
for a selected heart phase

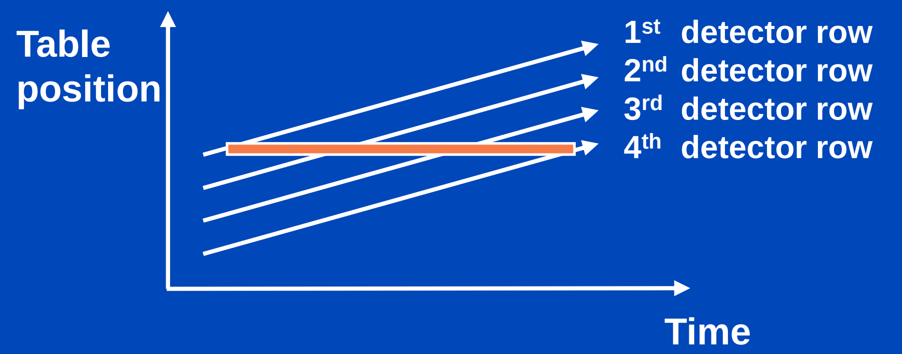

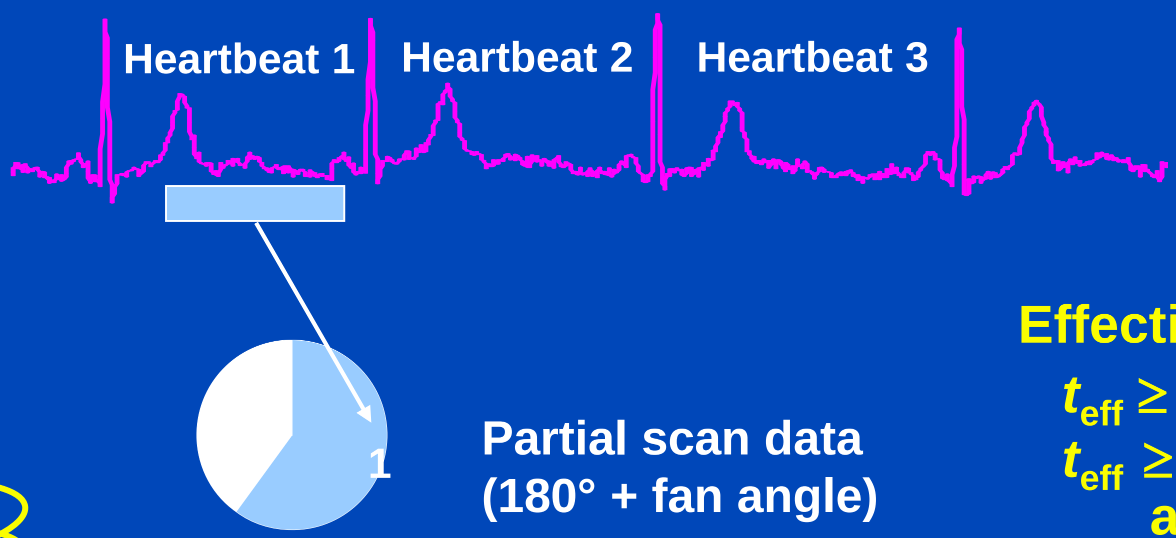

Partial scan data
(180° + fan angle)

Effective scan time

$t_{eff} \geq t_{rot}/2$

$t_{eff} \geq 200$ ms at $t_{rot} = 0.4$ s

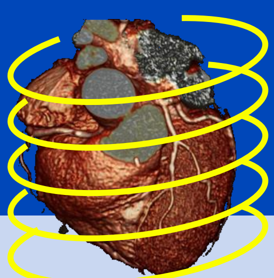

Kachelrieß, Ulzheimer, Kalender, Med. Phys. 27(8):1881-1902 (2000)

Multi-Segment Reconstruction

Combine n segments
to obtain 180°+δ
of phase-coherent data
for a selected heart phase

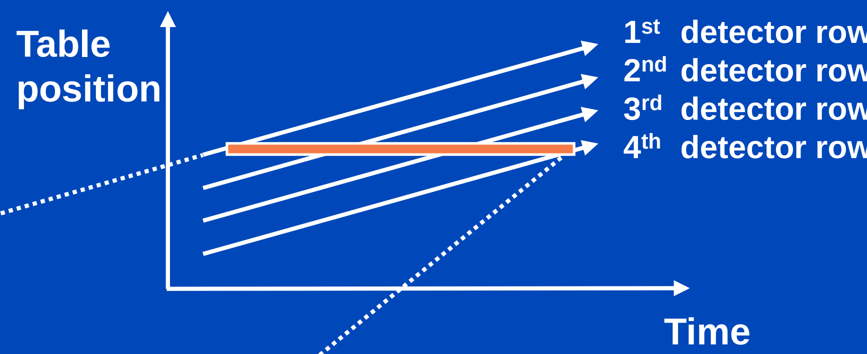

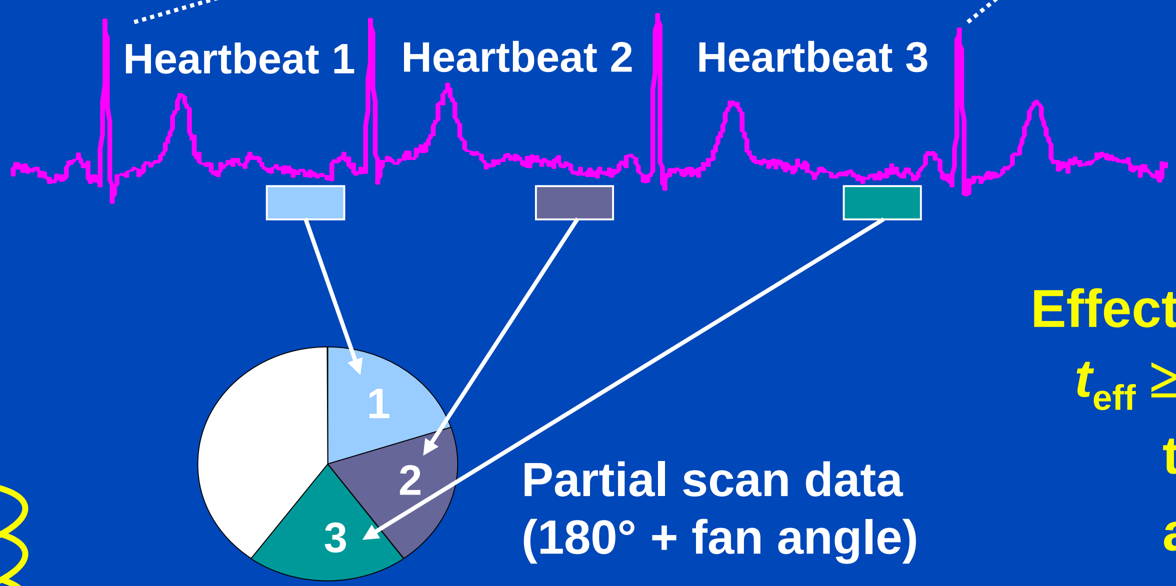

Effective scan time

$t_{eff} \geq 48$ ms

typ. 75-150 ms

at $t_{rot} = 0.4$ s

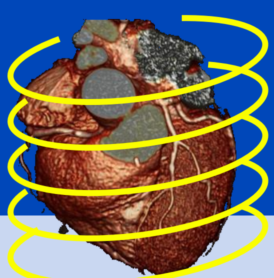

Kachelrieß, Ulzheimer, Kalender, Med. Phys. 27(8):1881-1902 (2000)

Early Cardiac Spiral CT

Single Slice CT (RSNA 1997)

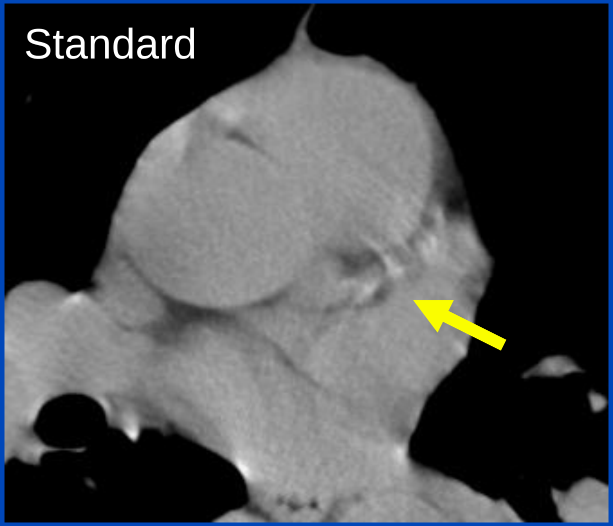

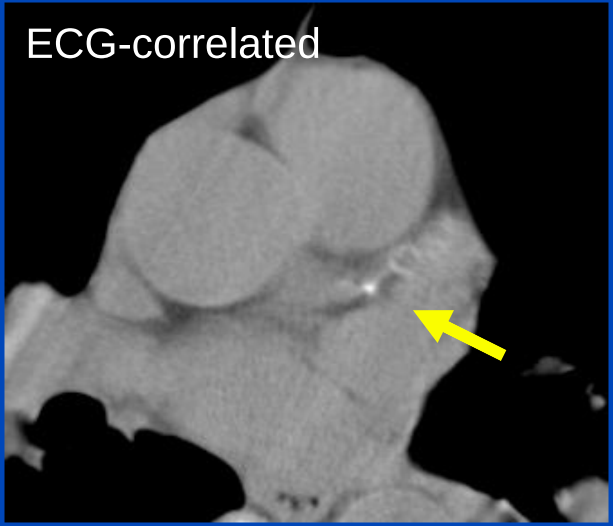

Kachelrieß et al. Electrocardiogram-correlated image reconstruction from subsecond spiral computed tomography scans of the heart. Med. Phys., 25(12):2417-2431, December 1998.

4-Slice CT (RSNA 1999)

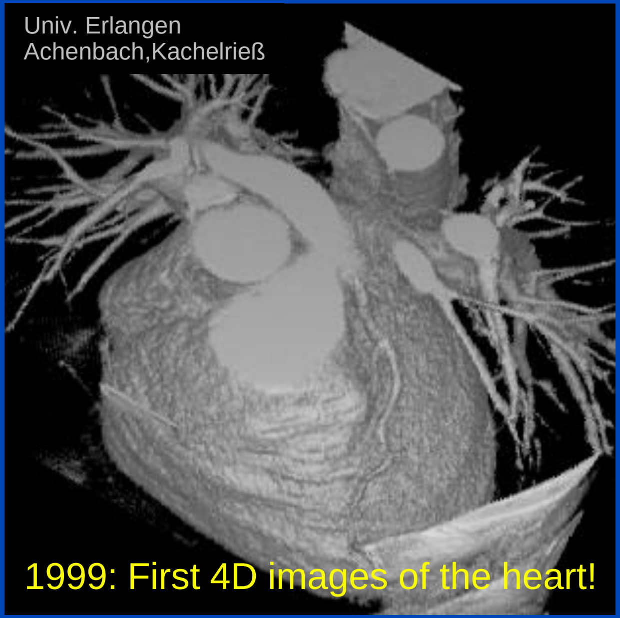

Kachelrieß et al. ECG-correlated imaging of the heart with subsecond multislice spiral CT. IEEE TMI, 19(9):888-901, September 2000.

Dual Source CT (DSCT)

Siemens SOMATOM Force
dual source cone-beam spiral CT

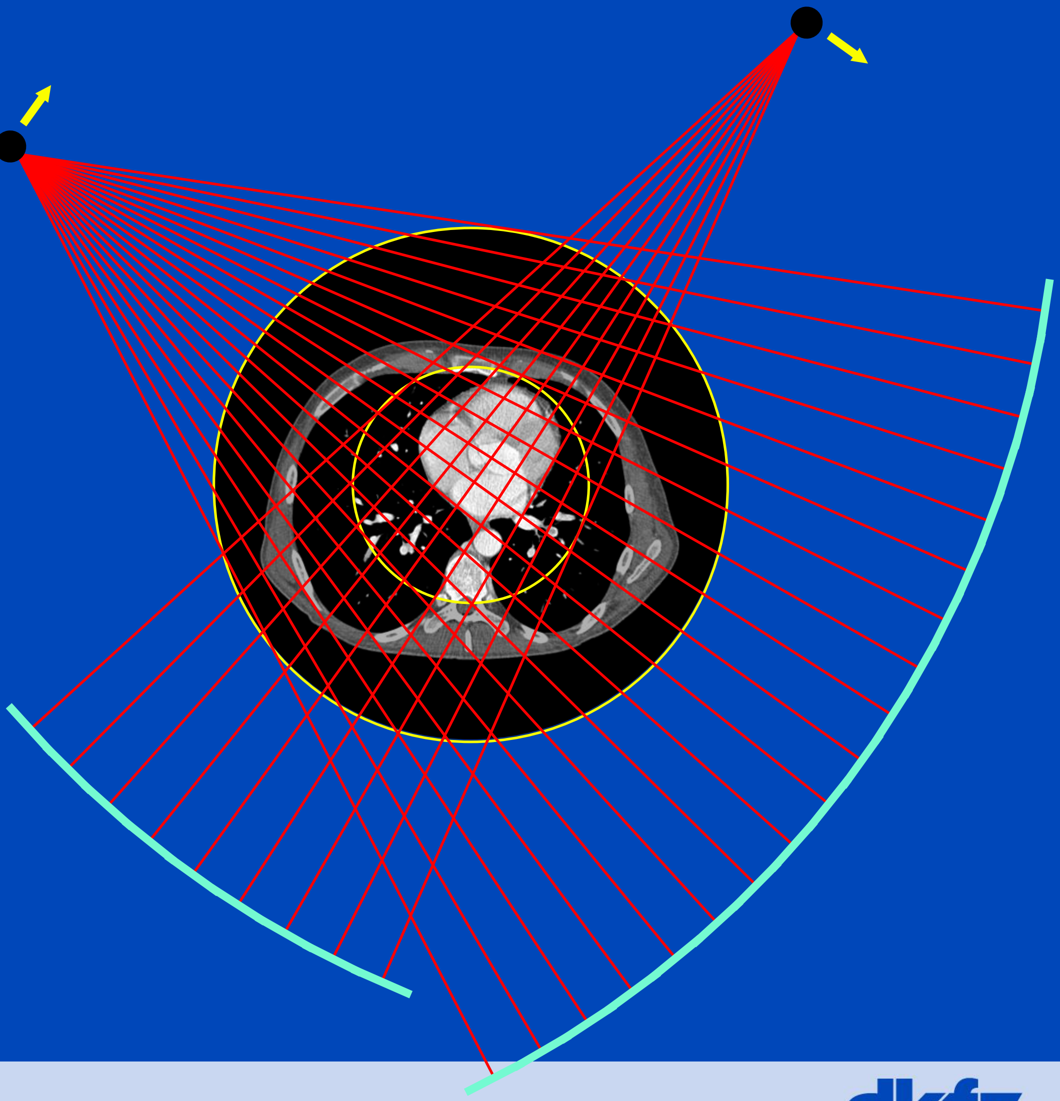

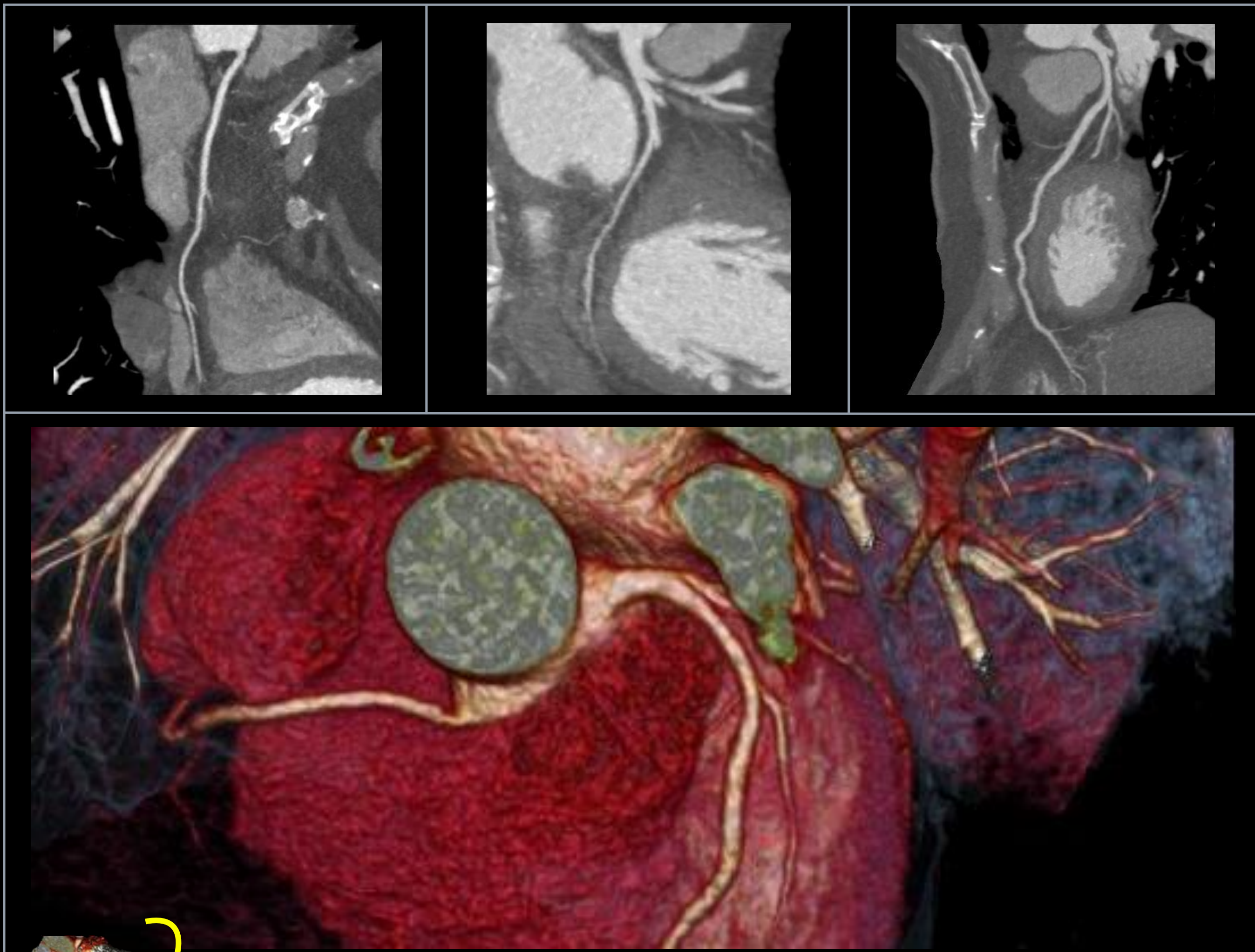

Adult

Temporal resolution: 75 ms
Collimation: 2·64×0.6 mm
Spatial resolution: 0.6 mm
Scan time: 0.28 s
Scan length: 128 mm
Rotation time: 0.28 s
80 kV, 300 mAs / rotation

Flash Spiral

Eff. dose: 0.36 mSv

Courtesy of Sir Run Run Shaw University HongKong / HongKong, China

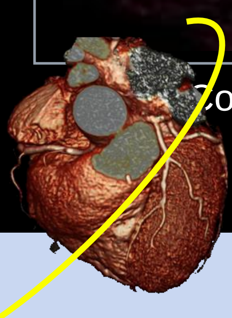

DSCT = Best Possible Cardiac CT

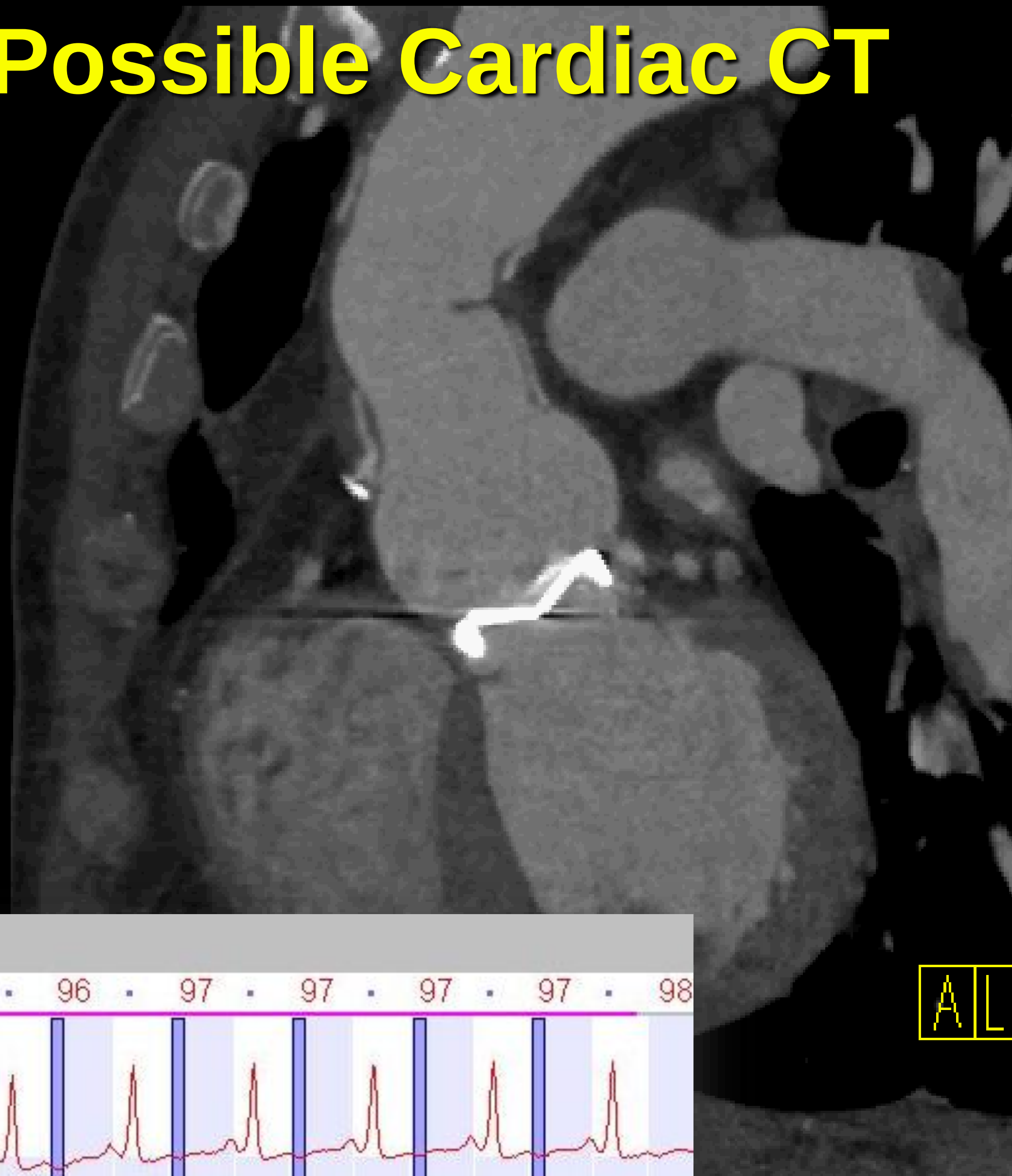

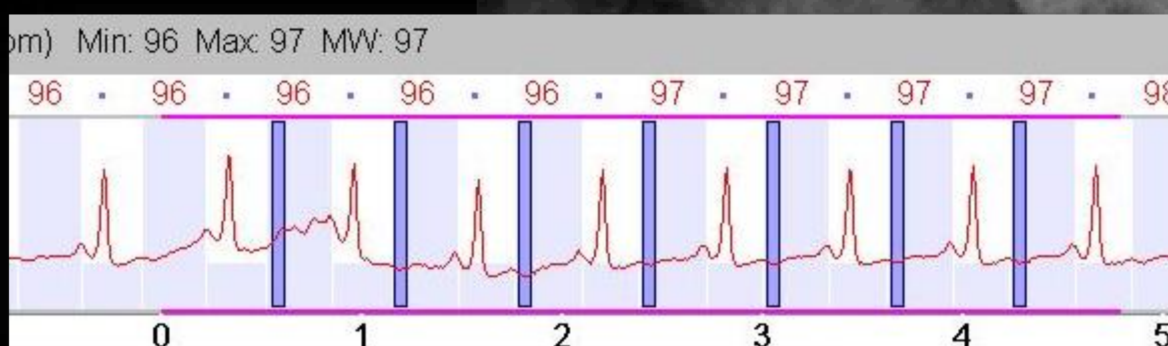

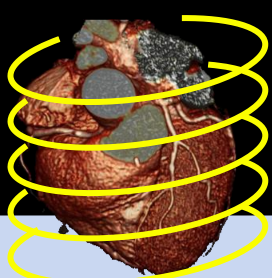

Data courtesy of Stephan Achenbach, Erlangen, Germany

DSCT = Best Possible Cardiac CT

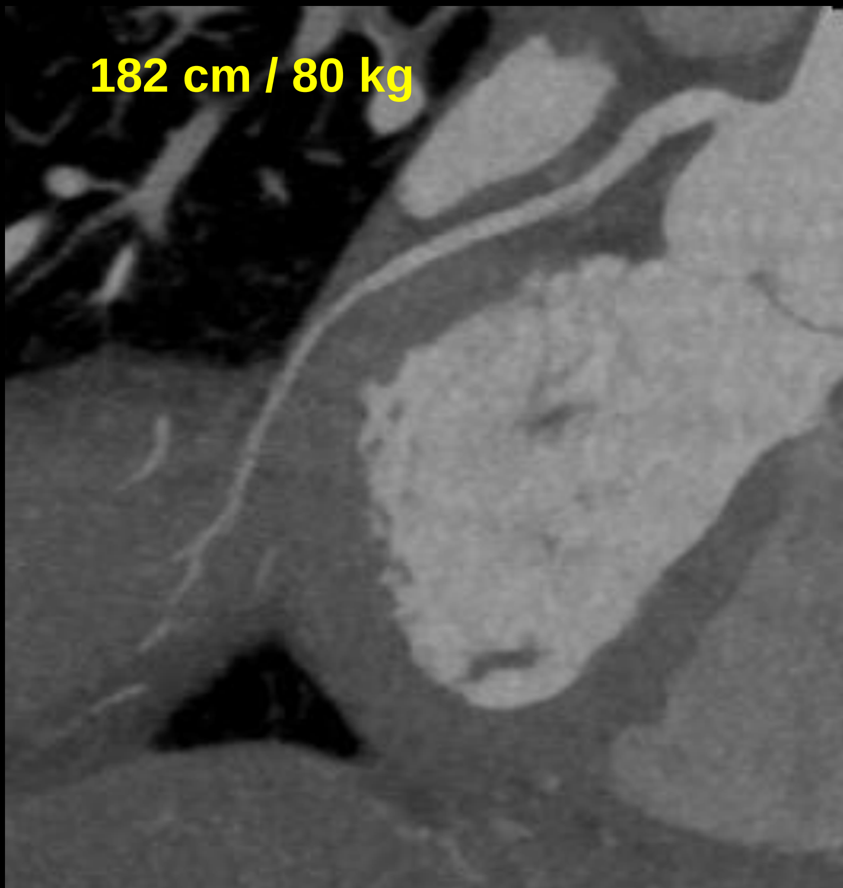

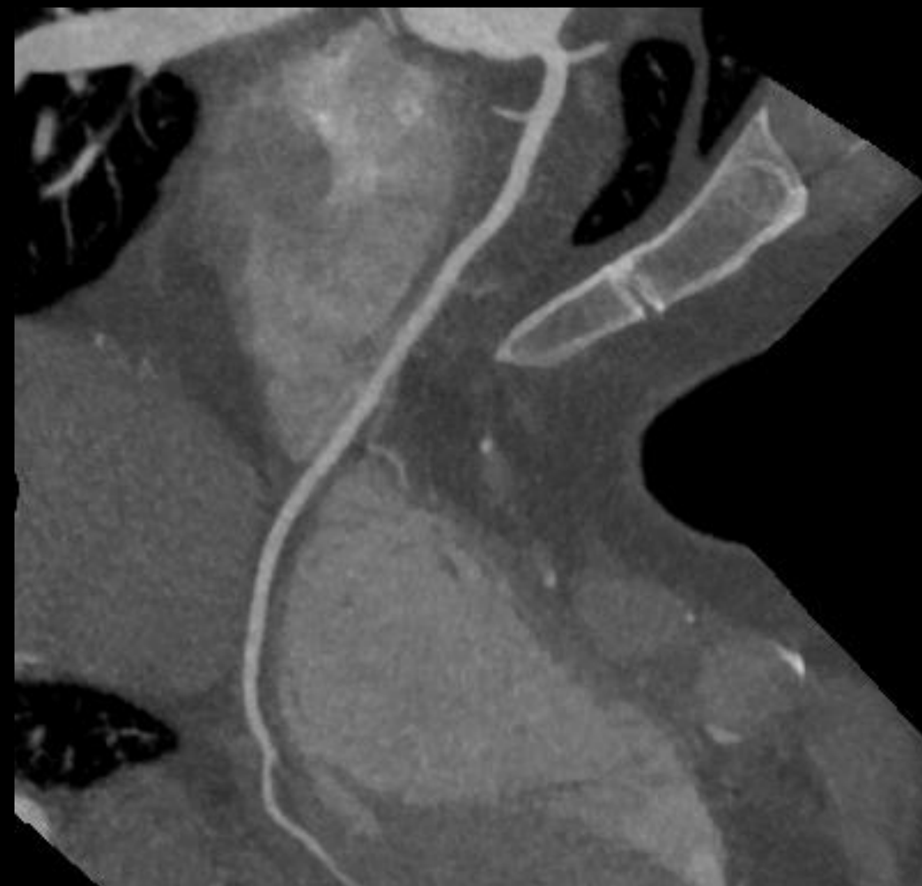

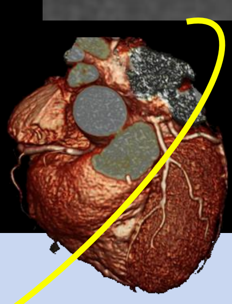

Emergency room patient,
70 kV, 450 mAs$_{eff}$ ref., 21 mGy cm, 0.3 mSv

Motion-Compensated (MoCo) Image Reconstruction

- **Main progress:**
  - Since about 2005
  - Still ongoing

Motivation

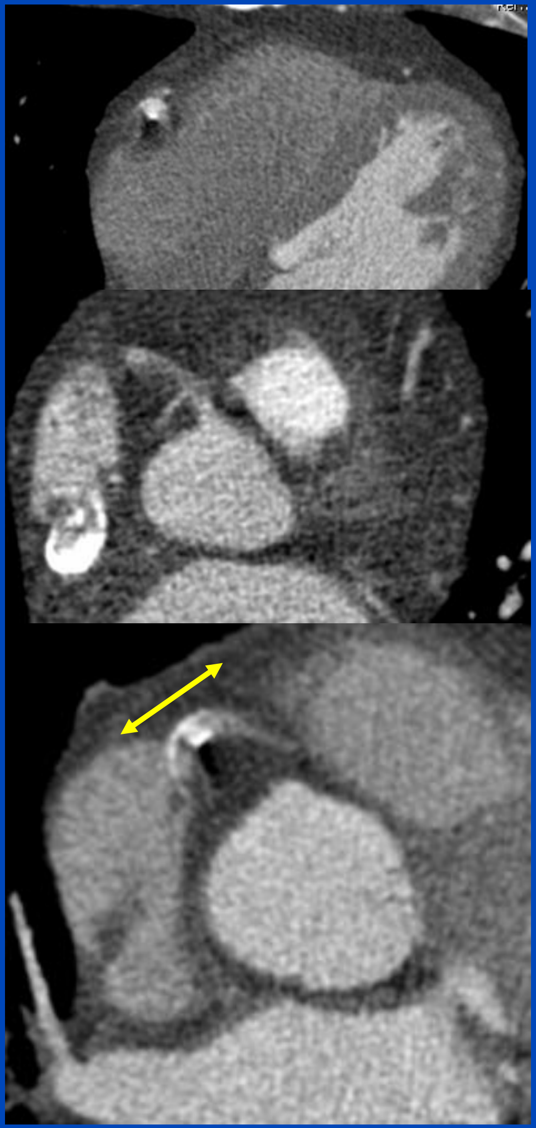

- In cardiac CT, the imaging of small and fast moving vessels places high demands on the spatial and temporal resolution of the reconstruction.
- Mean displacements of $d \approx \frac{trot}{2}\,\bar{v} \approx \frac{250}{2}\,\mathrm{ms}\; 50\,\frac{\mathrm{mm}}{\mathrm{s}} = 6.25\,\mathrm{mm}$ are possible according to RCA mean velocity measurements[1,2,3,4].
- Standard FDK-based cardiac reconstruction might have an insufficient temporal resolution introducing strong motion artifacts.

[1]Achenbach et al. In-plane coronary arterial motion velocity: measurement with electron-beam CT. Radiology, Vol. 216, Aug 2000.
[2]Vembar et al. A dynamic approach to identifying desired physiological phases for cardiac imaging using multislice spiral CT. Med. Phys. 30, Jul 2003.
[3]Shechter et al. Displacement and Velocity of the Coronary Arteries: Cardiac and Respiratory Motion. IEEE Trans Med Imaging, 25(3): 369-375, Mar 2006.
[4]Husmann et al. Coronary Artery Motion and Cardiac Phases: Dependency on Heart Rate - Implications for CT Image Reconstruction. Radiology, Vol. 245, Nov 2007.

Partial Angle-Based Motion Compensation (PAMoCo)

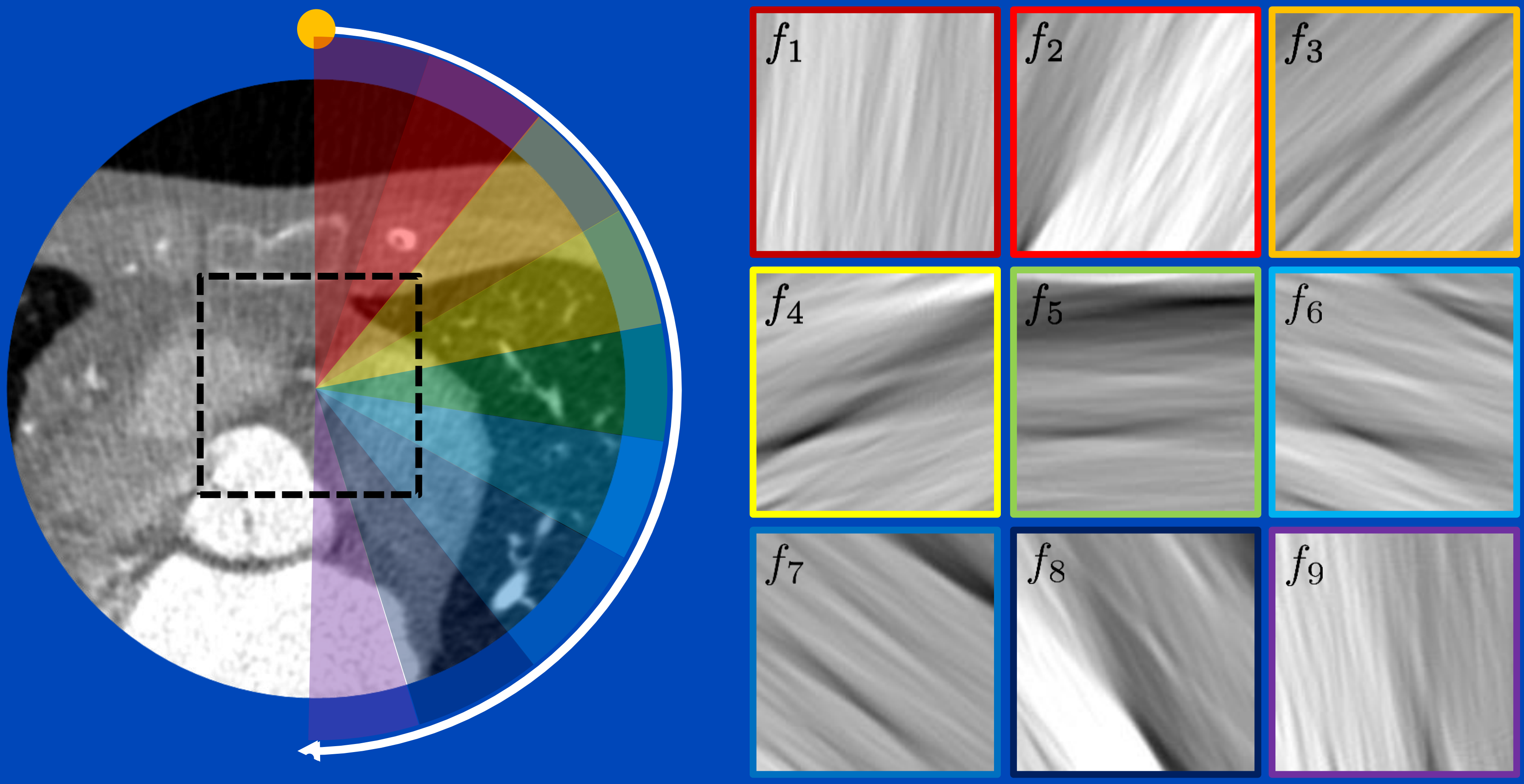

Animated rotation time = 100 × real rotation time

Partial Angle-Based Motion Compensation (PAMoCo)

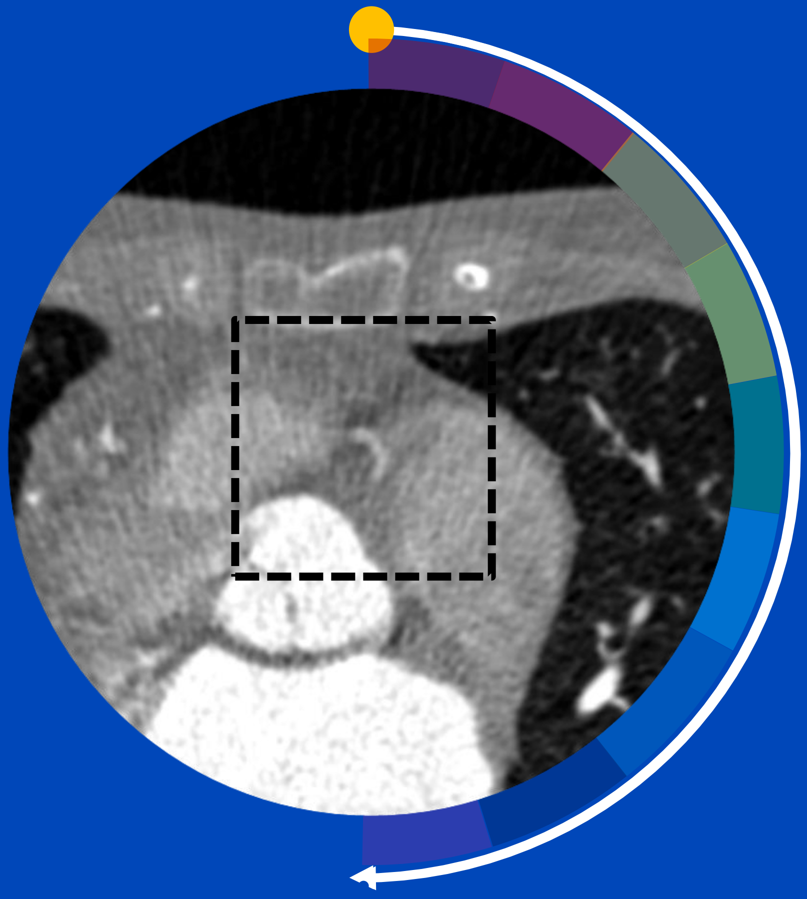

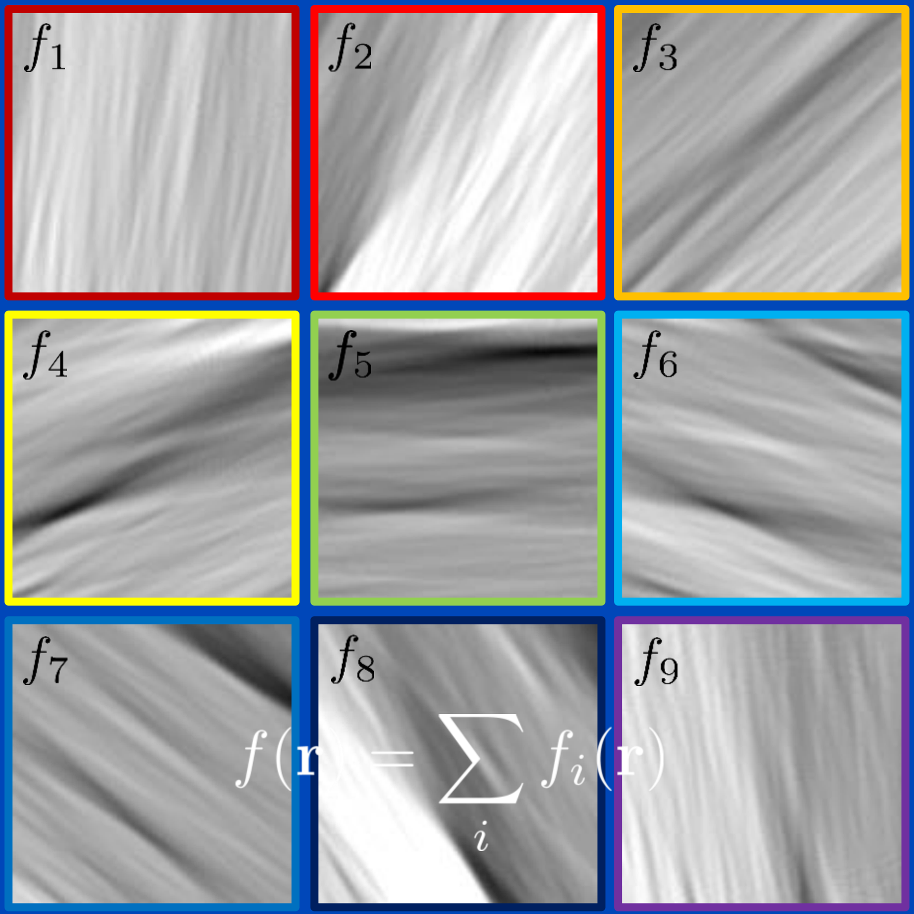

Partial Angle-Based Motion Compensation (PAMoCo)

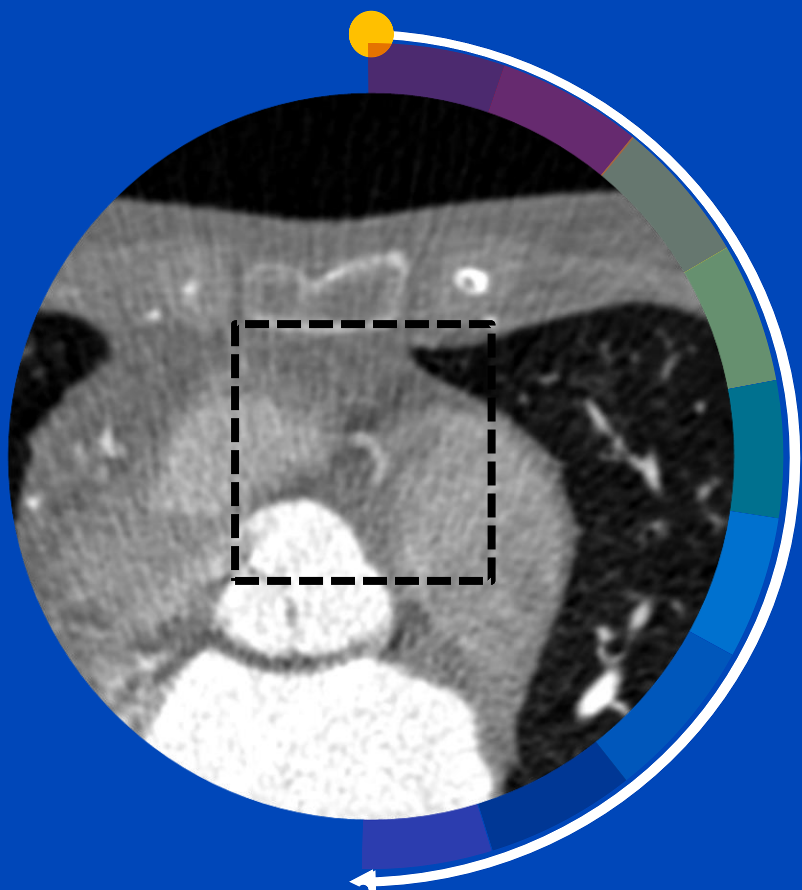

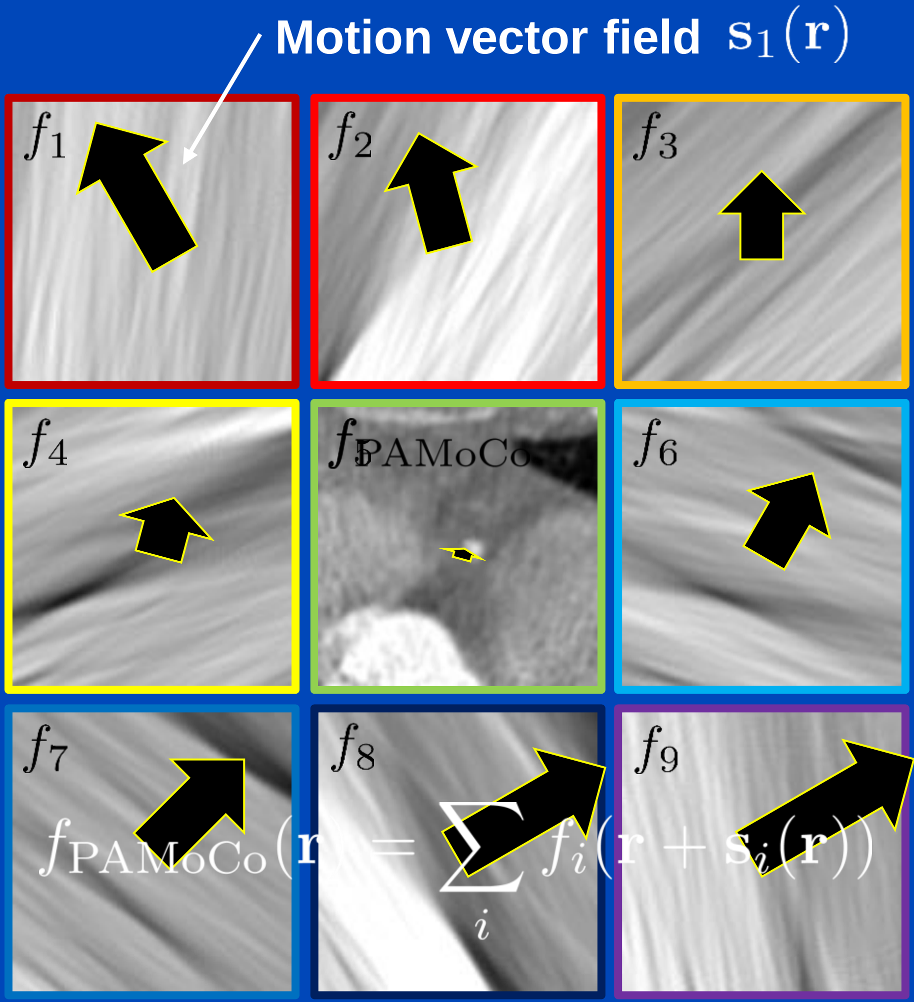

$$f_{\mathrm{PAMoCo}}(\mathbf{r}) = \sum_i f_i(\mathbf{r} + \mathbf{s}_i(\mathbf{r}))$$

Apply motion vector fields (MVFs) to partial angle reconstructions

dkfz.

Phantom Measurement

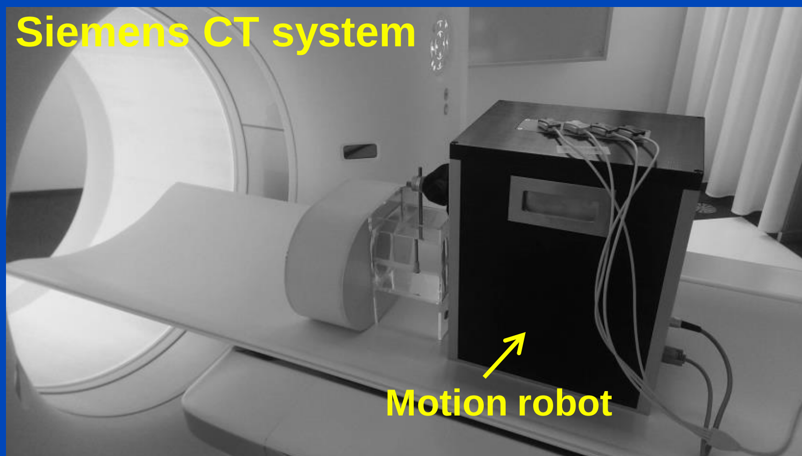

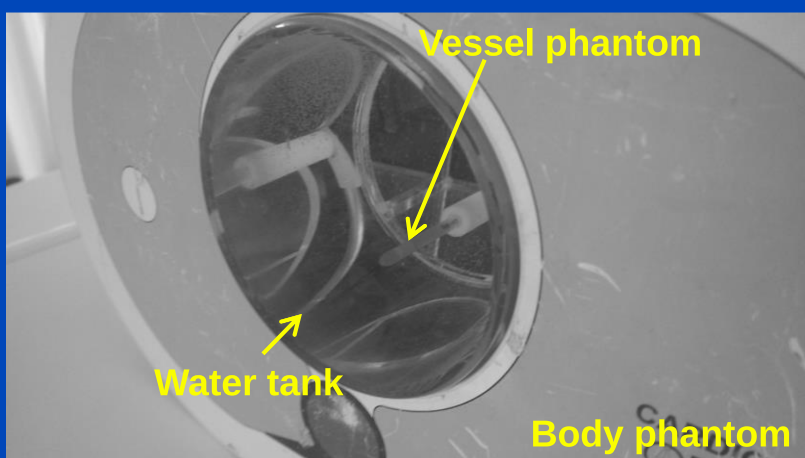

d = 1.5 mm 2.5 mm 3 mm

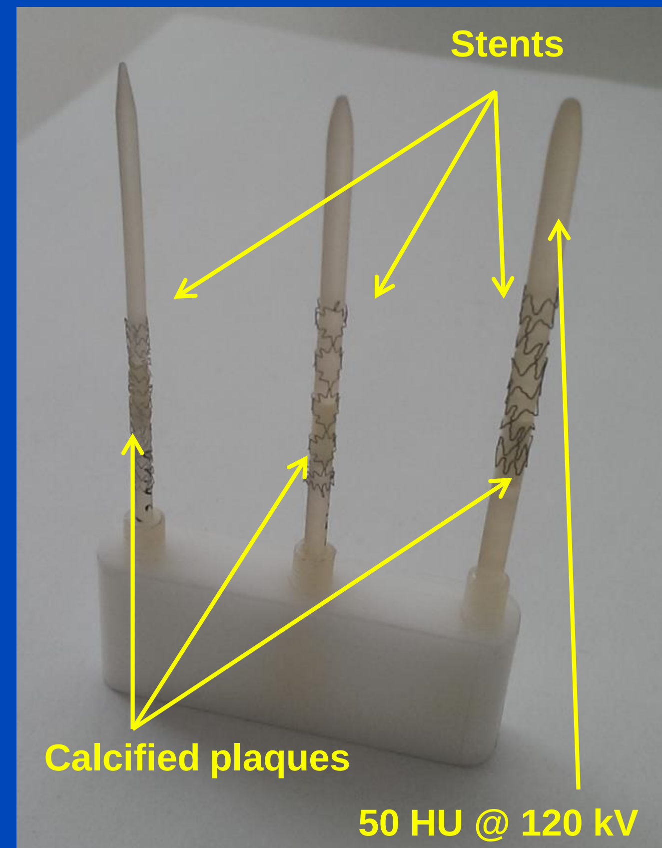

Phantom

Best Phase

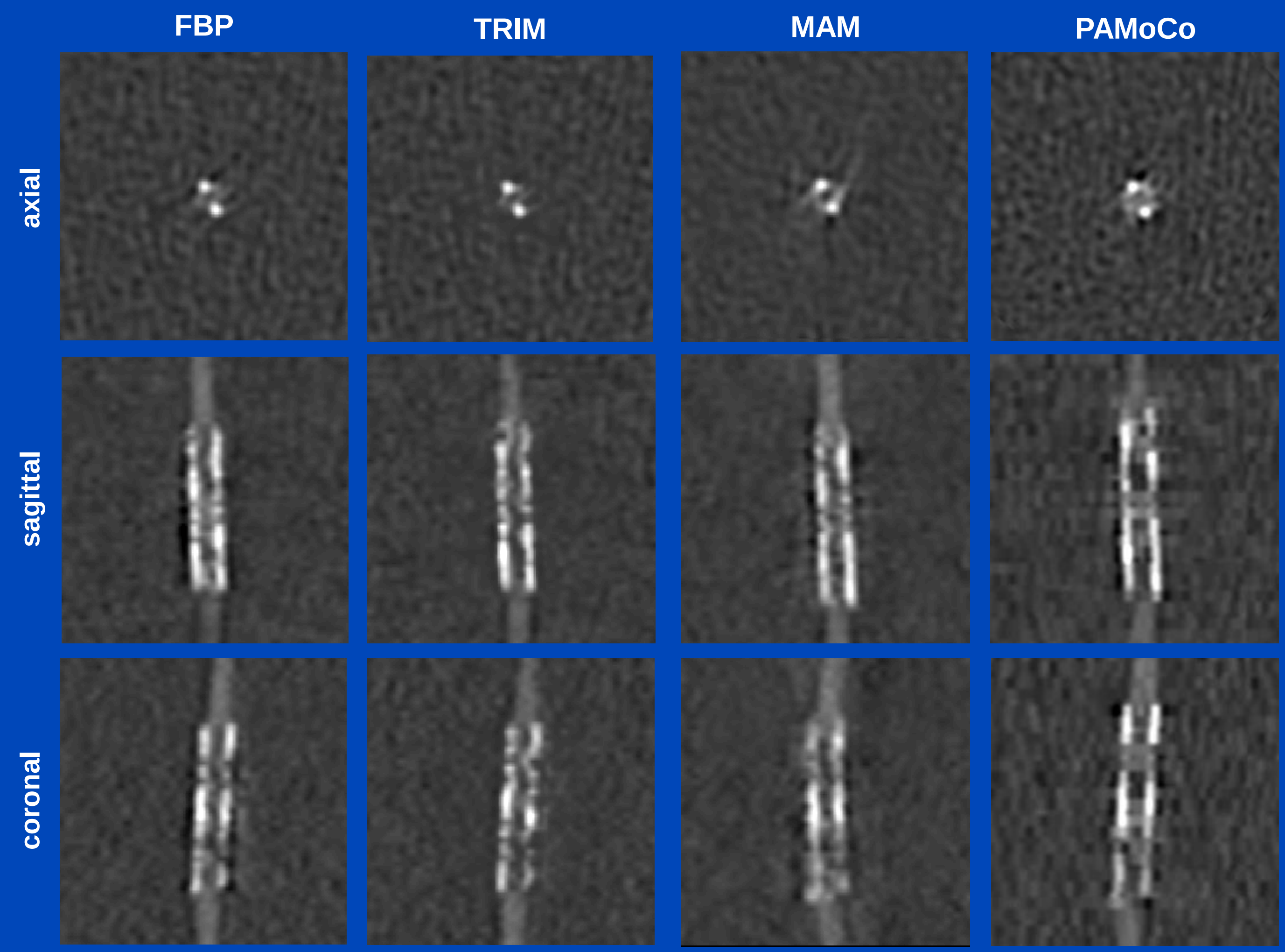

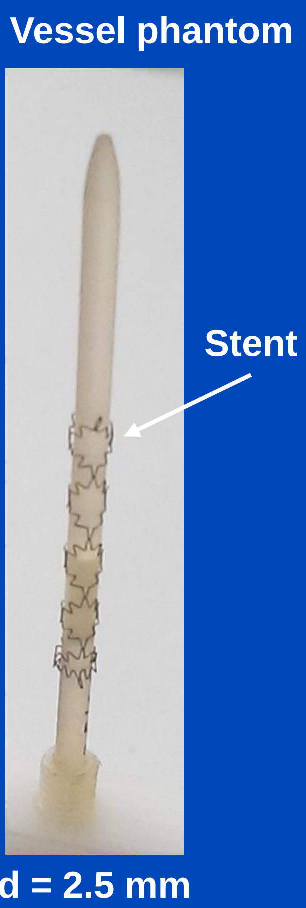

$\overline{\text{HR}}$ = 74 bpm, c = 74%,
C = 400 HU, W = 1500 HU

PAMoCo with $N_t \times N_\lambda \times 3 = 3 \times 3 \times 3 = 27$
parameter each stack

Phantom

5% off Best Phase

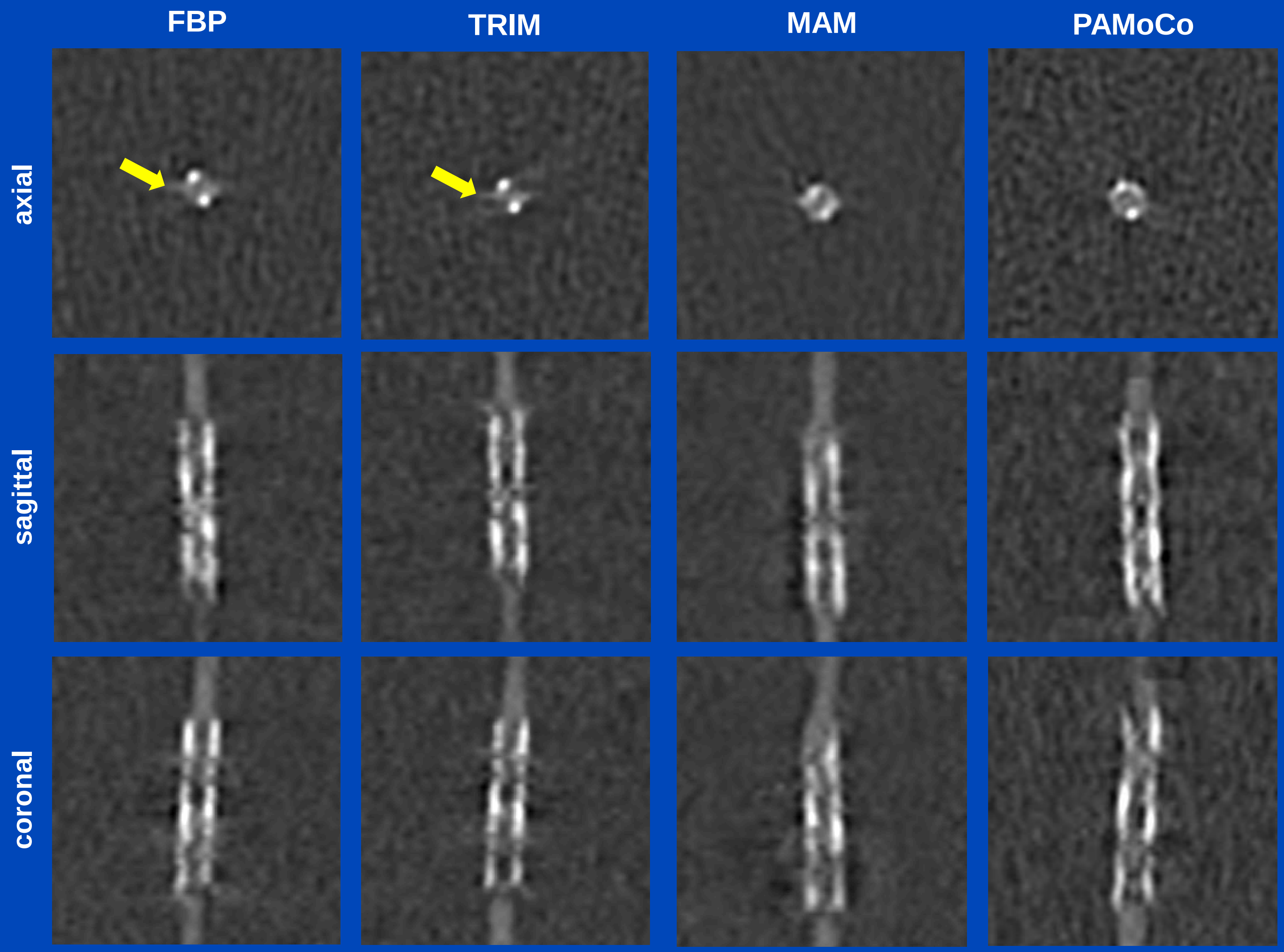

Vessel phantom

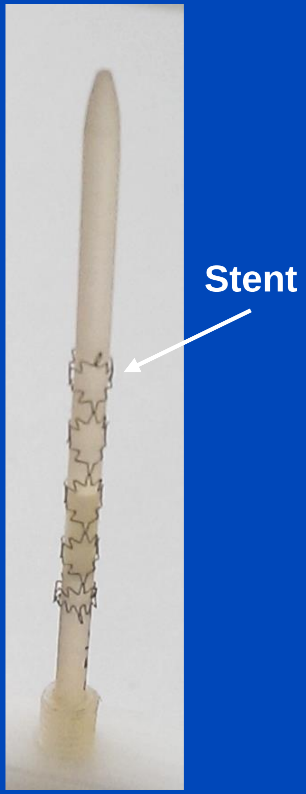

d = 2.5 mm

SIEMENS

$\overline{HR}$ = 74 bpm, c = 74%,
C = 400 HU, W = 1500 HU

PAMoCo with $N_t \times N_\lambda \times 3 = 3 \times 3 \times 3 = 27$
parameter each stack

dkfz.

Phantom

10% off Best Phase

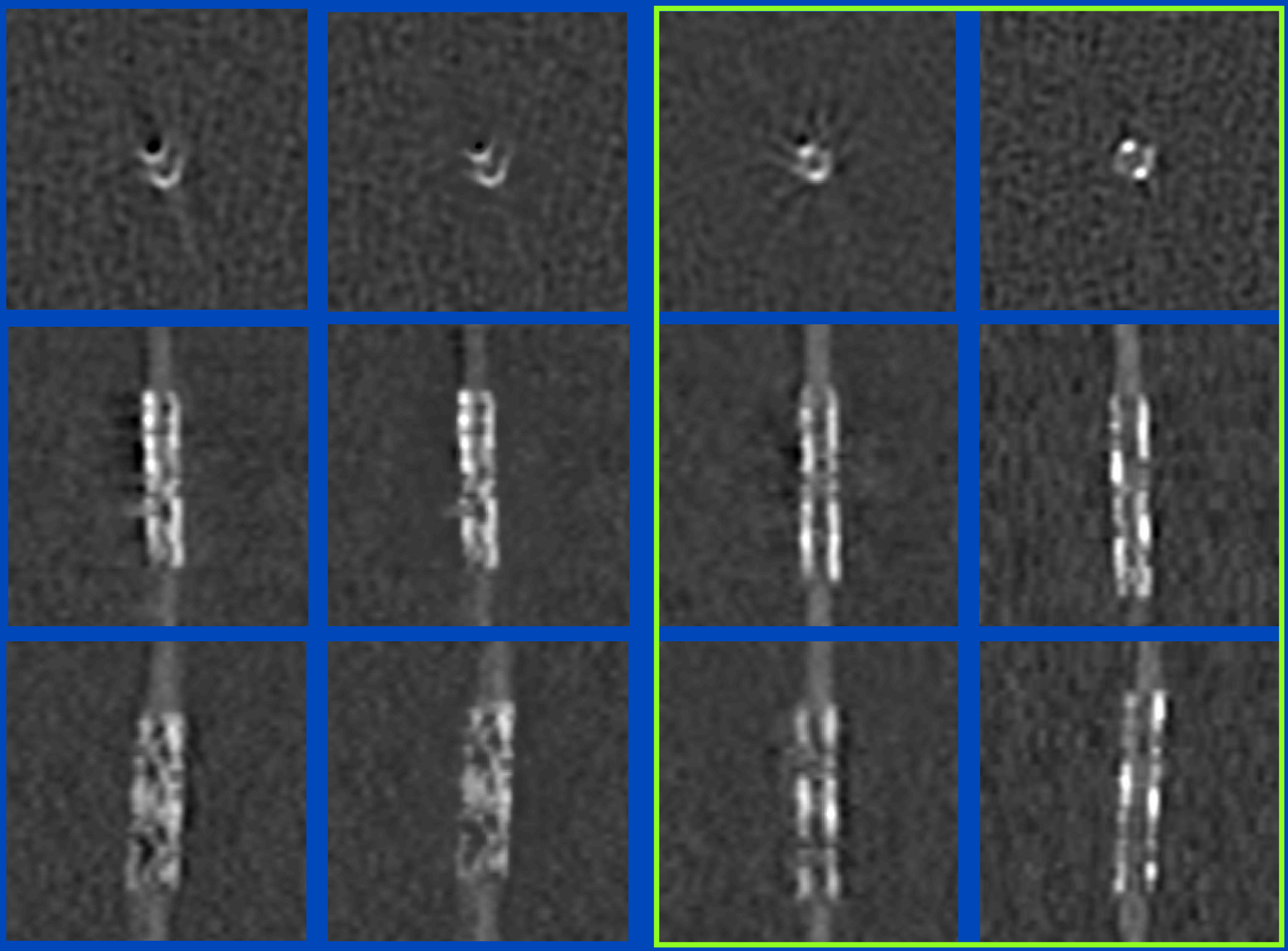

Vessel phantom

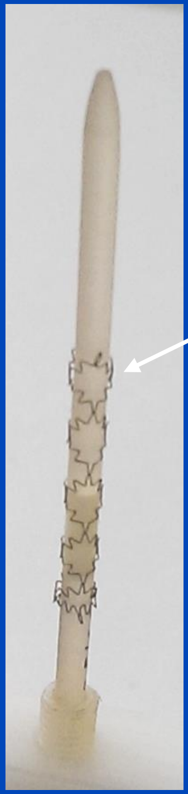

d = 2.5 mm

$\overline{HR}$ = 74 bpm, c = 74%,
C = 400 HU, W = 1500 HU

PAMoCo with $N_t \times N_\lambda \times 3 = 3 \times 3 \times 3 = 27$
parameter each stack

Deep Partial Angle-Based Motion Compensation (Deep PAMoCo)

PARs centered around coronary artery

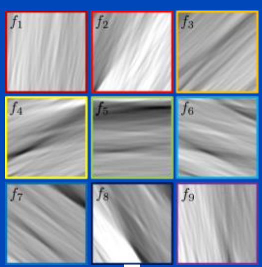

Neural network to predict parameters of a motion model

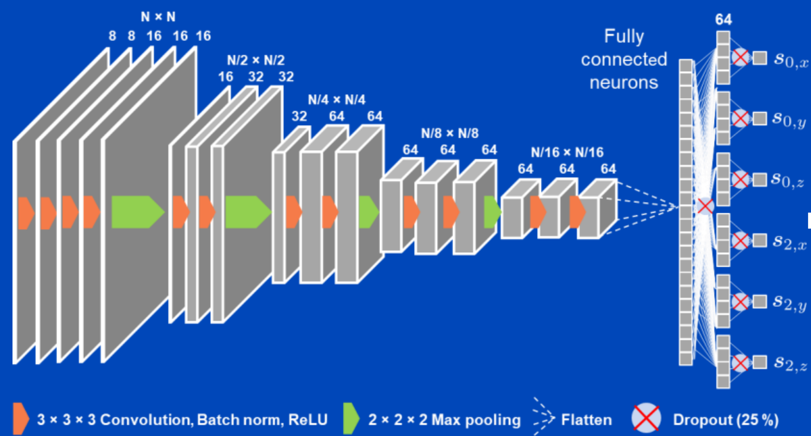

Reinsertion of patch into initial reconstruction

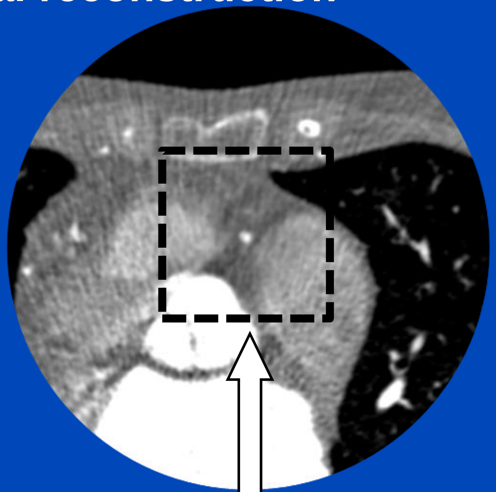

Spatial transformer

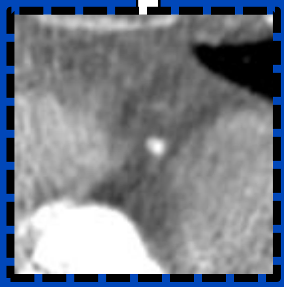

Application of the motion model to the PARs via a spatial transformer[1]

[1] M. Jaderberg et al., "Spatial transformer networks", NIPS 2015: 2017–2025 (2015).

Patient 2

FBP

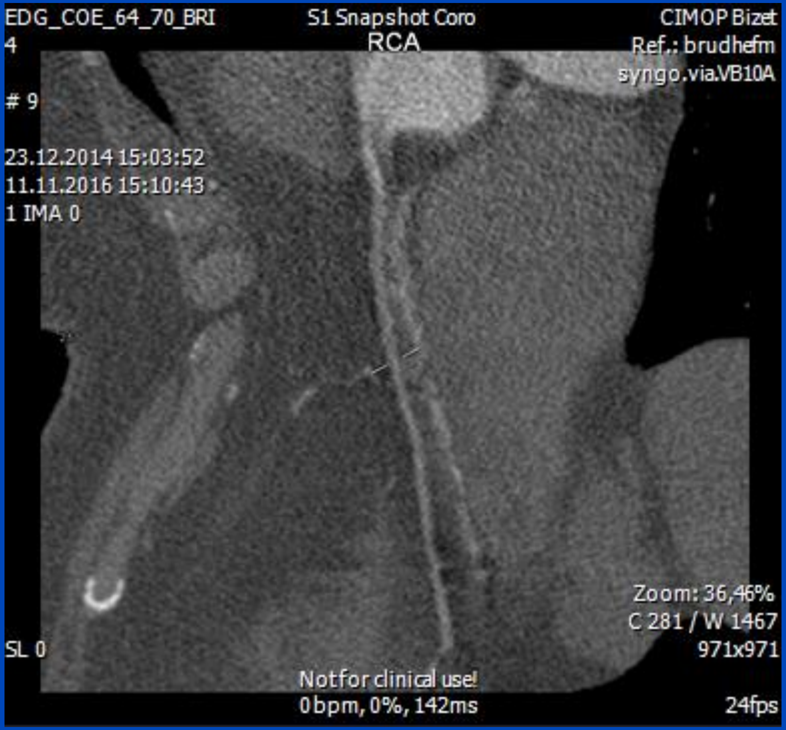

PAMoCo

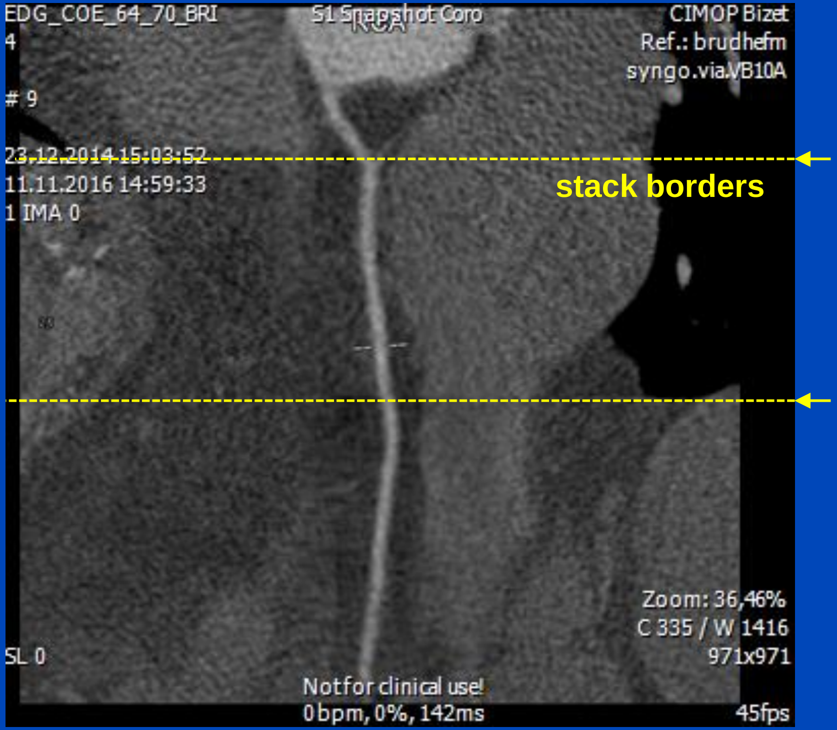

curved MPRs created with syngo.via

Patient 6

Original

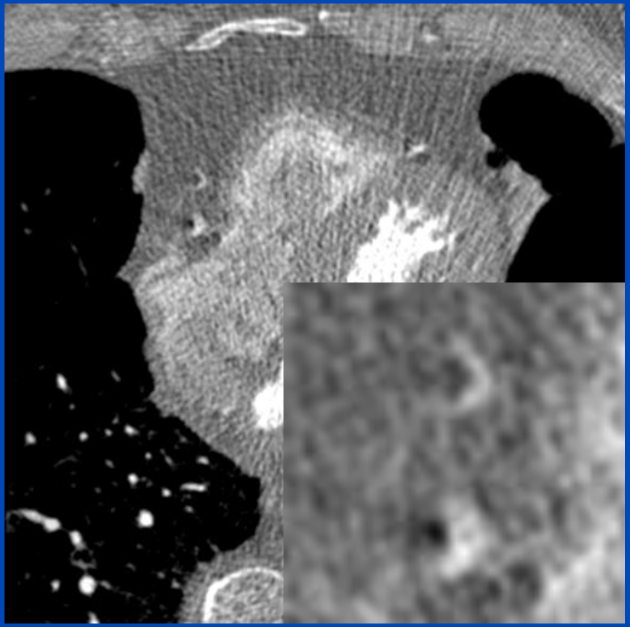

Deep PAMoCo

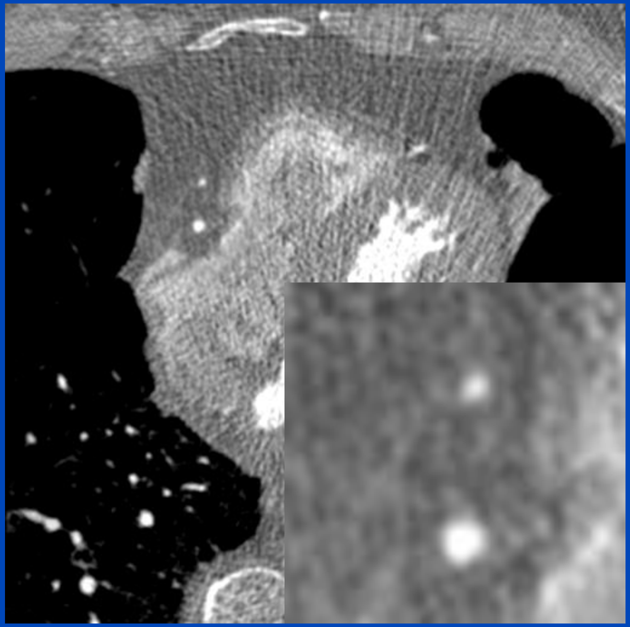

C = 0 HU, *W* = 1400 HU

J. Maier, S. Lebedev, J. Erath, E. Eulig, S. Sawall, E. Fournié, K. Stierstorfer, M. Lell, and M. Kachelrieß. Deep learning-based coronary artery motion estimation and compensation for short-scan cardiac CT. Med. Phys. 48(7):3559-3571, July 2021.

Patient 7

Original

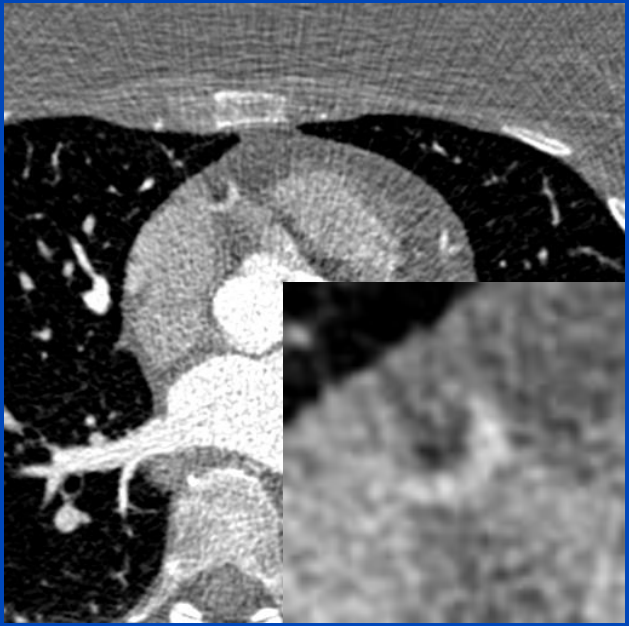

Deep PAMoCo

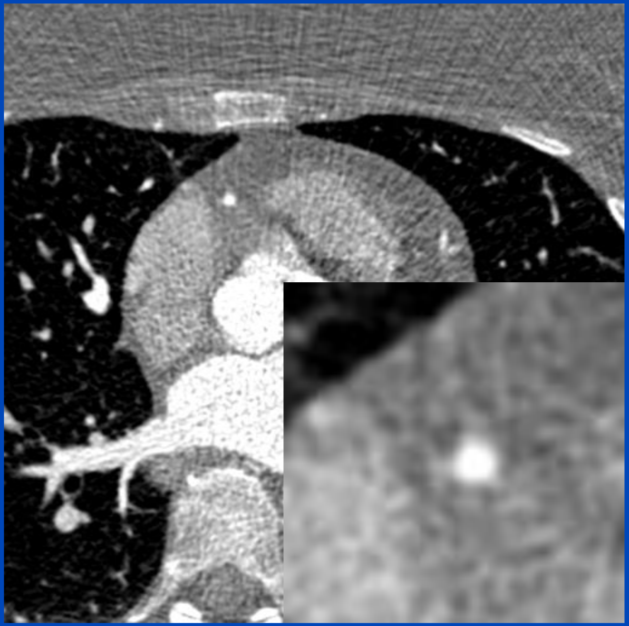

C = 0 HU, *W* = 1600 HU

J. Maier, S. Lebedev, J. Erath, E. Eulig, S. Sawall, E. Fournié, K. Stierstorfer, M. Lell, and M. Kachelrieß. Deep learning-based coronary artery motion estimation and compensation for short-scan cardiac CT. Med. Phys. 48(7):3559-3571, July 2021.

Patient 8

Original

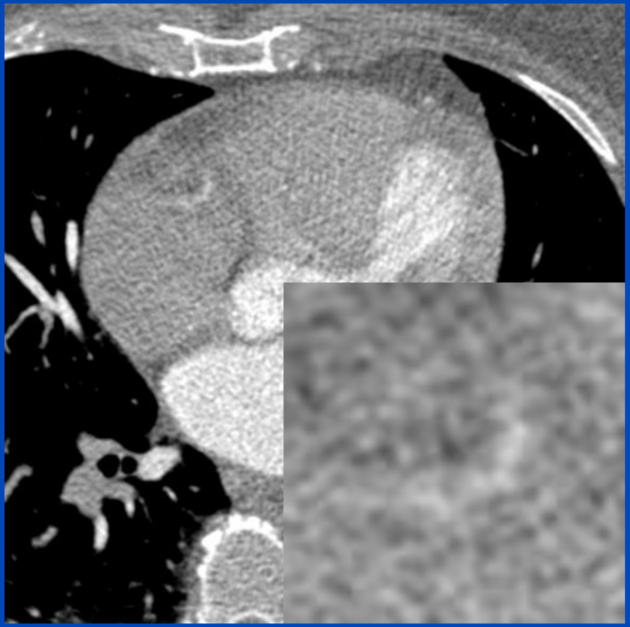

Deep PAMoCo

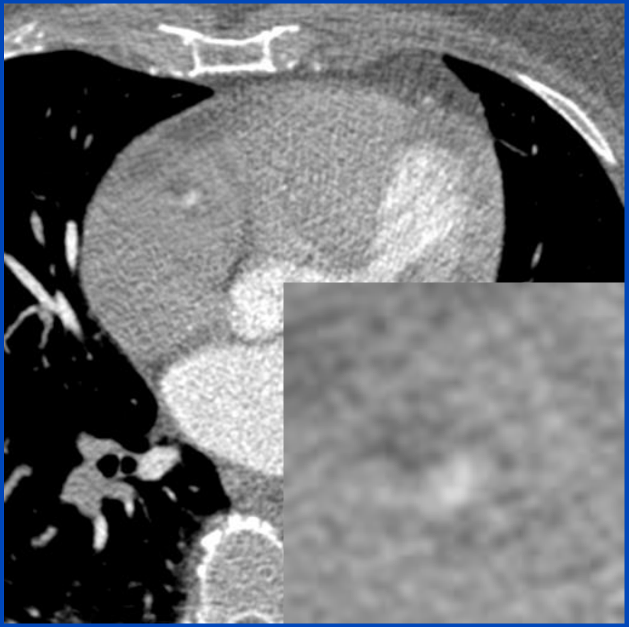

C = 0 HU, *W* = 1000 HU

J. Maier, S. Lebedev, J. Erath, E. Eulig, S. Sawall, E. Fournié, K. Stierstorfer, M. Lell, and M. Kachelrieß. Deep learning-based coronary artery motion estimation and compensation for short-scan cardiac CT. Med. Phys. 48(7):3559-3571, July 2021.

Motion Management for CBCT in IGRT

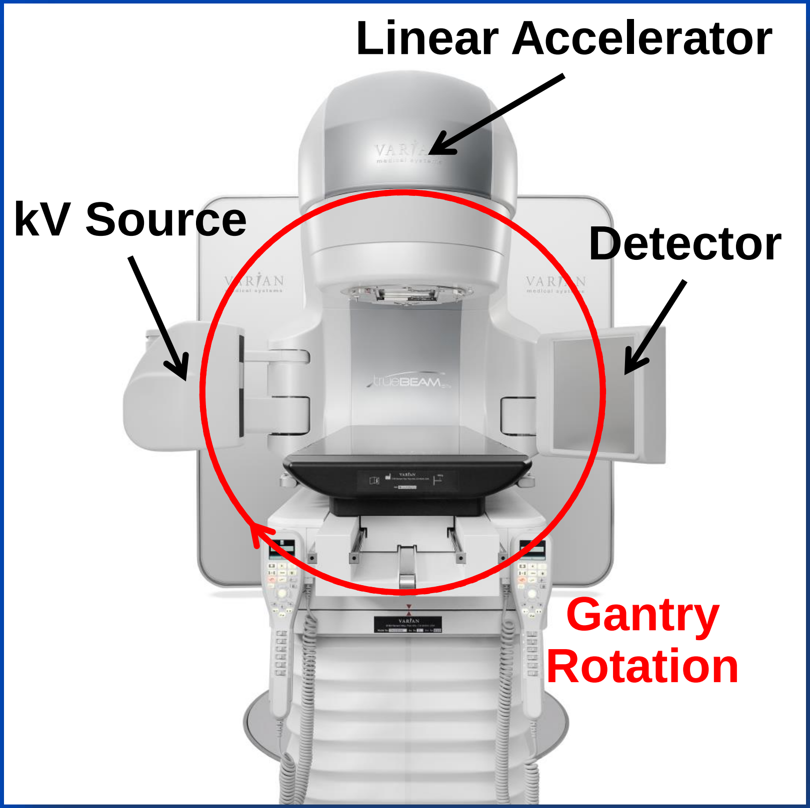

4D CBCT Scan with Retrospective Gating

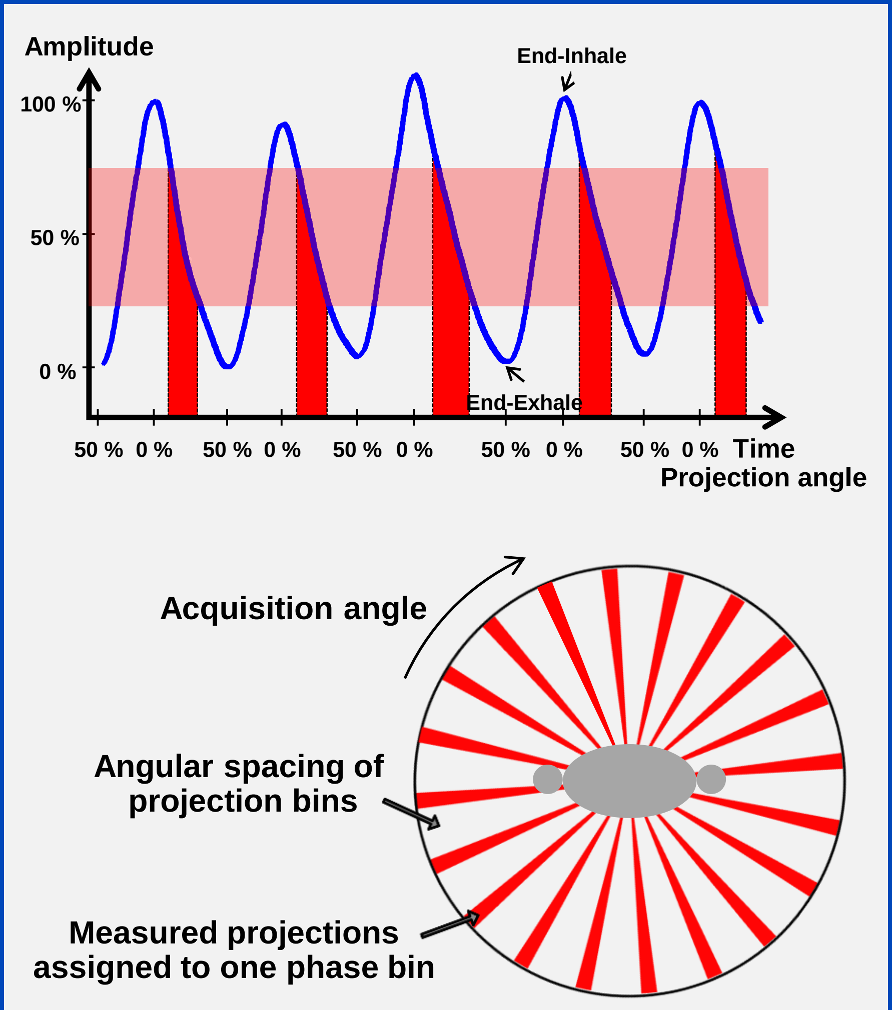

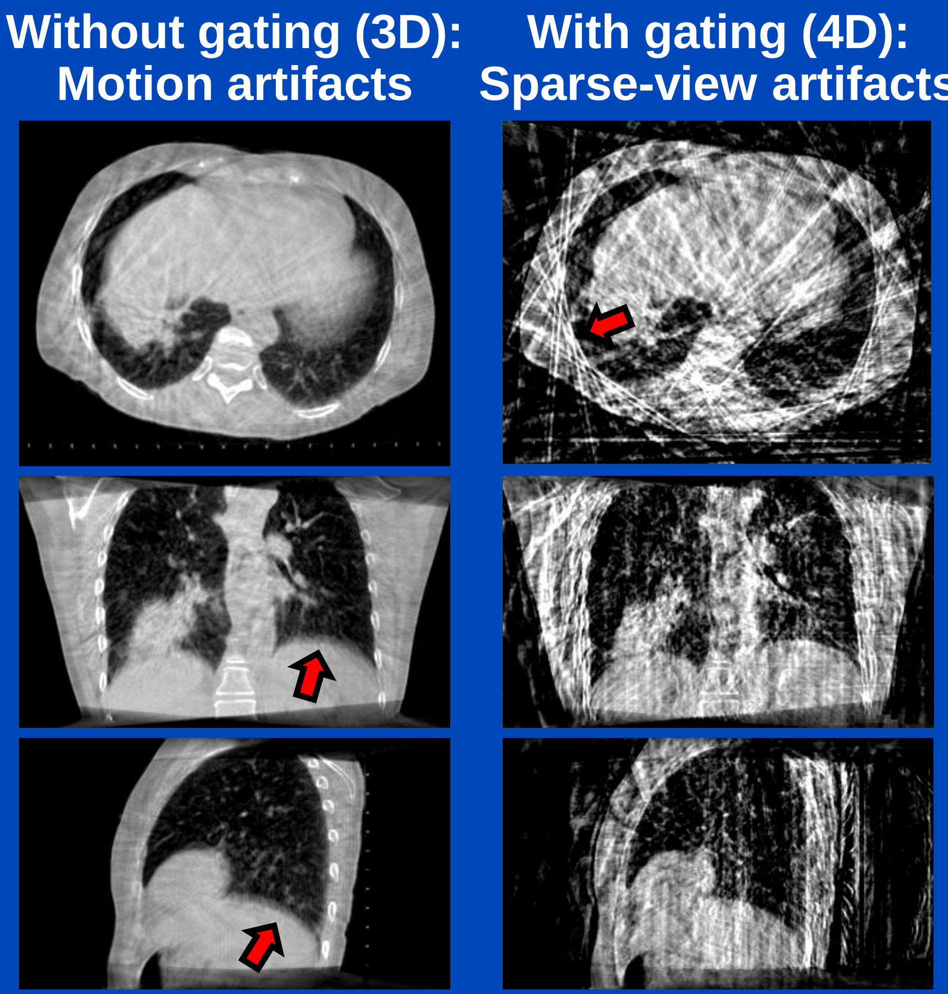

A Standard Motion Estimation and Compensation Approach (sMoCo)

- Motion estimation via standard 3D-3D registration

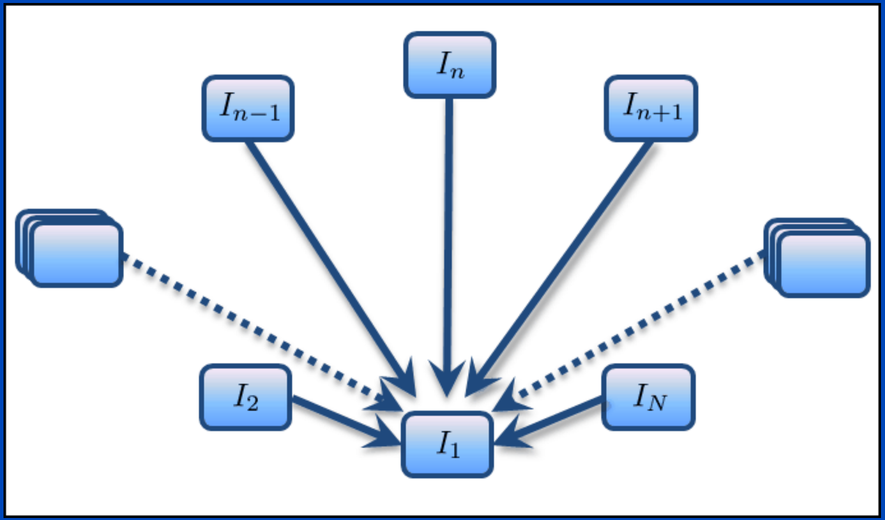

- Has to be repeated for each reconstructed phase

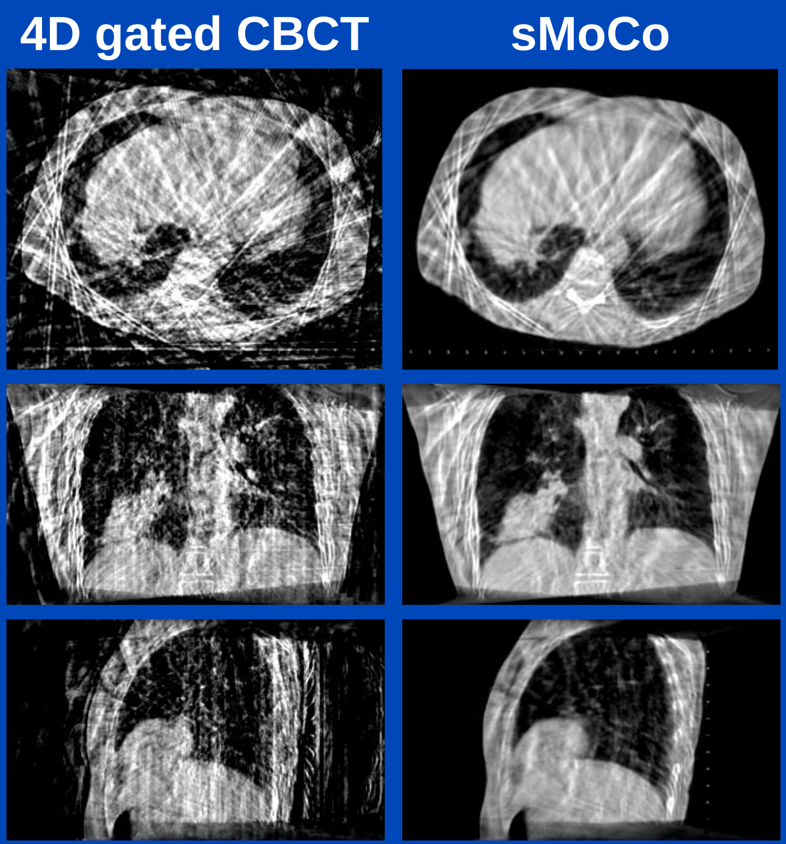

- Streak artifacts from gated reconstructions propagate into sMoCo results

Li, Koong, and Xing, "Enhanced 4D cone–beam CT with inter–phase motion model," Med. Phys. 51(9), 3688–3695 (2007).

The Cyclic Motion Estimation and Compensation Approach (cMoCo)

- Motion estimation only between adjacent phases
- Incorporate additional knowledge
  - A priori knowledge of quasi periodic breathing pattern
  - Non-cyclic motion is penalized
  - Error propagation due to concatenation is reduced

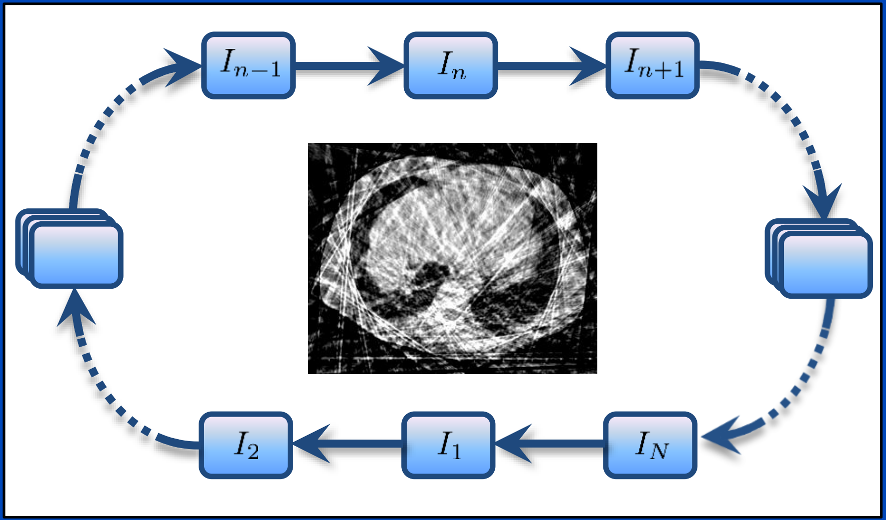

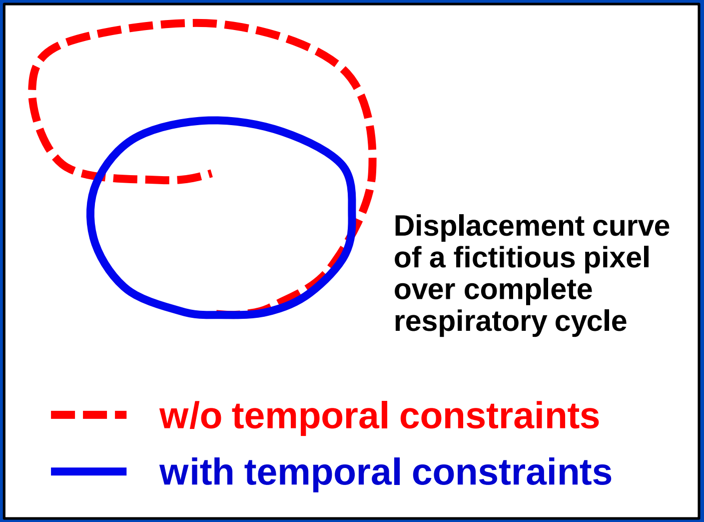

Brehm, Paysan, Oelhafen, Kunz, and Kachelrieß, "Self-adapting cyclic registration for motion-compensated cone-beam CT in image-guided radiation therapy," Med. Phys. 39(12):7603-7618, 2012.

dkfz.

Artifact Model-Based MoCo (aMoCo)

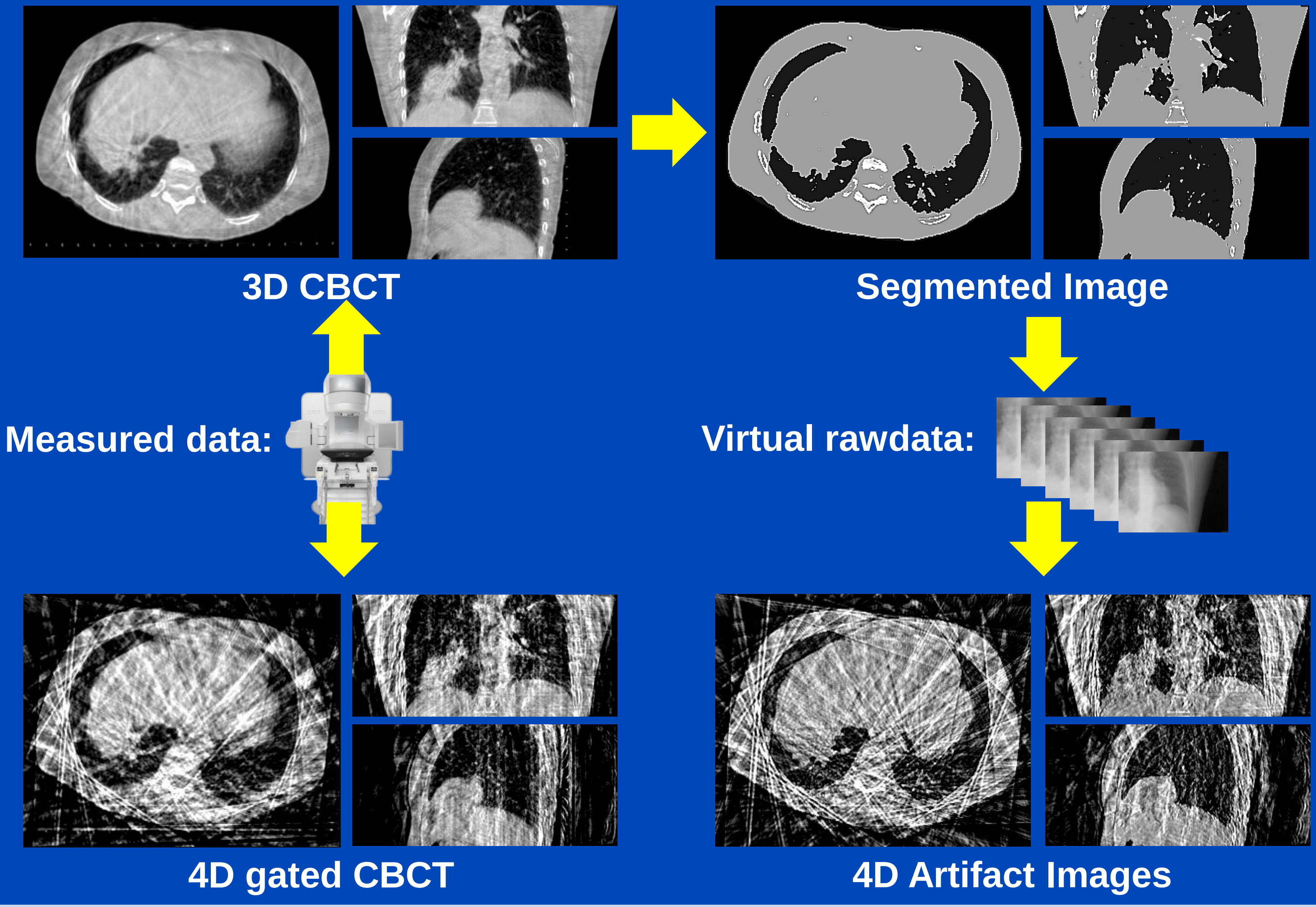

Brehm, Paysan, Oelhafen, and Kachelrieß, "Artifact-resistant motion estimation with a patient-specific artifact model for motion-compensated cone-beam CT" Med. Phys. 40(10):101913, 2013.

Examples for CBCT MoCo

3D CBCT Standard	4D gated CBCT Conventional Phase-Correlated	sMoCo Standard Motion Compensation	acMoCo Artifact Model-Based Motion Compensation

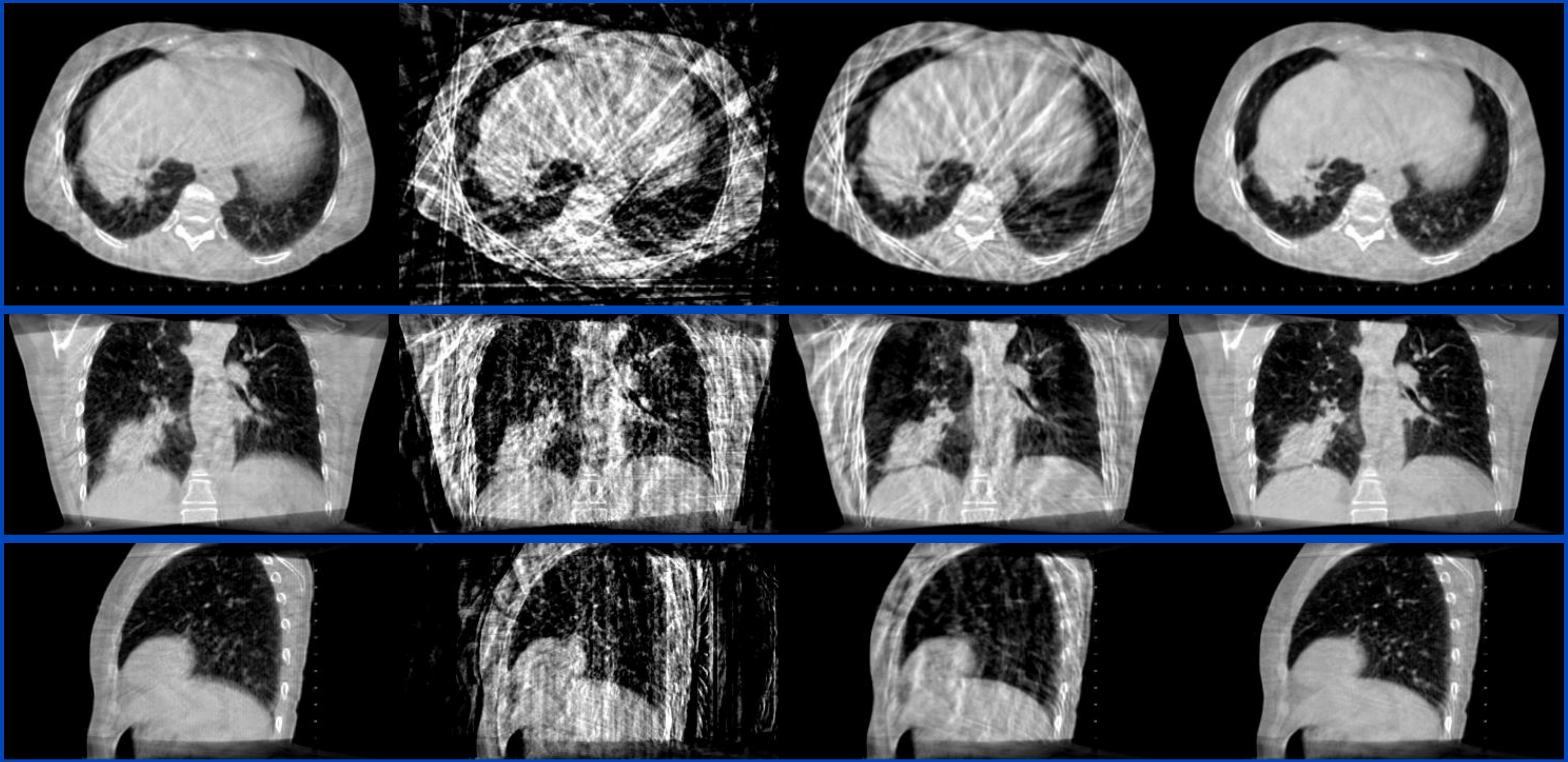

sMoCo: Li, Koong, and Xing, “Enhanced 4D cone–beam CT with inter–phase motion model,” Med. Phys. 51(9), 3688–3695, 2007.
cMoCo: Brehm, Paysan, Oelhafen, Kunz, and Kachelrieß, “Self-adapting cyclic registration for motion-compensated cone-beam CT in image-guided radiation therapy,” Med. Phys. 39(12):7603-7618, 2012.
acMoCo: Brehm, Paysan, Oelhafen, and Kachelrieß, “Artifact-resistant motion estimation with a patient-specific artifact model for motion-compensated cone-beam CT” Med. Phys. 40(10):101913, 2013.

1 min shifted detector CBCT scan with about 12 respiratory cycles, displayed with 30 rpm.
Patient data provided by Memorial Sloan–Kettering Cancer Center, New York, NY. C = -200 HU, W = 1400 HU

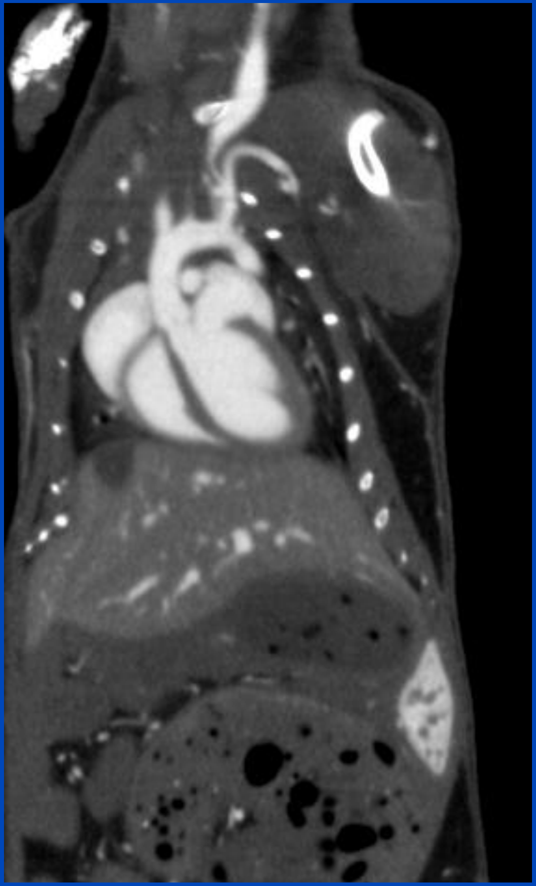

<u>Data displayed as:</u>

Heart: 280 bpm

Lung: 150 rpm

Mouse with 150 rpm and 280 bpm.

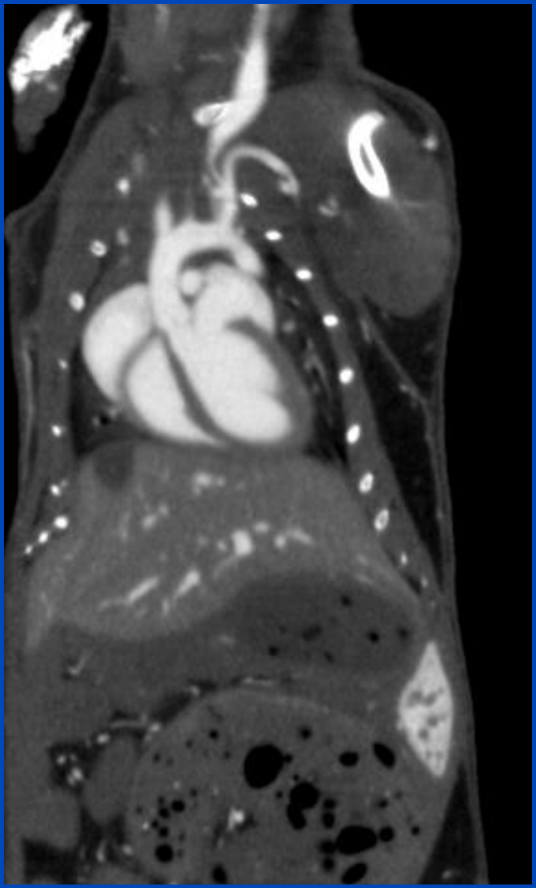

Data displayed as:

Heart: 180 bpm

Lung: 90 rpm

Mouse with 180 rpm and 240 bpm.

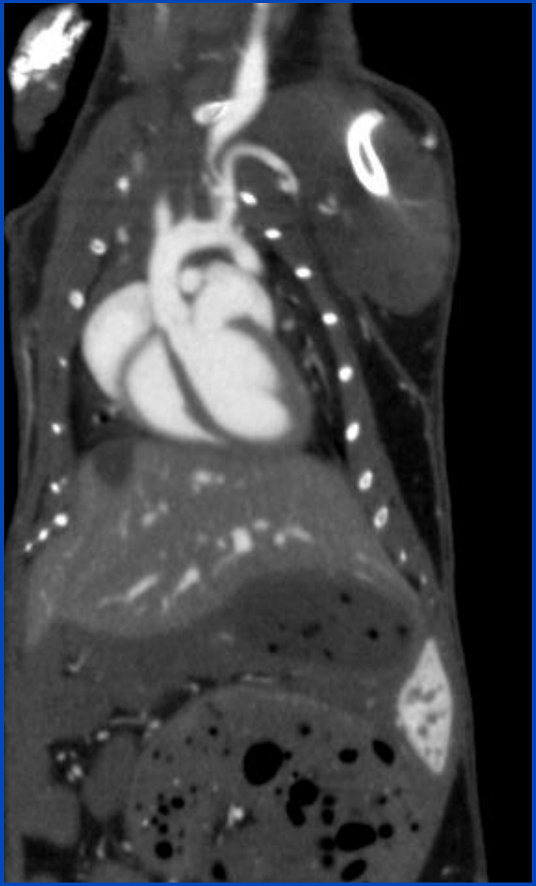

Data displayed as:

Heart: 90 bpm

Lung: 90 rpm

Mouse with 180 rpm and 240 bpm.

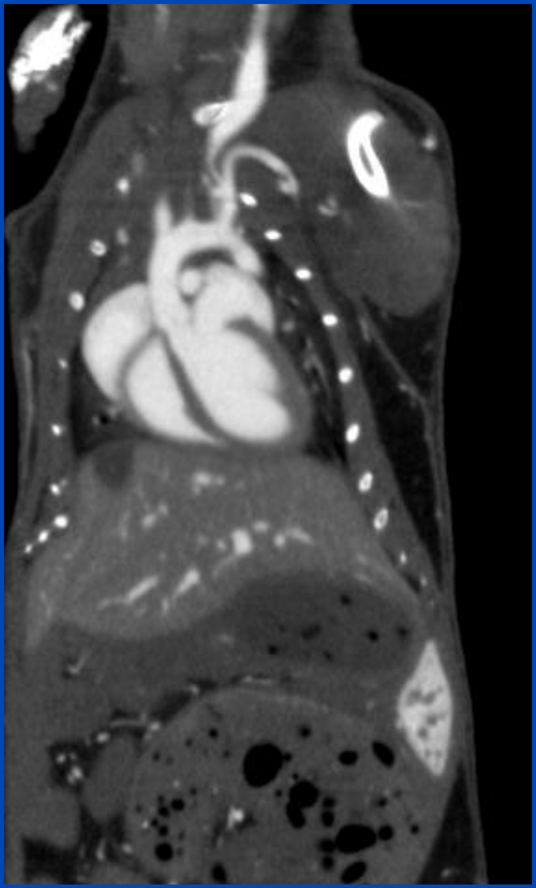

Data displayed as:

Heart: 0 bpm

Lung: 90 rpm

Mouse with 180 rpm and 240 bpm.

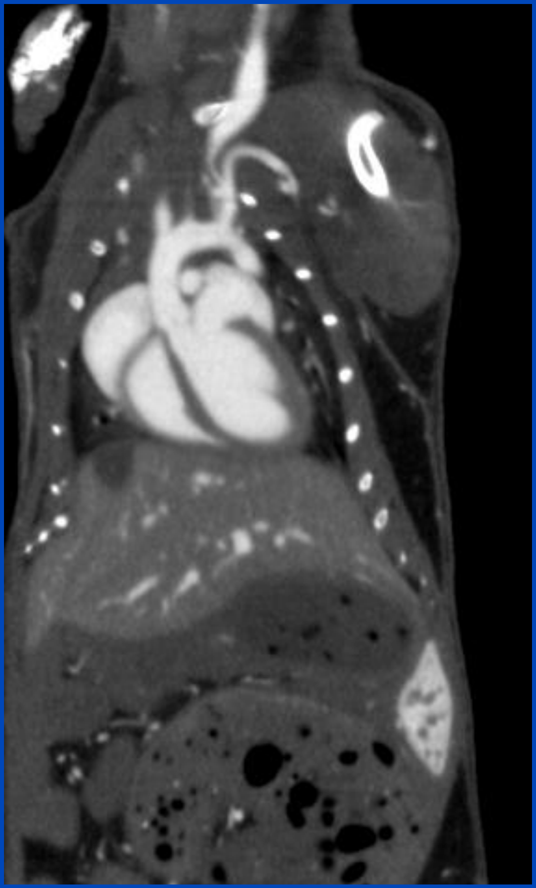

<u>Data displayed as:</u>

Heart: 90 bpm

Lung: 0 rpm

Mouse with 180 rpm and 240 bpm.

5D Motion Compensation

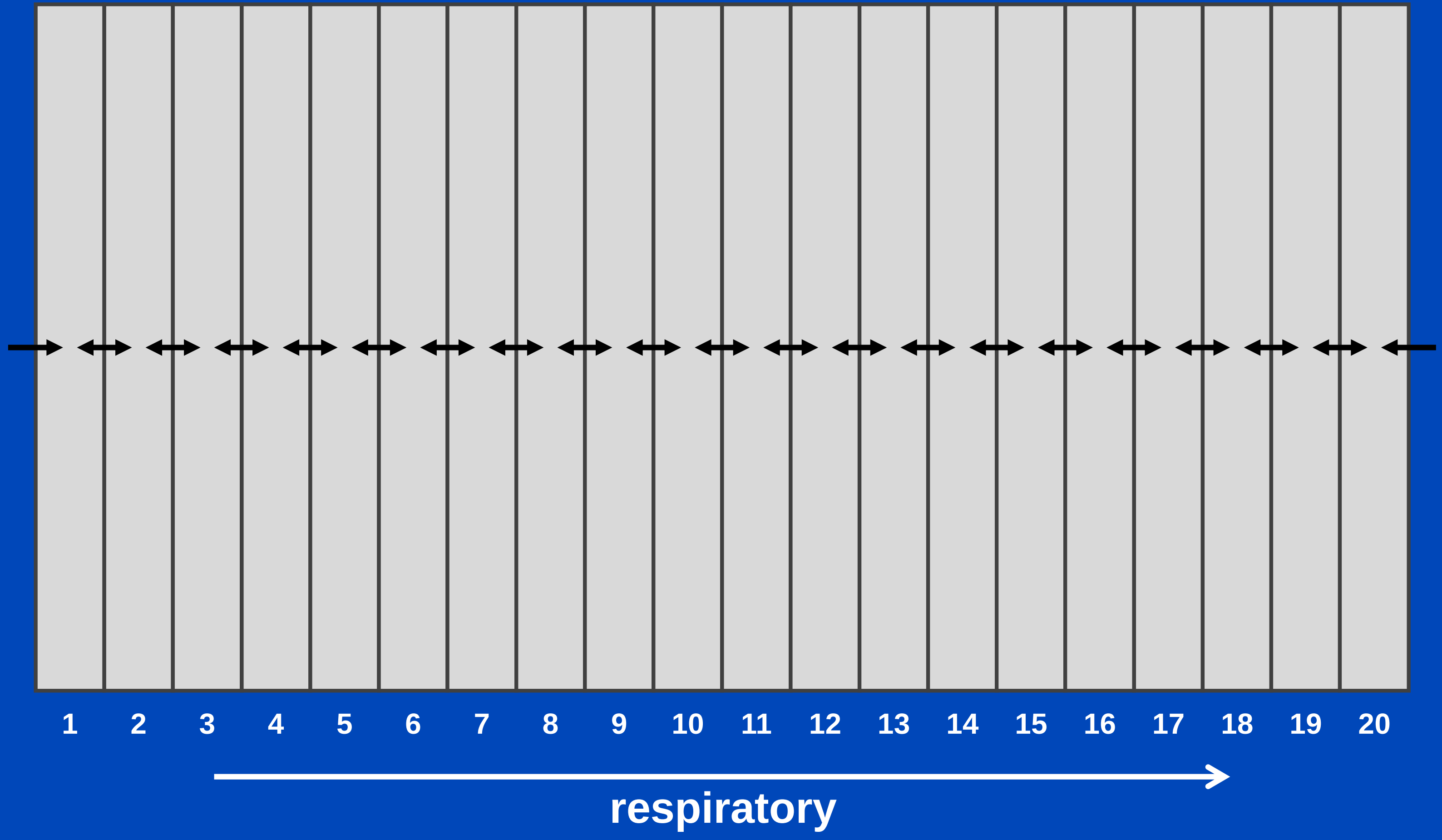

Brehm, Sawall, Maier, and Kachelrieß, “Cardio-respiratory motion-compensated micro-CT image reconstruction using an artifact model-based motion estimation” Med. Phys. 42(4):1948-1958, 2015.

dkfz.

5D Motion Compensation

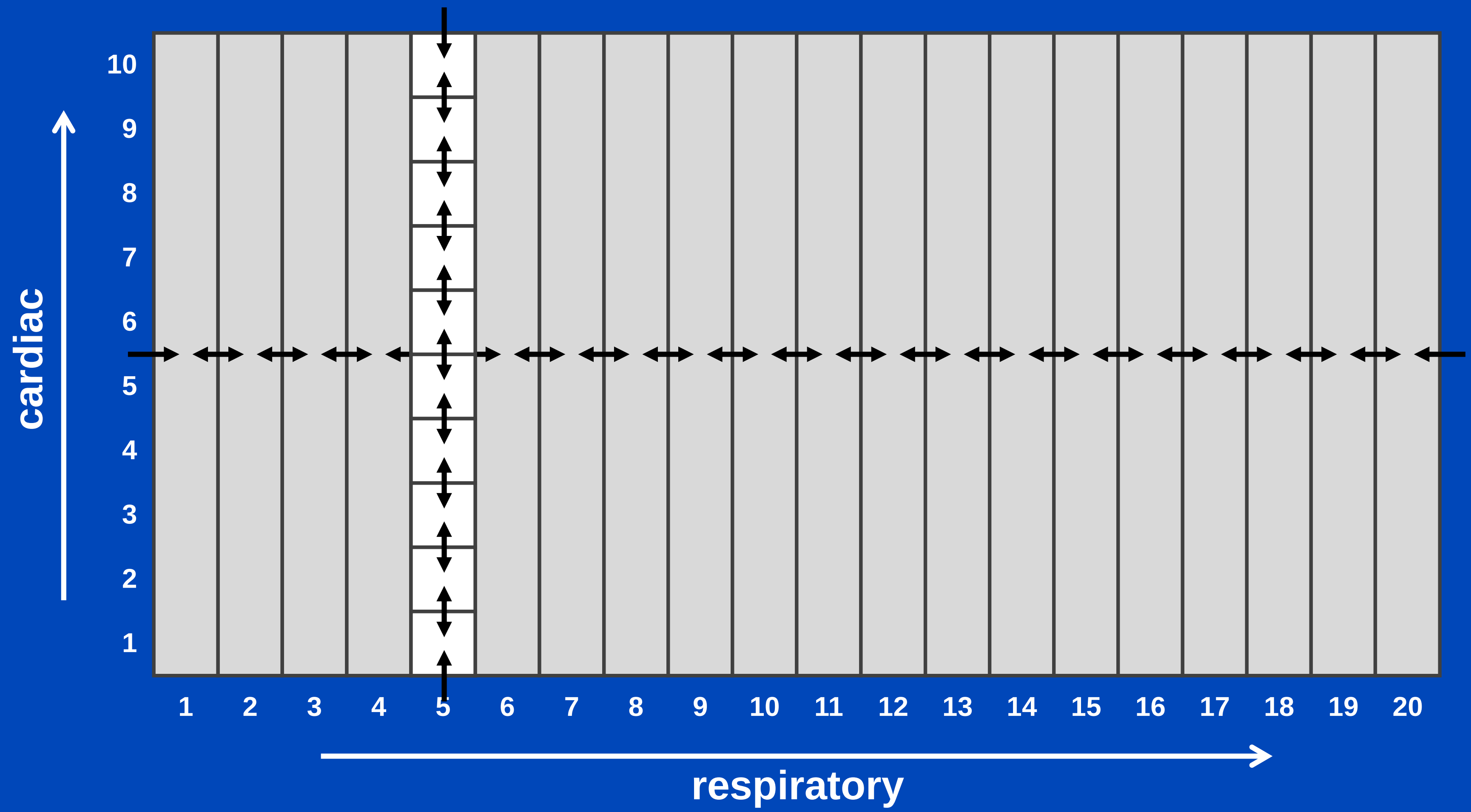

Brehm, Sawall, Maier, and Kachelrieß, “Cardio-respiratory motion-compensated micro-CT image reconstruction using an artifact model-based motion estimation” Med. Phys. 42(4):1948-1958, 2015.

5D Motion Compensation

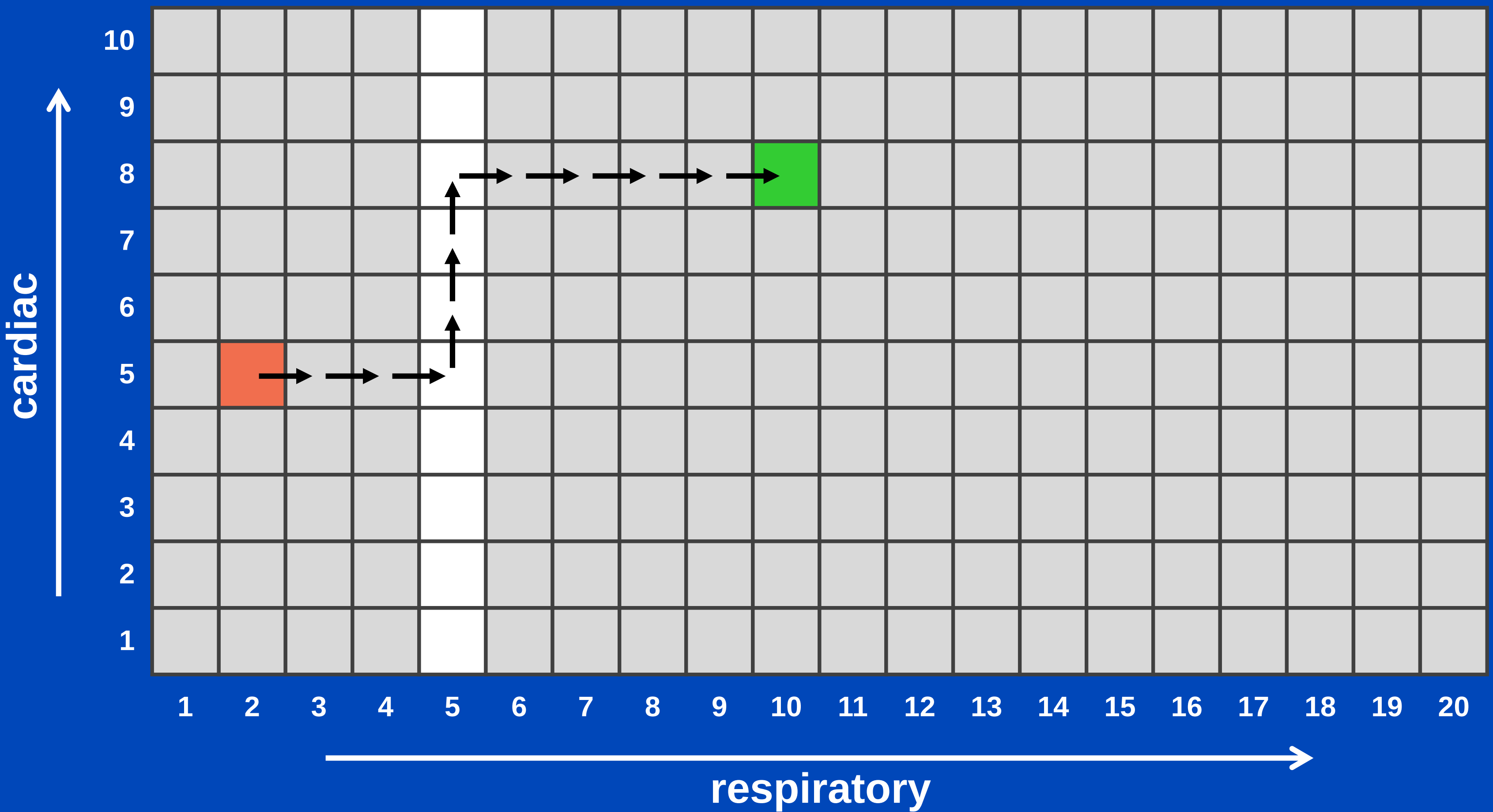

Brehm, Sawall, Maier, and Kachelrieß, “Cardio-respiratory motion-compensated micro-CT image reconstruction using an artifact model-based motion estimation” Med. Phys. 42(4):1948-1958, 2015.

5D Motion Compensation

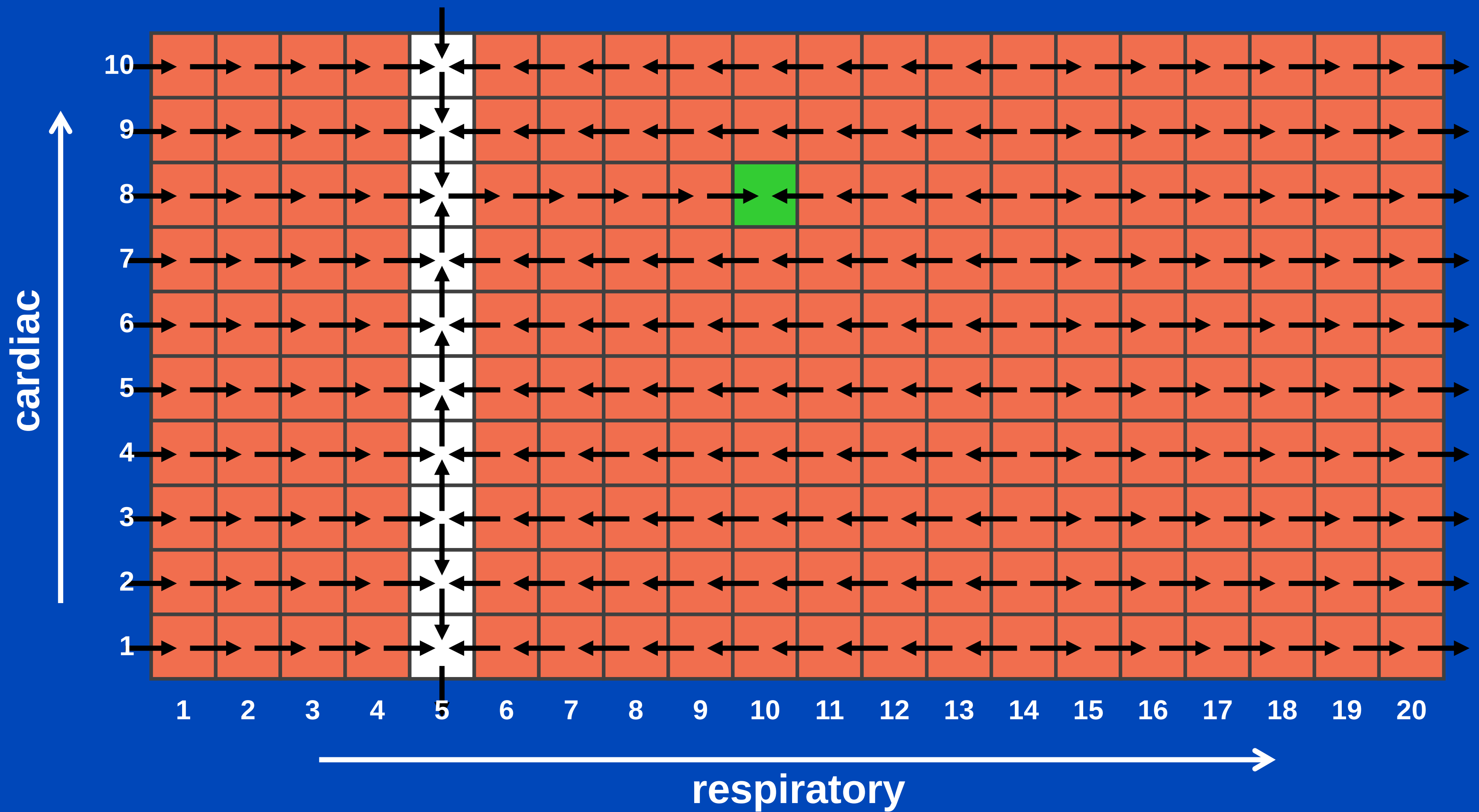

Brehm, Sawall, Maier, and Kachelrieß, “Cardio-respiratory motion-compensated micro-CT image reconstruction using an artifact model-based motion estimation” Med. Phys. 42(4):1948-1958, 2015.

7200 Projections

3D CBCT | 5D double-gated CBCT | 5D Motion Compensation

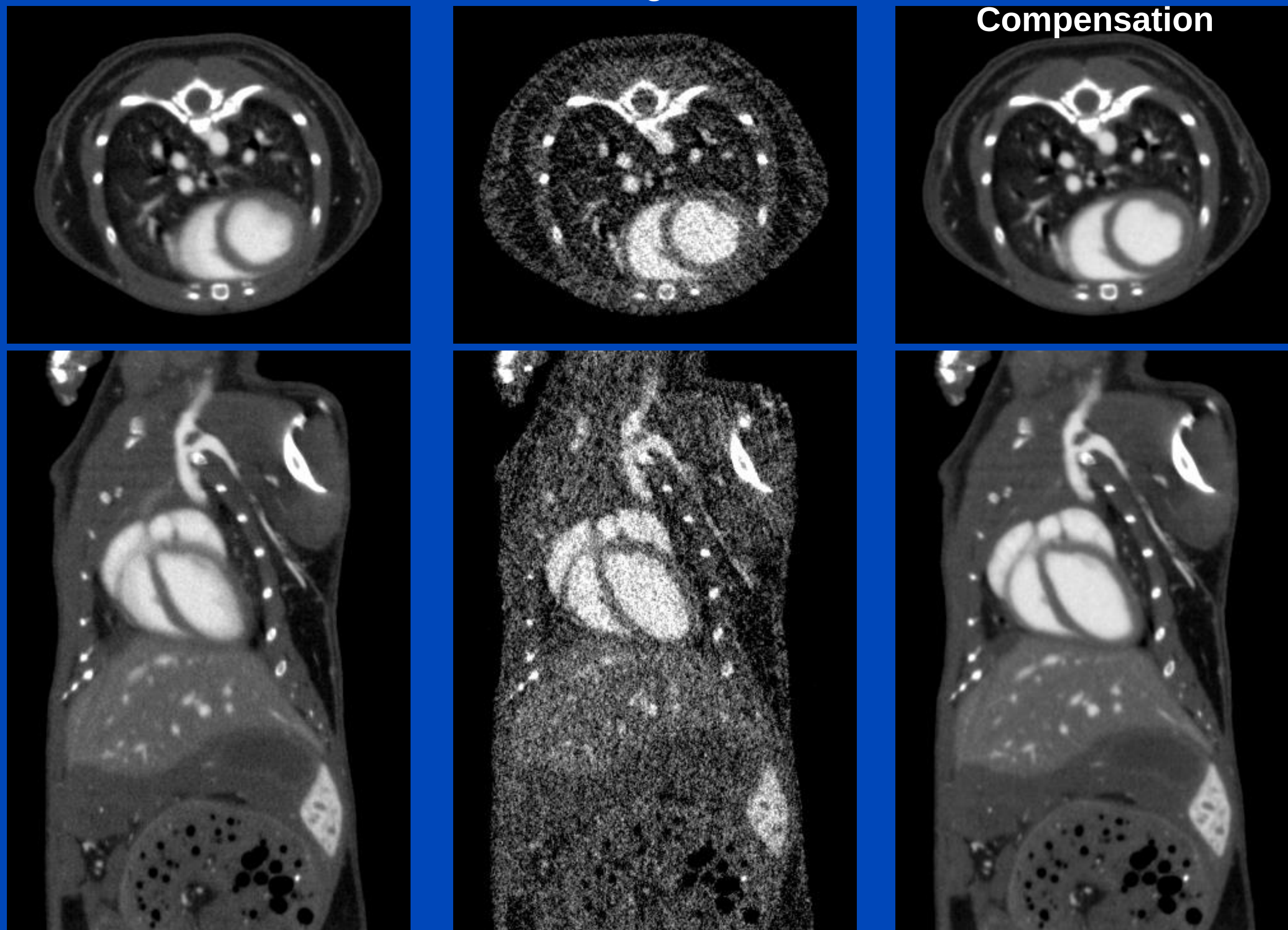

The images show a fixed respiratory and cardiac phase.

Brehm, Sawall, Maier, and Kachelrieß, “Cardio-respiratory motion-compensated micro-CT image reconstruction using an artifact model-based motion estimation” Med. Phys. 42(4):1948-1958, 2015.

3600 Projections

3D CBCT | 5D double-gated CBCT | 5D Motion Compensation

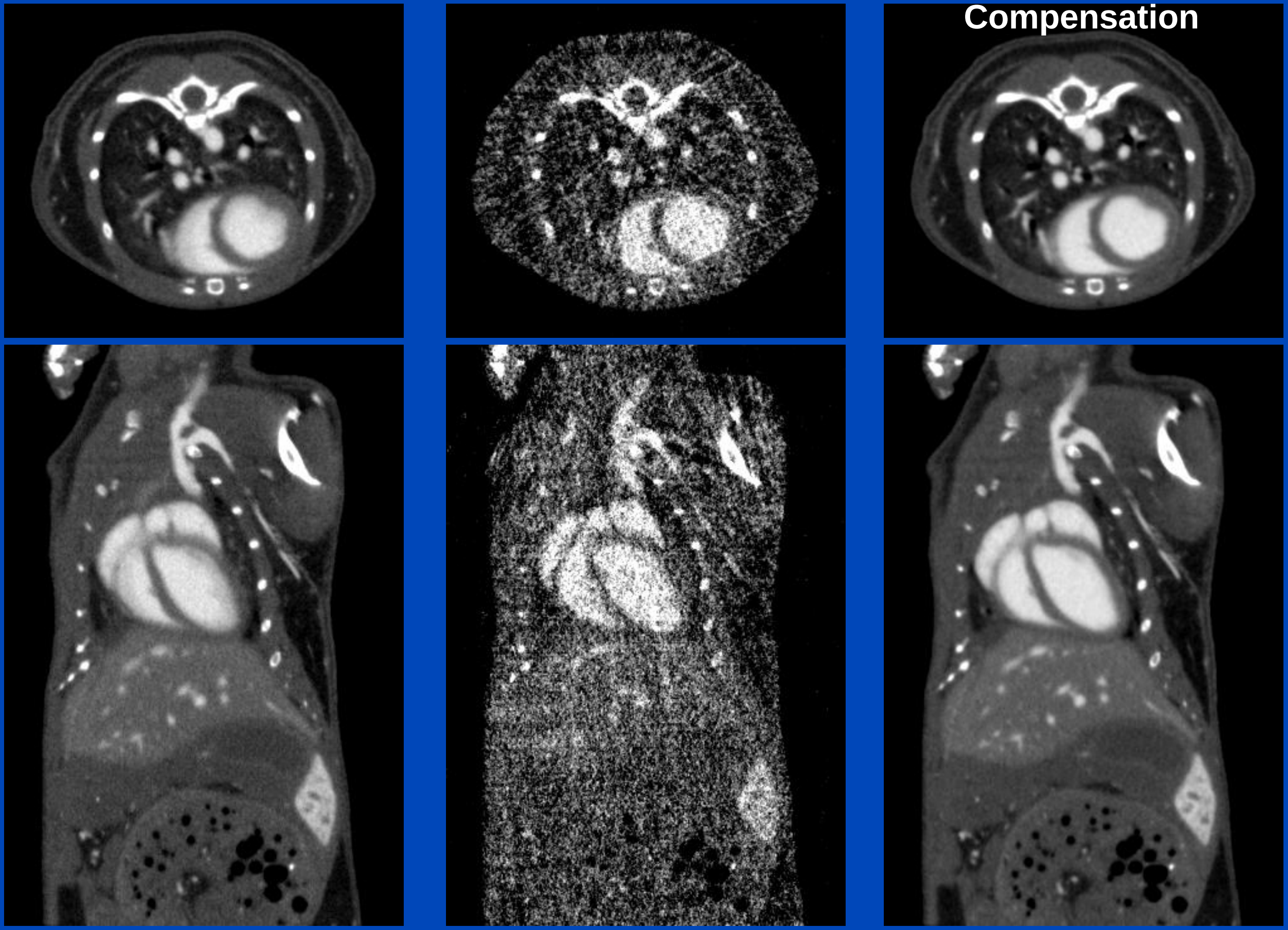

The images show a fixed respiratory and cardiac phase.

Brehm, Sawall, Maier, and Kachelrieß, “Cardio-respiratory motion-compensated micro-CT image reconstruction using an artifact model-based motion estimation” Med. Phys. 42(4):1948-1958, 2015.

720 Projections

3D CBCT | **5D double-gated CBCT** | **5D Motion Compensation**

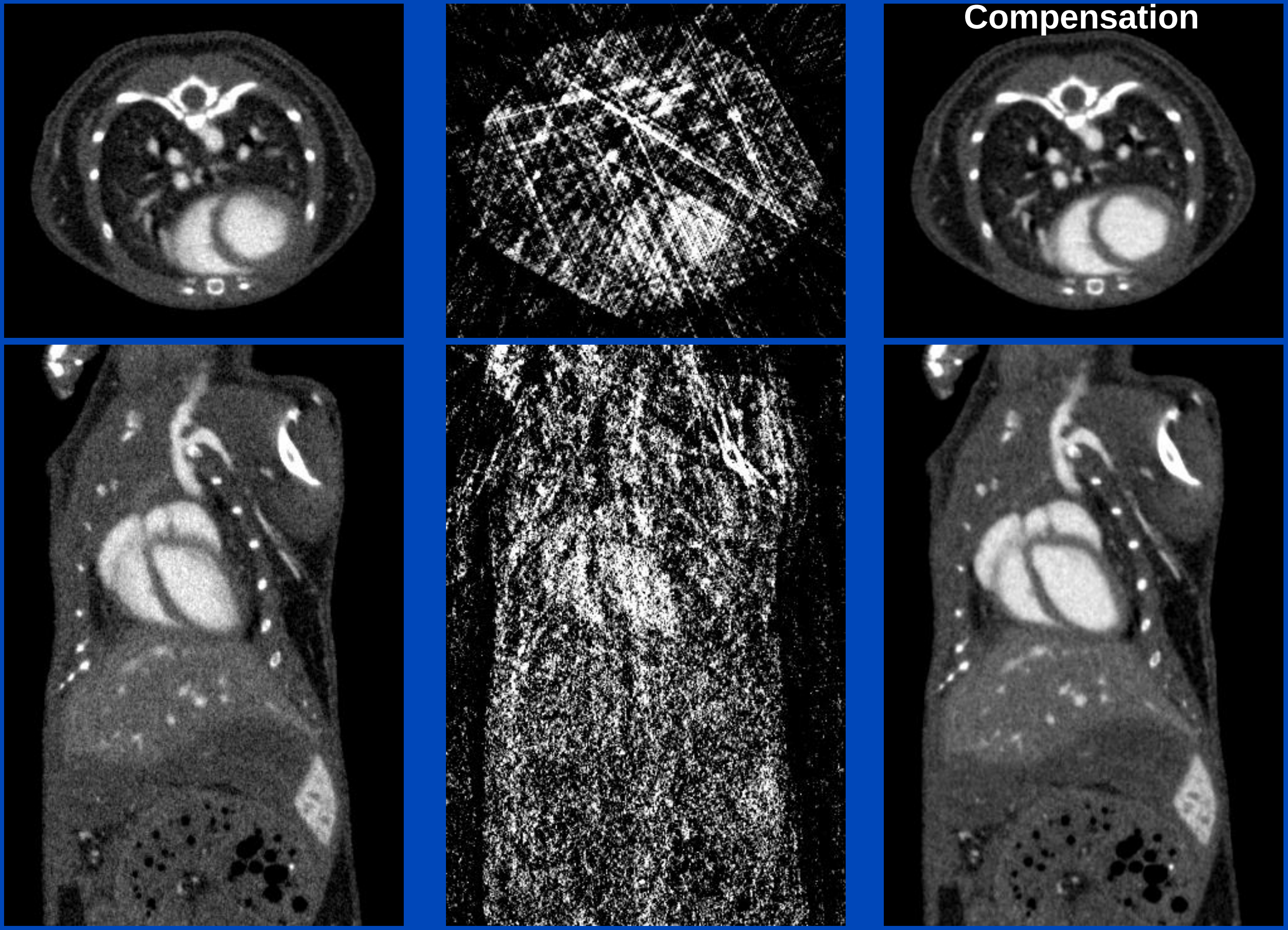

The images show a fixed respiratory and cardiac phase.

Brehm, Sawall, Maier, and Kachelrieß, "Cardio-respiratory motion-compensated micro-CT image reconstruction using an artifact model-based motion estimation" Med. Phys. 42(4):1948-1958, 2015.

Thank You!

This presentation will soon be available at www.dkfz.de/ct.

Job opportunities through DKFZ's international PhD or Postdoctoral Fellowship programs (marc.kachelriess@dkfz.de).

Parts of the reconstruction software were provided by RayConStruct® GmbH, Nürnberg, Germany.